MOLECULARLY IMPRINTED NANOPARTICLES FOR DIAGNOSTIC APPLICATIONS

Thesis submitted for the degree of

Doctor of Philosophy

at the University of Leicester

by

Francesco Canfarotta MSc

Department of Chemistry

University of Leicester

February 2016

ABSTRACT

MOLECULARLY IMPRINTED NANOPARTICLES FOR DIAGNOSTIC APPLICATIONS

Francesco Canfarotta

Molecularly imprinted polymers (MIP) are gaining increasing interest thanks to their low cost of manufacturing, robustness and stability compared to their bio-analogues such as antibodies. The molecular imprinting process can be defined as the generation of molecular recognition sites in a synthetic polymer. The template-derived sites thus created within the polymeric matrix allow MIPs (often referred as plastic antibodies, due to their synthetic nature) to selectively recognise and bind the target molecule. In light of these properties, MIPs have been successfully applied in sensors, assays and separation applications. Due to their small size, MIP nanoparticles (NPs or nanoMIPs) can be used in biomedicine, since the nanoscale format is potentially suitable for cellular or *in vivo* applications. The aim of this work is to demonstrate the suitability of the nanoMIPs as tools for imaging in cells. For this purpose, the choice of appropriate fluorescent moieties to be included in the nanoMIPs is crucial and depends on the intended application. Several fluorescent monomers were characterised and chosen as imaging functionalities to be employed in the synthesis of MIP NPs (Chapter 2). The innovative solid-phase approach used in this work enables the synthesis of nanoMIPs both in organics (for small templates) and in water (for peptides and proteins), with the possibility to tailor the particle's surface chemistry according to the intended use. (Chapter 3 and 4). Only few examples of MIP NPs for cellular imaging have been reported so far. Such nanosystems should be biocompatible and physiochemically stable under physiological conditions, as demonstrated in Chapter 5 and 6. Thanks to their good biocompatibility and recognition properties, MIP NPs were successfully applied as membrane-targeted diagnostic tools (Chapter 7) in both cancer and senescent cells, thus paving the way for their *in vivo* use as diagnostic and imaging tools.

ACKNOWLEDGEMENTS

TABLE OF CONTENTS

LIST OF TABLES

LIST OF FIGURES

LIST OF ABBREVIATIONS

ACN   Acetonitrile

AIBN   Azobisisobutyronitrile

APTS   [(3-aminopropyl)triethoxysilane]

ATRP   Atom transfer radical polymerisation

DEDTC N,N-diethyldithiocarbamate

DLS   Dynamic light scattering

DMF N,N'-dimethylformamide

EGDMA   Ethylene glycol dimethacrylate

EPR   Enhanced permeability and retention

FRET   Fluorescence resonance energy transfer

GA   Glutaraldehyde

IVD   In vitro diagnostic

LOD   Limit of detection

MAA   Methacrylic acid

MIP   Molecularly imprinted polymer

MNPs   Magnetic nanoparticles

M_w Weight-average molecular weight

MWCO   Molecular weight cut off

NIR   Near infra-red

NPs   Nanoparticles

PBS   Phosphate buffered saline

PEG   Polyethylene glycol

QDs   Quantum dot

RAFT   Reversible addition–fragmentation chain transfer

RES   Reticuloendothelial system

SEM   Scanning electron microscopy

SPR   Surface plasmon resonance

TEM   Transmission electron microscopy

TEOS   Tetraethyl orthosilicate

TRIM   Trimethylolpropane trimethacrylate

1 LITERATURE REVIEW – NANOTECHNOLOGY IN DIAGNOSTICS

The recent improvements in both diagnostics and therapy have led to a rise in the human life expectancy. Nanotechnology has been proven to be a powerful tool and several nano-formulations are currently employed in clinical practice. For instance, magnetic nanoparticles (NPs) are currently being used for imaging, therapy and in bioassays for analyte quantification. Nanotechnology enables the user to handle only a small volume of sample, allowing at the same time a low limit of detection (LOD) to be achieved. Sometimes, certain nanosytems in diagnostics have demonstrated to perform faster and achieve an higher sensitivity than comparable assays which use biomolecules[1]. Moreover, depending on the final application, NPs can be engineered to impart the required properties. In general, NPs should possess specific properties according to the final use. For instance, the use of a stable, bright and cheap dye is crucial for the manufacture of optical-based diagnostic assays. On the other hand, other generic properties such as the monodispersity of the produced nanosystem are highly desirable, since many properties depend on the particle size distribution[2].

The use of NPs in molecular diagnostics can be termed "nanodiagnostics" and several nanosystems have been successfully employed in both *in vivo* and *in vitro*[3]. Recently, the global market for *in vitro* diagnostics (IVD) has grown at an incredible rate, from US$44 Billion in 2010 to a predicted US$ 74.65 billion by 2020[4]. The largest part of the IVD global market is represented by the "point-of-care" sector, followed by immunochemistry and molecular diagnostics[5].

1.1 POLYMERIC NANOPARTICLES FOR OPTICAL DIAGNOSTICS

Polymeric nanoparticles have attracted increasing interest in the past decade thanks to their overall ease of synthesis and straightforward functionalisation. Indeed, the possibility of tailoring their properties (e.g. optical, magnetic, electrochemical) made polymeric NPs a "winning tool" in diagnostics. One of the most exploited features of

polymeric NPs in diagnostics is their possibility of being optically detected, by means of fluorescence analysis or monitoring colour changes. Currently, the optical diagnostic sectors in which polymeric NPs are widely employed are biomarker analysis, diagnostic imaging, cancer diagnosis and immunoassays. The binding of the target biomolecule to NPs is the crucial step in many assays based on nanoparticles. In order for the target analyte to be detected, the binding should produce a measurable signal that can be quantified. To this end, the most commonly employed labels are enzymes, that are able to catalyse the formation of coloured molecules which in turn can be monitored by a change in colour or fluorescence of a solution. Dyes have been widely used in optical diagnostics, enabling the detection of analytes with excellent sensitivity, either by emission of fluorescence or by means of colour changes. Unfortunately, dyes suffer from photobleaching and typically exhibit an asymmetric emission spectrum. Photostability is crucial especially for prolonged observations, where photobleaching issues would severely impact on the dye's capability to detect single molecules. Moreover some dyes, such as rhodamines and fluoresceins, suffer from quenching phenomena beyond a certain concentration in solution[6]. Despite these drawbacks, organic dyes have been widely used thanks to their ease of use and low cost. However, when the dye molecule is incorporated in a polymeric matrix, enhanced photostability is often achieved due to the "protective" effect of the polymer. Furthermore, by covalently linking the dye to the polymer it is possible to reduce the chance of leakage, which is often detected with physically entrapped dyes that can still diffuse out of the polymer. Since hundreds of dye molecules can be entrapped within a single NP, the intensity of colour or the brightness of emission result enhanced. Moreover, the hydrophobic microenvironment usually present in a polymeric NP can enhance the quantum yield of some fluorescent dyes[7-10]. In addition, the polymer can be engineered in order to bear specific reactive functional groups along its backbone, to allow specific labelling with other fluorescent reporters as well as conjugation with other (bio)molecules for specific applications.

In general, reporters for optical sensing can be classified in two main categories. The first consists of reporters used as *molecular sensors* in systems able to detect changes in their surroundings and/or give a response upon exposure to a specific target molecule.

The second includes reporters used as *labels*, whose aim is to generate a fluorescent signal which depends only on the presence of the reporter itself, without any changes in the fluorescence properties[6]. The ideal reporter should possess high quantum yield and high molar absorption coefficient, it should be thermally and photochemically stable, and produce an optical response proportional to the concentration of the analyte to be detected, without interacting with other molecules in the sample. A large Stokes shift is highly desirable since it enables the fluorescent signal to be monitored without issues related with the overlapping of excitation and emission spectra of the reporter[11]. For *in vivo* use, dyes must be non-toxic and their biodistribution profile well-known.

1.2 SYNTHESIS OF POLYMERIC NANOPARTICLES

Polymeric NPs can be made from inorganic materials (e.g. silica) or organic polymers. Typically, the latter are produced either by polymerisation of monomers or by processing of preformed polymers. In the latter case, the methods most frequently employed are: salting-out, nanoprecipitation, solvent evaporation, supercritical fluid technology and dialysis[12]. Polymeric NPs are also produced from single monomers by several methods, such as dispersion, precipitation and interfacial polymerisations. The most commonly used methods are emulsion and living free radical polymerisation (LFRP). The former is performed in water, with or without surfactant, and enables a good control over the size distribution of the particles. Similarly, LFRP allows an excellent control over the molecular weight and polydispersity of NPs[13]. In general, living polymerisations relies on the establishment of dynamic equilibria between a small number of growing radicals and a large majority of dormant species. Although the colloidal stability of NPs prepared by living polymerisation (LP) can be sometimes problematic, LPs are an excellent method for the production of functionalised NPs. Furthermore, in contrast to conventional free radical polymerisations, living polymerisations are not subject to autoacceleration phenomena, allowing a better control over polymer chain length and particle size.

Table 1. Comparison of the most frequently employed methods for the synthesis of polymeric NPs for biomedical application

Organic nanoparticles			
Synthetic method	Particle size/initiator	Advantages	Drawbacks/issues
Mini- and micro-emulsion polymerisation	10-200 nm Initiator: persulfate; azoisobutyronitrile	Performed both in water and organics. Good monodispersity	Size control. Surfactant needed to obtain smaller particles
Living radical polymerisation	30-300 nm Initiator: alkoxyamines, thioesters, alkyl halides, iniferters	Performed both in water and organics. Ideal for synthesis of functionalised nanoparticles	Residues of initiator and surfactant (if employed). Colloidal stability
Precipitation and dispersion polymerisation	200 nm – 10 μm Initiator: persulfate; azoisobutyronitrile	With/without surfactant. Moderate-good monodispersity	Size control. Possible irregular shape. Difficult to obtain particles<200 nm

1.3 ORGANIC POLYMERIC NANOPARTICLES FOR IN VITRO OPTICAL DIAGNOSTICS

Regardless of their composition, NPs can be engineered to act as signal transducers, converting the presence of the analyte into a quantifiable optical response generated by variations in photophysical characteristics of the dye. It should be noted that some general requirements for the fluorophores are often mutually exclusive: for instance, a high quantum yield is usually correlated with a small Stokes shift, or a high molar extinction coefficient (ε) with short fluorescence lifetimes[11]. According to the photochemical process implicated in the optical detection, three processes can be distinguished: (1) generation of fluorescence emission, (2) modulation of fluorescence emission, (3) Förster resonance energy transfer (FRET) processes[14]. In the first mechanism, fluorescence emission is produced by specific recognition phenomena or chemical reactions in the presence of the target molecule. For instance, the fluorescence emission of Rhodamine B (RhB) changes depending on whether it is in the spirolactam or the acyclic form[15, 16]. This phenomenon was used by Hu and colleagues in the

development of RhB-based polymeric micelles for detection of Hg^{2+}. A thermo-responsive copolymer containing RhB moieties was synthesised by reversible addition−fragmentation chain-transfer (RAFT) polymerisation. The ring-opening reaction of RhB moieties occurs upon addition of Hg^{2+}, thus generating an intense emission of fluorescence[16]. Similarly, a polyethylenglycol (PEG)-based thermo-responsive copolymer embedding coumarin moieties was employed for the detection of fluoride (Figure 1-1)[17]. In a similar approach, polymeric micelles based on Eu(III) complexes and fluorescein isothiocyanate (FITC) showed multicolour fluorescent emission, acting both as pH and temperature sensors[18]. Spiropyran is another example of reporting group which, upon exposure to UV light, undergoes heterocyclic ring cleavage forming the open chain merocyanine form. The latter absorbs in the visible region, whereas the spiropyran (closed form) is colourless[19-21]. Spiropyran-based nanosystems based on this mechanism have been developed as fluorometric and colorimetric temperature sensors[22].
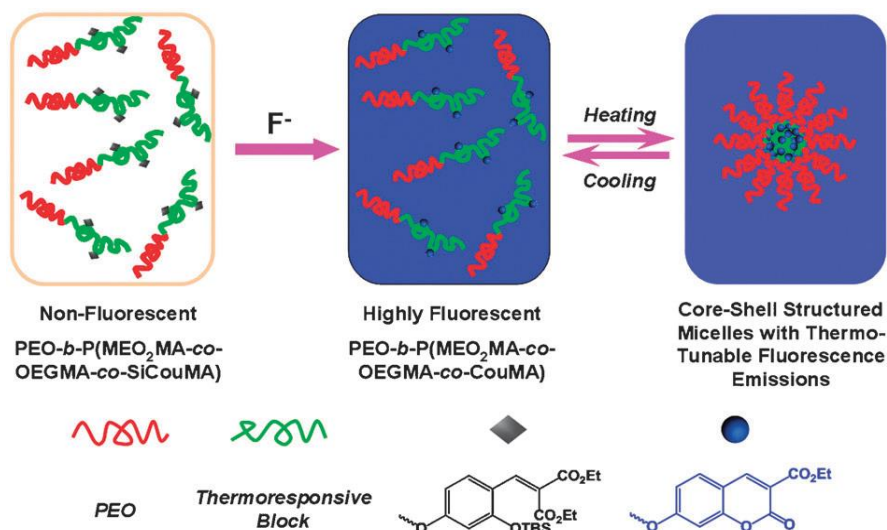
Figure 1-1. Illustration for the generation of responsive NPs for fluoride ions sensing. The system exploits fluoride ions-induced cyclisation reaction of non-fluorescent portions to form fluorescent coumarin moieties within the polymer, where PEO, MEO$_2$MA, and OEGMA are poly(ethyleneglycol), di(ethyleneglycol) monomethyl ether methacrylate, and oligo(ethyleneglycol) monomethyl ether methacrylate, respectively (reprinted with permission from Jiang Y. *et al.*, Macromolecules 2011, 44, 8780. Copyright 2016, American Chemical Society).

Another fluorogenic mechanism involves the so-called "click" reaction, in which highly fluorescent products are generated from the non-fluorescent alkyne- and azide-derivatives (Figure 1-2). By means of this principle, fluorescent polymeric NPs embedding cyanine dyes have been used for *in vivo* targeting of tumour angiogenesis[23]. In particular, amphiphilic copolymers conjugated with PEG, folate and indocyanine green by click reaction were produced. The resulting NPs showed to accumulate in the tumour proximity, thanks to the synergistic effect of PEG and folate targeting[24]. The advantage of click chemistry is its high selectivity and easiness: it can be used to produce multifunctional systems by means of simple synthetic procedures. Recently, this technique has been used for *in vitro* imaging of glioma cells by using an azido-terminal fluorescein derivative, which was reacted with an alkyne-modified copolymer[25]. As reported elsewhere[26], click chemistry can also be used to functionalize inorganic nanosystems, such as gold and magnetic NPs[27, 28], silica beads or quantum dots (QDs)[29]. The latter are semiconductor nanocrystals, between 1 and 10 nm, made of selenides, sulphides or tellurides of heavy metals characterised by wide absorption spectrum, high photostability, narrow and intense emission spectrum, large Stokes shift and size-tunable emission[30]. In fact, their emission wavelength can be tuned from the UV to the near infrared (NIR) region just by changing their size and chemical composition, thus allowing simultaneous detection of multicolour QDs using an appropriate excitation wavelength. Furthermore, they exhibit high fluorescence in the region of 650–900 nm, which makes them ideal for *in vivo* applications. On the other hand, due to the presence of heavy metals, they are potentially cytotoxic and for this reason they are often coated with a polymer layer to reduce the risk of heavy metal loss and to improve their solubility in water[31].
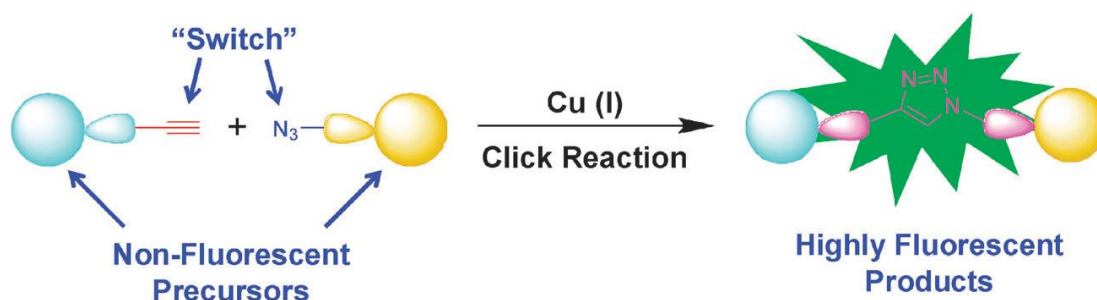
Figure 1-2. Representation of a typical fluorogenic click reaction (reproduced from from Li, C. *et al.*, Chemical Communications 2012, 48, 3262, with permission from the Centre National de la Recherche Scientifique and The Royal Society of Chemistry).

Another fluorogenic example is given by some non-fluorescent reporters (in their single-molecule state) which can undergo self-aggregation, turning on their fluorescent emission[32-34]. Polymeric NPs based on *N*-isopropylacrylamide (NIPAM) and tetraphenylethene (TPE) were employed as a fluorescent thermometer, showing variations in temperature within the thermal phase transition of the polymer, due to the aggregation process triggered by water (a poor solvent for TPE) and heat[35].

The second detection principle (fluorescence modulation of the reporter) is based on the intrinsic properties of the dye and/or on the responsiveness of the polymer matrix upon exposure to the target molecule. Benzylselenide-tricarbocyanine (BzSe-Cy) and fluorescein are two fluorescent reporters which undergo changes in their emission spectrum in response to environmental factors. The emission intensity of fluorescein changes according to the pH of the solution due to its transition between mono- and di-anionic states[36]. BzSe-Cy was used to develop fluorescent micelles for peroxynitrite detection in living cells. Upon exposure to ONOO⁻, BzSe-Cy undergoes oxidation, with a consequent reduction in its fluorescence emission[37]. Another example of responsive reporter is based on the polarity-sensitive benzoxadiazole (BD) motifs. Uchiyama *et al.* developed temperature-sensitive fluorescent nanogels based on these BD moieties[38,39]. Their quantum yield is enhanced by the thermally-induced aggregation determined by a reduction in polarity of the microenvironment within the polymer (Figure 1-3). At low temperature, the polymer undergoes swelling due to the absorption of water and the

polarity-sensitive BD motifs are quenched by the surrounding water molecules. As the temperature increases, the polymer shrinks, releasing water molecules and enhancing its fluorescence emission. Such nanosystems can be used to monitor intracellular phenomena, as demonstrated in COS7 cells[40].
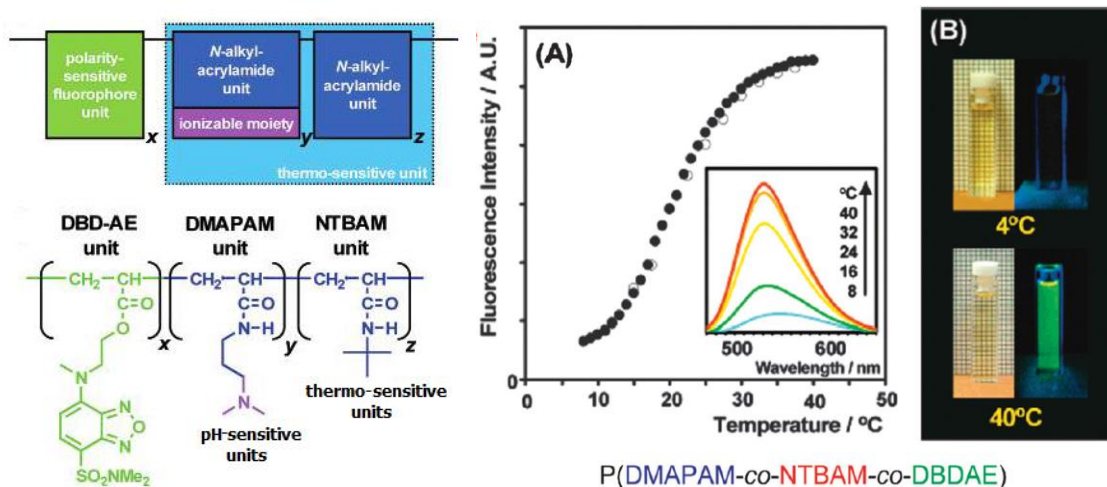
Figure 1-3. Thermo-responsive copolymer, composed of *N,N*-dimethylaminopropylacrylamide (DMAPAM), *N*-t-butylacrylamide (NTBAM) and 4-*N*-(2-acryloyloxyethyl)-*N*-methylamino-7-*N,N*-dimethylamino-sulfonyl-2,1,3-benzoxadiazole (DBD-AE), which acts as a fluorescent molecular thermometer in buffer. Changes in the fluorescence emission upon heating and cooling cycles (a). Visible and fluorescent images of the sample (b) (adapted with permission from Uchiyama S. *et al*., JACS 2004, 126, 3032. Copyright 2016 American Chemical Society).

Gao and colleagues recently produced copolymers consisting of tertiary amine-containing (TA) segments and poly(ethyleneoxide) (PEO) which demonstrated excellent pH sensitivity. When the pH is higher than the pKa of the TA segments, the polymers self-assemble into micelles ("hiding" the TA blocks in the core), leading to fluorescence quenching due to homo-FRET mechanisms. By increasing the pH, the TA segments become positively charged and therefore the micelles undergo disassembly, with a consequent fluorescence enhancement. These NPs exhibited a fast response (< 5 ms) to changes in pH, in the range 5.0-7.4[41]. Thanks to the ability of this system to distinguish between variations of pH values around 0.25 pH units, such nanosystem can be used to monitor pH variations within intracellular compartments[42]. However, no

long-term photostability and cytotoxicity studies have been carried out. In contrast, FITC-based particles were coated with dextran to increase their long-term biocompatibility, resulting in no cytotoxic effect observed over a 22 day period[43].

The encapsulation of a gold core within polymeric NPs is another method to generate nanosystems which can be used in luminescence-based assays. For instance, the metallic core can quench the fluorescence emission of a cationic polyfluorene, allowing the detection of target analytes at subpicomolar concentrations[44]. In another example, Rotello and colleagues grafted a fluorescent polymeric shell around gold NPs for detection of proteins and for differentiation between normal and cancer cells by means of this quenching mechanism[45, 46]. The novelty of this nanosystem lies in the exploitation of morphological changes that occur on the cell surface, according to various disease states. Similarly, pyrene dimers having –O–Si–O– or –O–Si–Si–O– linkages exhibited different excimer/monomer emission upon exposure to fluoride anions[47]. Upon exposure to fluoride, the Si–O bond is cleaved, giving rise to fluorescence emission characteristic of the pyrene monomer. The aforementioned probes were loaded in NPs made of poly(D,L-lactic acid) (PLA) and used as F^- sensor in living HeLa cells. When these cells were incubated for 2 hours together with both fluoride (100 μM) and NPs, the distinctive fluorescence emission specific of pyrene monomers was detected. More interestingly, no optical changes were seen in the presence of other interfering ions.

The third detection principle (FRET) consists in a non-radiative transfer of energy from a "donor" dye to an "acceptor" through long-range dipole–dipole interactions. This energy transfer depends on the spectral overlap of the donor (D) emission band and the acceptor (A) absorption band. Moreover, the distance between the fluorescent reporters is critical since, for FRET to occur, a separation between donor and acceptor between 1 and 10 nm is needed. In light of such distance-dependent features, FRET can be used as a technique to investigate events that lead to variations in molecular distances[6]. Such energy transfer resolves in a quenching effect if A is non-fluorescent. Otherwise, if A is a fluorophore, a longer-wavelength emission occurs according to the acceptor emission. By varying the D-A ratio, multicolour detection can also be accomplished, as

demonstrated by Wang and Tan[48]. Usually the fluorescence is either enhanced or quenched upon addition of the target molecule[49, 50]. Other nanoparticles which show on/off FRET behaviour have been synthesised, depending only on the presence or absence of the target analyte[51-54]. FRET-based polymeric NPs have been employed to detect ions, as demonstrated by Chen and colleagues who produced core–shell polymeric particles for quantification of Cu^{2+}. In their system, the poly(methyl methacrylate) (PMMA) core was embedded with Nile red, while polyethyleneimine (PEI) was used as a shell and ensure binding to Cu^{2+}. Upon exposure to copper ions, complexation of Cu^{2+} with PEI at the NP surface quenches the fluorescence emission of Nile red, due to FRET from dye to the aforementioned Cu^{2+}/PEI complexes. Interestingly, almost no fluorescence quenching was detected in presence of other cations[53]. In another example, Ma and colleagues developed FRET-based polymeric micelles based on a Fe^{3+}-reactive RhB derivative, with switchable fluorescence emission upon Fe^{3+}-induced ring-opening reaction. The system exhibited a good sensitivity, but its practical application might be limited by the irreversible nature of the sensing mechanism[52].

1.3.1 Molecularly imprinted polymers

The use of antibodies and enzymes in diagnostic assays is widely accepted and, to date, represents the gold standard in terms of sensitivity and affinity. Antibodies (Abs) are routinely used in many diagnostic assays but, unfortunately, they suffer from short shelf-life, high costs of manufacturing and relatively poor stability, especially in organic solvents and at extremes of temperature and pH. Furthermore, it is not easy to produce antibodies against immunosuppressants or toxins due to their action on the immune response[55]. Moreover, generating antibodies against small molecules is not straightforward since chemical coupling to haptens is first required[56]. Finally, it is often difficult to immobilize Abs on the supports used in diagnostic assays[57]. The use of molecularly imprinted polymer (MIP) nanoparticles can overcome these problems. In molecular imprinting, monomers and cross-linkers are polymerised in an appropriate solvent in the presence of the molecules to be imprinted (called "template"). After

removal of the template, the polymer matrix will retain recognition cavities that are complementary to the template, in terms of size, shape and functionality (Figure 1-4). More specifically, the three-dimensional arrangement of binding sites is driven by the structure of the template molecule. Therefore, the synthesised polymer is capable of rebinding the template. Compared with antibodies, the synthesis of MIPs is simpler and cheaper, and without any involvement of animals. In addition, MIPs show high stability and excellent mechanical properties and can be prepared for a wide variety of targets[58, 59 55, 60]. Template removal, however, is often difficult and incomplete, with the potential for subsequent leaching of analyte from the matrix, resulting in inaccurate performance in analytical applications[61]. Moreover, it is quite laborious to integrate them in sensors or to convert the template binding into an electric signal[60, 62].
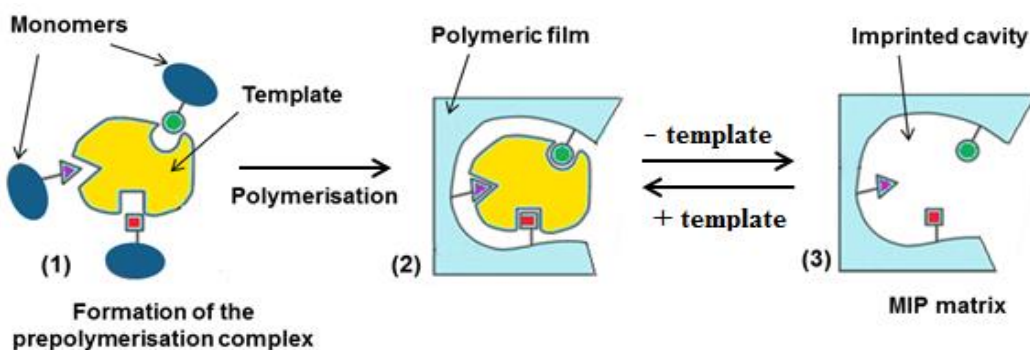
Figure 1-4. Schematic diagram of a general MIP process.

Regarding their synthesis, MIPs can be produced by means of two main approaches, the covalent and the non-covalent imprinting. In the former, developed by Wulff and co-workers, reversible chemical bonds are created between monomer and template during the polymerisation, and the same bonds are then re-formed in the rebinding step. The advantage is that only the monomer's functional groups interact with the template and more homogeneous binding sites are generated. However, not many compounds are suitable for this approach and they need a prior derivatisation with the monomer. Furthermore, the template removal is quite difficult and the re-binding step is slower compared to other approaches[62, 63]. On the other hand in the non-covalent approach, pioneered by Mosbach and co-workers, hydrogen bonds, electrostatic and hydrophobic

interactions are involved. Since weaker interactions take place, an excess of monomer is usually employed to stabilise the monomer-template complex. This method is easier and more versatile, although issues related with the heterogeneity of the binding sites might arise[64]. Considering the advantages of the aforementioned two approaches, some authors have combined them, thus using a template covalently linked to the monomer and the following rebinding step designed in a non-covalently way[62].

Currently MIPs are employed as solid-phase extraction matrices and this is the only MIP-based product commercialised so far, mainly by Sigma-Aldrich and MedTech (USA), Polyintell (France), Chrysalis Scientific (Canada) and Biotage (Sweden). However, imprinted polymers have been successfully applied also in sensors[65-67] and for analyte quantification[68-70], although such systems have not reached the market yet.

In general, MIPs can be manufactured in different ways (Table 2) and in several formats, for example as films or membranes, microparticles or nanoparticles. Compared to the other formats, the nanosize one presents several advantages: it allows the system to exhibit a much higher surface-to-volume ratio and greater total surface area per weight unit of polymer. The imprinted sites are more easily accessible by the templates, thus improving binding kinetics and template removal, and hence enhancing their recognition capabilities[71, 72]. Several authors have started developing nanoMIPs for diagnostic and therapeutic applications, for instance as drug delivery systems[73-75] and sensing elements in assays or sensors[76-79].

Table 2. List of synthetic approaches available for the synthesis of MIPs.

Approach	Procedure	Advantages	Drawbacks	Ref.
Bulk	Performed in organics. A block is obtained and then crushed and sieved	Simple method	Wide particle size distribution and heterogeneity of active sites	80-82
Precipitation polymerisation	Polymer chains grow in solution, precipitating when their size makes them insoluble	Easy and fast. Leads to good yields. Low amount of reagents required	The low monomer concentration required might affect the interactions with the template.	68, 83
Emulsion	Use of surfactants and high-shear homogenisation to	Possible to obtain very small NPs	Surfactants might interfere with the imprinting process.	68, 84

polymerisation	emulsify the water phase with the organic one.	(50nm)	Difficult removal of surfactants	
Core-shell emulsion polymerisation	Deposition of a MIP layer on preformed nanoparticles (made of metals, silica, polymers)	Suitable for large-scale production. High yields	The presence of surfactants and the aqueous phase can reduce the imprinting effect	85, 86
Core-shell grafting	Chemical linkage of MIP to preformed nanoparticles modified with double bonds or iniferter	Excellent control over shell thickness. Sequential shell polymerisation	Imprinted shell might be too thin for imprinting of bulky templates like proteins	87-89
Living radical polymerisation	Use of nitroxide species, metal-containing or dithiocarbonyl initiators. The polymer chains grow at similar rate	Excellent control over particle size and PD. Good for thermolabile templates	Low yield. Removal of catalyst needed (in NMP and ATRP). Not suitable for photolabile templates	90, 91

PD: polydispersity. NMP: nitroxide-mediated polymerisation. ATRP: atom-transfer radical polymerisation.

MIP nanoparticles for optical sensing

Imprinted polymers are gaining increasing interest in the diagnostic field, due to continuous improvements in their synthetic approaches and recognition properties. Many fluorescent nanosystems based on imprinted polymers for detection of different target molecules have been developed to date, although, only a few of them are based on fluorescent monomers. In one example, 1-pyrenemethylamine (PMA) was linked to the matrix of MIP NPs through Michael addition reaction between the residual C=C bonds of the cross-linker (*N,N'*-methylene-*bis*-acrylamide) and the $-NH_2$ of the fluorescent dye[92]. By distillation precipitation, 260 nm NPs imprinted for *R,S*-propranolol were synthesised and employed for selective quantification of propranolol in complex matrices. In another example, fluorescent MIP NPs for atrazine were synthesised by using a zinc(II) protoporphyrin-derivative as both fluorescent reporter and functional monomer[93]. The fluorescence of the MIP was quenched upon template rebinding with a LOD of 1.8 μM, with a low cross-reactivity. Very recently, fluorescent nanoMIPs imprinted for tetracycline were used for quantification in real samples (bovine and pig serum)[94]. An anthracene-derivative monomer was first synthesised and

then used as signalling functionality capable of being quenched upon addition of the drug, down to sub-micromolar concentrations.

Other fluorescent MIP nanosystems are based on core-shell approaches, with other nanomaterials such as QDs, gold NPs, or upconverting materials embedded in the imprinted matrix[95-98]. For instance, QDs have been used as fluorescent reporters in MIP-based sensors. When QDs are in proximity to the imprinted cavities, the analyte rebinding event can quench the emission of the QDs. This is due to a FRET process, which can lead to a 4-fold reduction in the QD emission for some analytes[99]. Recently, composite nanoMIPs embedding QDs have been produced for detection of target molecules in saliva[100]. Interestingly, the size of the nanoMIPs was not affected by the inclusion of QDs. The binding of the target biomolecules (lysozyme, amylase and lipase) to the composite nanosystem was monitored following the reduction in fluorescence emission upon addition of the target. The detection limits were well within the physiological concentrations of the three biomolecules, making it suitable for diagnostic applications (diagnosis of pancreatic cancer). These nanoMIPs were also compared with the Architect *ci* 8200 system (the gold standard for this type of analysis), showing high average accuracy for all three targets.

In another example, Lin and colleagues produced composite QD-nanoMIPs for caffeine detection, using QDs previously derivatised with 4-vinylpyridine[101]. Even in this case, the rebinding event resulted in a reduction of the fluorescence emission from the QDs, exhibiting also high specificity in the presence of caffeine analogues (theobromine and theophylline). Following the same rationale, Diltemiz and colleagues used methacryloylamidocysteine (MAC) to introduce methacryloyl groups onto the surface of QDs. Afterwards, the activated QDs were imprinted for guanosine by using the metal-monomer complex: methacryloyl-amidohistidine-Pt(II)[102]. This metal complex enables selective rebinding through interactions between the N7 of guanine and Pt(II) (Figure 1-5). Like QDs in general, this nanosystem showed a broad separation between excitation and emission (300 nm and 600 nm respectively), and it could be used in mutagenesis studies for the diagnosis of DNA errors.
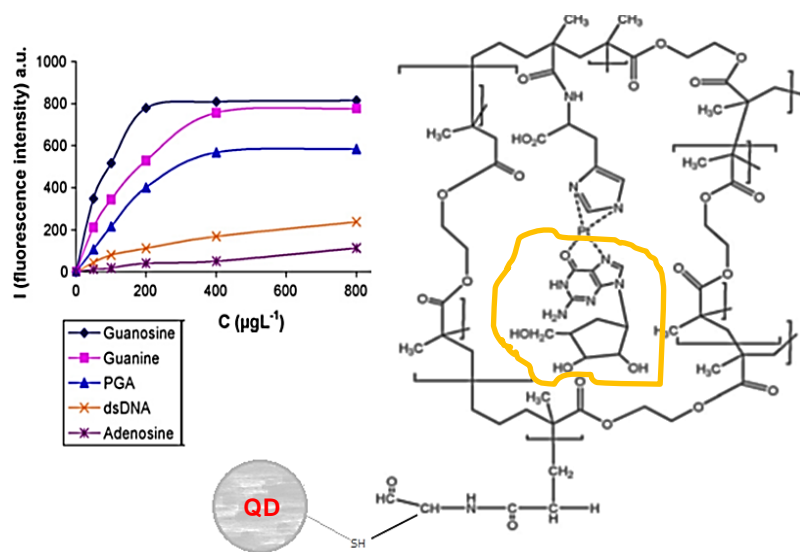
Figure 1-5. On the top left, the effect of increasing concentrations of guanosine and its analogues on the change of the fluorescence of QDs-MIP NPs. On the right, schematic representation of QD-MIP system binding the guanosine template (yellow line) (adapted with permission from Diltemiz *et al.* Talanta, 2008, 75. Copyright 2016, Elsevier).

The number of composite QD-MIPs systems has been rapidly increasing in the past 5 years. Very recently, other three QD-nanoMIP complexes based on a quenching mechanism have been developed for detection of cocaine, ferritin, amanitin and nicotinic acid[103-106]. Notably, ferritin and amanitin imprinted nanoMIPs performed well also in serum samples, while nicotinic acid could be detected even in urine.

The exploitation of surface-enhanced Raman spectroscopy (SERS) represents a way to increase the sensitivity of the nanosystem. To this end, a gold core was embedded in a MIP matrix imprinted for (*S*)-propranolol by emulsion polymerisation[107]. The sensitivity obtained by this system (0.1 μM) was several orders of magnitude higher than for plain nanoMIPs. Furthermore, the rebinding capability was also preserved when a 100-fold excess of interfering compounds caffeine or acetylsalicylic acid) were present.

Other metal-based MIPs have been employed to develop a glucose sensor: silver NPs were produced by in situ synthesis of Ag NPs within a MIP matrix[108]. This synthetic

protocol allowed silver NPs to be restrained in close proximity to each other, so that plasmon coupling effect could occur. Upon exposure to glucose, swelling/shrinking process of the polymer matrix occurs, altering the distance between the silver NPs embedded in the polymer and leading to a change in colour of the solution from yellow to red.

Applications of fluorescent nanoMIPs in cells

Very recently, several groups have started applying the molecular imprinting technology for the recognition of specific targets on the surface of cells. For instance, Haupt's group developed for the first time fluorescent nanoMIPs for molecular imaging of cells and tissues by imprinting glucuronic acid, a monosaccharide present as the terminal unit on larger oligosaccharides[109]. The produced nanoMIPs were then employed to image the hyaluronan on human keratinocytes and on adult skin specimens (Figure 1-6a). Interestingly, other potential interfering molecules such as galactose, *N*-acetylglucosamine, *N*-acetylgalactosamine and glucose did not bind to the nanoMIPs, possibly due to the lack of the charged carboxyl group.

Another target exploited by other groups for cellular targeting is sialic acid. Sellergren's group developed nanoMIPs targeted towards cell surface glycans, via sialic acid imprinting[110]. The overexpression of glycans terminating with sialic acid (SA) residues on the surface of cells has been found to be correlated with various diseases such as cancer. 200 nm silica nanoparticles were used as cores for the subsequent grafting of the sialic acid-imprinted layer. The authors speculate that a specific mixture of functional monomers is ideal for the nanoMIPs to bind strongly to the template. In particular, hydroxyl groups of the sialic acid would interact with a boronate-based monomer, while the carboxyl group would be targeted by an urea-based fluorescent monomer synthesised in-house. The produced fluorescent nanoMIPs were capable of selectively staining different cell lines depending on the SA expression level (Figure 1-6b). Similarly, Yin *et al.* produced sialic acid-imprinted nanoMIPs for selective imaging of cancer cells[111]. In this case, the authors employed Raman-active nanotags (silver

nanoparticles) as signalling core. By surface imprinting based on silanes, an imprinted layer based on boronate as a functional monomer was then created around the silver core. Raman spectroscopy provides significant advantages, such as high photostability and sensitivity, as well as multiplexing capacity. Healthy human hepatic cells and hepatocarcinoma cells (HepG-2) were used as a model to test the selectivity of the nanoMIPs. HepG-2 cells showed an evident SERS signals at 1435 cm^{-1}, much stronger than the one in healthy cells, proving the specific binding of the nanoMIPs to SA on the cell surface.
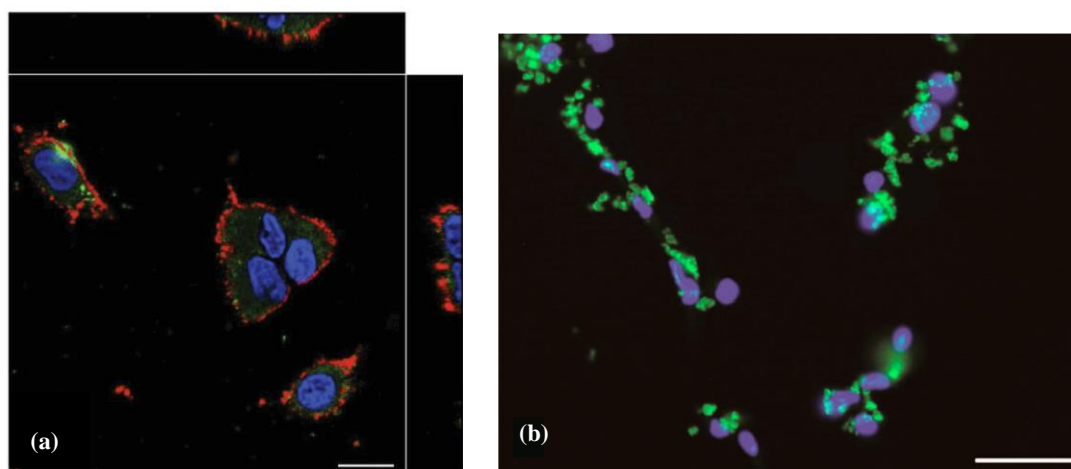
Figure 1-6. Confocal microscopy of fixated human keratinocytes (HaCaT) exposed to nanoMIPs (a). DAPI blue signal (cell nucleus), rhodamine red signal (MIPs), 3,3′-dioctadecyloxacarbocyanine perchlorate (DiO) green signal (cell membrane). Scale bar: 20 μm (reprinted with permission from Kunath *et al.*, Advanced Healthcare Materials, 2015, 4). Confocal image of DU145 cells incubated with SA-MIP (20 μg/mL) (b). Scale bar = 10 μm (reprinted with permission from Shinde *et al.*, JACS 2015, 137. Copyright 2016, American Chemical Society).

An intriguing application of nanoMIPs involves their use as a theraupetic tool for selective protein/enzyme sequestration in cells. Once the nanoMIPs capture the protein/enzyme, this latter would not be able to carry out its physiological function, thus altering the cellular metabolism. Very recently, Liu *et al.* demonstrated this principle by imprinting silica coated iron oxide nanoparticles with DNase I, a cytoplasmic enzyme involved in cell apoptosis[112]. The nanoparticles were also fluorescently tagged to visualize their distribution inside the cell. As done by several other groups, a silica layer

was inserted between the magnetic core and the fluorescent reporter to minimise potential quenching issues. The nanoMIPs demonstrated to successfully inhibit the DNAase activity without affecting the short-term cell viability.

These examples prove that nanoMIPs hold great potential as molecular recognition and imaging tools since, in contrast with antibodies where multistep staining processes are required, multiple labelling can be easily achieved by using a panel of nanoMIPs, each one incorporating a specific dye for a given target. Furthermore, it is possible to link drugs or add magnetic functionalities to the nanoMIPs, thus allowing their use as drug delivery systems or in hyperthermia therapy. Therefore, it is expected that the number and complexity of these multifunctionalities in nanoMIPs will grow in the next years.

Applications of unlabelled nanoMIPs in assays and in vivo

In the last decade, even unlabelled nanoMIPs have been successfully applied in diagnostic assays for analyte quantification. In one such example, nanoMIPs imprinted for vancomycin were used in the first ELISA-like assay, where the use of antibodies was replaced by the said particles (Figure 1-7)[77]. In this assay, a HRP-vancomycin conjugate was first prepared and then employed in competitive binding experiments: several solutions of free vancomycin (between 1 pM and 70 nM) were added to the wells together with the HRP conjugate. After incubation and washing, the 3,3′,5,5′-tetramethylbenzidine (TMB) was added, leading to colour generation in solution due to reaction with HRP. The assay showed linearity from 1 pM to 70 nM and a LOD of 2.5 pM. Interestingly, this sensitivity is much higher than the other ELISA reported in the literature, whose LOD was only 0.1 μM[113].
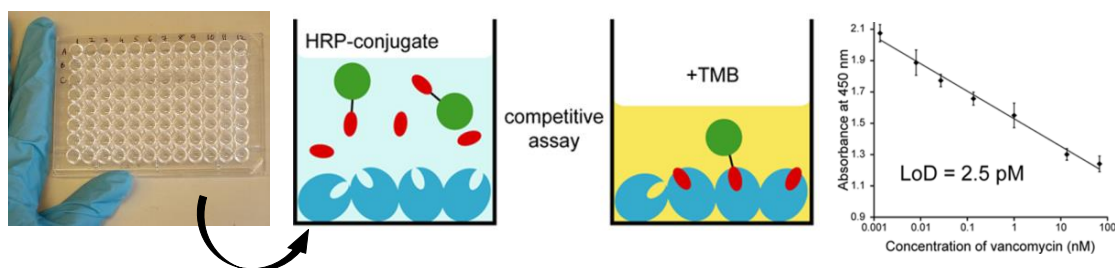
Figure 1-7. Scheme of the ELISA protocol with vancomycin-imprinted MIPs (adapted with permission from Chianella *et al.*, Anal. Chem. 2013, 85. Copyright 2016, American Chemical Society).

In a similar example, multifunctional MIP NPs were recently used in a novel ELISA-like assay with no biomolecules involved[78]. Imprinted NPs produced by solid-phase synthesis and embedding an iron oxide core with catalytic properties act simultaneously as recognition and signalling elements. In light of the intrinsic peroxidase-like activity, iron oxide can be employed in a variety of assays[114]. The iron oxide particles were first modified with double bonds and then used as "reactive seed" for the further polymerisation in the presence of the solid-phase bearing vancomycin as a template. The assay was developed by initially conjugating vancomycin onto the well surface. Then upon addition of free vancomycin and magnetic MIPs, competition occurs, in a similar manner as the aforementioned ELISA. After addition of the substrate TMB, a blue colour was detected due to the catalytic activity of the core-shell MIPs, allowing detection of vancomycin in the nanomolar range.

Despite the aforementioned successful applications of MIP NPs within sensors or assays, such nanoparticles have not been widely applied for *in vivo* diagnosis/therapy. The first *in vivo* application of imprinted nanoparticles had been reported by Hoshino *et al.*, who employed MIP NPs imprinted against melittin (a peptide that is the principal component of bee venom) to remove the said molecule from the bloodstream of living mice (Figure 1-8)[115]. The mice were intravenously injected with melittin and, afterwards, MIPs were administered via the tail vein. The MIPs successfully cleared melittin, improving the survival rate of mice over 24 h and reducing melittin toxic effects (e.g. weight loss and peritoneal phlogosis). This study demonstrates the potential of MIP NPs for the selective recognition of molecules *in vivo*.

The only other *in vivo* study has been recently performed by Wu and colleagues who prepared amoxicillin loaded nanoMIPs imprinted against an epitope of Lpp20, a membrane lipoprotein expressed in *Helicobacter pylori*[116]. *In vivo* imaging demonstrated a prolonged permanence of the nanoMIPs in stomachs of *H. pylori* infected mice. In particular, the nanoMIPs showed a better antibacterial effect than free amoxicillin, after intragastric administration.
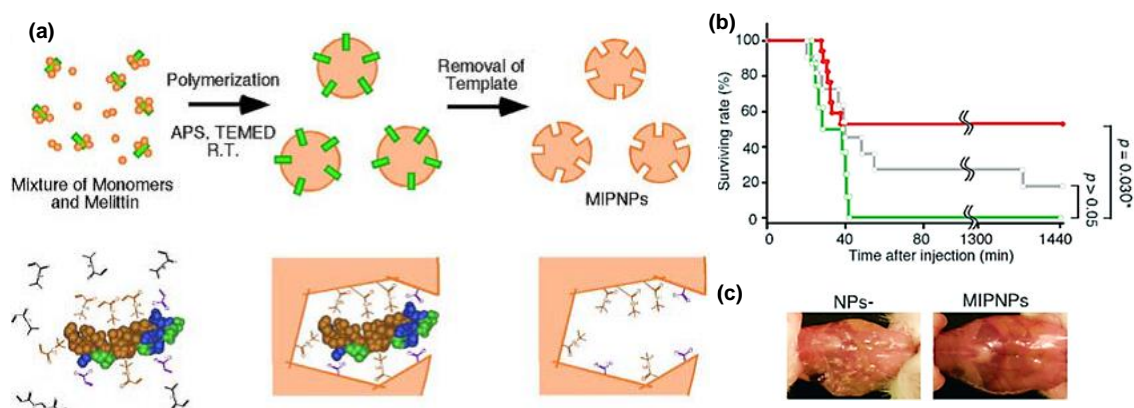
Figure 1-8. Schematic of the mellitin imprinting process (a). Neutralisation of the mellitin toxicity by MIP NPs (b). Pathology of peritoneal inflammation in mice previously injected with melittin (4.0 mg kg^{-1}), with no treatment (left) or MIPNPs (30 mg kg^{-1}) injection (right) (adapted with permission from Hoshino *et al.*, JACS 2010, 132. Copyright 2016, American Chemical Society).

1.4 INORGANIC NANOPARTICLES

Nanosystems made of inorganic polymers (i.e. silica) have been employed in different biomedical areas thanks to their biocompatibility and straightforward surface chemistry. As previously mentioned, embedding organic dyes within a silica matrix increases their photostability over the time. Photostability is crucial when prolonged observation is needed, for instance in imaging: photobleaching issues can jeopardise image acquisition and the biological environment in cells can lead to degradation of some organic reporters. The inert nature of silica can help to overcome these issues, as proven by Shi and colleagues, who embedded carboxytetramethylrhodamine (TAMRA) within silica nanoparticles (SNPs). Such NPs accumulated in lysosomes of HeLa cells, and were able to be detected over 5 days, showing a photostability 30 times higher than the widely used reporter LysoTracker Green. Interestingly, the cell viability was not negatively affected by the presence of these NPs. Furthermore, their capability of staining lysosomes was independent of the fluorophore embedded in the NPs, suggesting that a variety of other analogous SNPs could be used for multicolour labelling in cells[117].

By monitoring the intracellular pH conditions, evaluation of potential cellular diseases can be achieved. Usually, membrane-permeant esters of dyes are employed for pH evaluation in cells[118]. However these dyes are not targeted towards specific organelles and also tend to form complexes, thus invalidating pH measurements[119]. One way to overcome these drawbacks relies in the incorporation these dyes in silica NPs, since NPs in general can minimize organelle sequestration and reduce any potential cytotoxic effects of the free organic fluorophores[43].

For instance, Xu and colleagues produced SNPs (60 nm) embedding two dyes ($Ru(phen)_3^{2+}$ and FITC) which were then used as a ratiometric intracellular pH sensor[120]. This entails the use of two reporters, one pH insensitive and the other pH sensitive, included in a polymer or silica matrix. The emission intensity ratio of the two dyes can be correlated to the pH. Ratiometric pH sensors are more accurate than those containing only the pH-sensitive dye, because the ratios in emission intensity is less sensitive to changes in experimental conditions and variations in intensity of the excitation source. By means of a modified Stöber method, the authors synthesised co-doped SNPs with the reference dye located in the core of the particle, protected from the environment by the silica matrix. The surface of the SNPs was grafted with pH sensitive molecules, to maximize their interactions with the environment. These particles were capable of generating visible colour changes over a pH range from 2.0 to 8.0 in hepatoma cells (Figure 1-9).

Considering that many reporter molecules can be included in a single particle, the resulting signal generation will be enhanced, allowing ultrasensitive detection[121,122]. However, when the amount of dye reaches a certain concentration, self-quenching phenomena might occur[123].
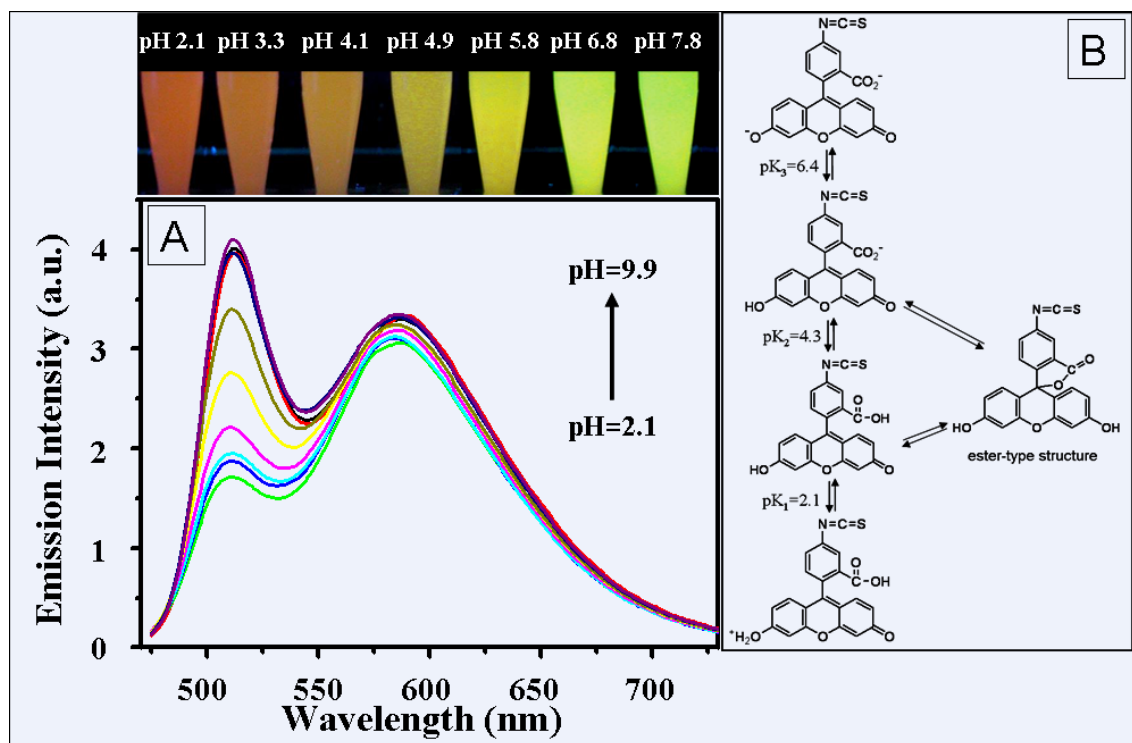
Figure 1-9. Emission spectra of silica nanoparticles (a). Structures of FITC at different pH (b). Insert shows the images of SNPs at different pH (reproduced with permission from Xu J. *et al.*, Nanoscale Research Letters 2011, *6*).

However, as mentioned before, physically embedded dyes may undergo leaching from the polymer. The amount of dye leached from SNPs can be as high as 45% (of the initial loaded amount) over 48 h, due to the weak interactions between the dye molecules and the matrix[119]. By conjugating FITC with (3-aminopropyl)triethoxysilane (APTS), stable fluorescent SNPs were produced and used for detection of γ-globulin, with reduced photobleaching and good sensitivity (LOD of 0.04 μg/mL)[124].

SNPs have been widely employed in diagnostics thanks to their several advantages. Firstly, they are biocompatible and their size is not influenced by variations in pH unlike polymer particles, which may swell in organic solvents, causing the dye to leak out. Furthermore, they do not absorb light in the range between 300 and 800 nm[125]. However, silica particles show poorer multiplexing capabilities compared with QDs because of the overlapping in the dye excitation spectra. Nevertheless, several researchers tried to produce SNPs containing different reporters. In one of these rare

examples, three dyes were embedded inside a single SNP and their emission finely tuned, such that they displayed several colours under a single excitation wavelength[48]. Such NPs were then labelled with biotin and employed in a biotin-avidin binding assay. The biotin-SNPs were used to functionalise microparticles previously coated with streptavidin (Figure 1-10).
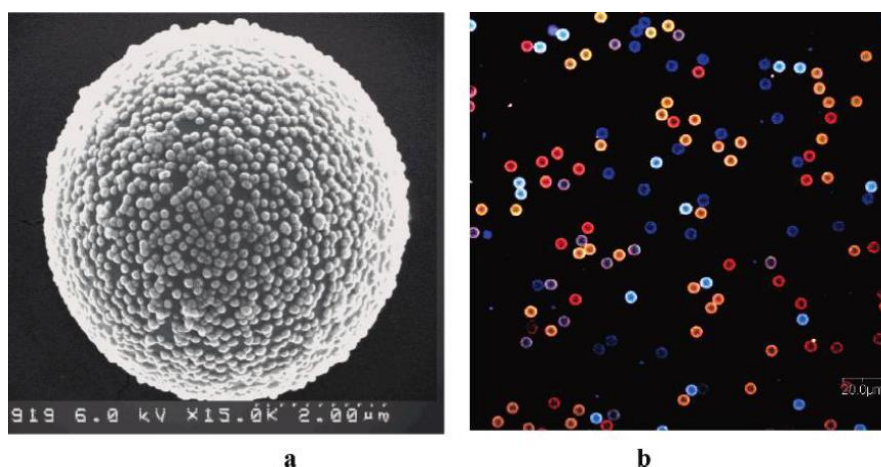
Figure 1-10. SEM image of one composite microsphere-SNP (a). Confocal image of a mixture of microsphere-SNP complexes, each one containing a different dye, under 488 nm excitation (b) (reproduced with permission from Wang and Tan, Nano Letters 2006, *6*. Copyright 2016, American Chemical Society).

1.5 MULTIFUNCTIONAL POLYMERIC NANOPARTICLES

Multifunctional NPs hold great potential in diagnostics and therapy as the simultaneous exploitation of different features embedded in the same nanoparticle enables to obtain systems that can be used in more complex assays, improving data acquisition or the efficacy of a given treatment[126]. Magnetic particles can be combined with fluorescent reporters for simultaneous separation and imaging, both for *in vivo* and *in vitro* applications[127-130]. Similarly, magnetic NPs and QDs can be included in the same polymeric matrix. The magnetic moiety embedded in a multifunctional particle can be exploited for hyperthermic cancer treatment, thanks to the capability of iron oxide NPs to produce heat under the influence of an external magnetic field. Nanocomposites made of magnetic NPs embedded in a polystyrene matric along with NIR-emitting QDs

have been developed[131]. The system is capable of achieving *in vivo* active targeting, with multimodal therapeutic and imaging features thanks to the incorporation of paclitaxel (a chemotherapeutic agent) in the matrix (Figure 1-11). This is an excellent example of versatility, since the system can achieve both bimodal imaging diagnosis and therapeutic treatment. In order to manufacture multifunctional magnetic-QDs, iron oxide particles can be employed as cores for the subsequent growth of QDs, adding a further silica layer to ensure bioconjugation and biocompatibility[132]. Very recently, Ranzoni and colleagues developed a method to trap around 10^4 QDs within a single core nanoparticle, called "papaya particle"[133]. The latter can then act as a scaffold to produce multi-layered shell. To produce these QD-doped NPs, polystyrene NPs (200-500 nm in diameter) were placed in an organic solvent which caused them to swell. Then the added free QDs underwent diffusion-driven migration towards the swollen polystyrene NPs. The subsequent polymerisation helped to physically constrain the QDs. The model dengue immunoassay developed using this system exhibited a 15-fold lower limit of detection thanks to the higher fluorescence emission of the papaya particle compared to commercial reagents.
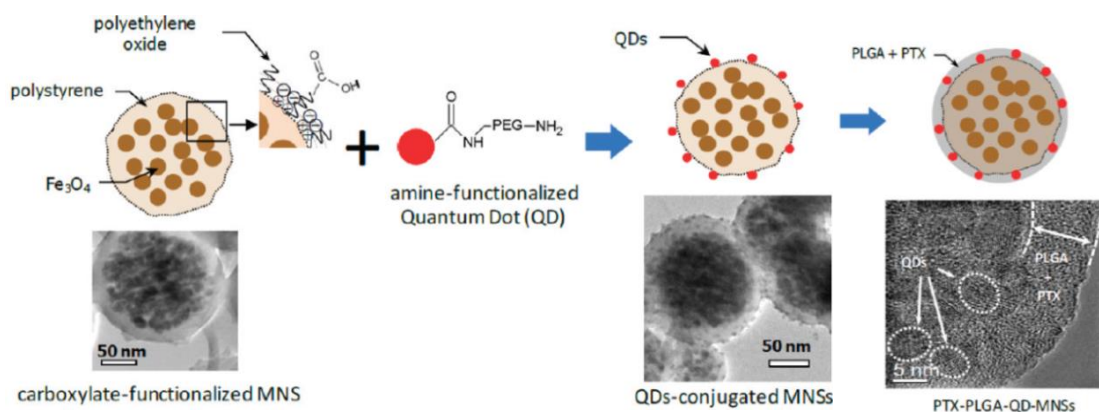
Figure 1-11. Fe_3O_4 NPs are included in a polystyrene matrix, which was functionalised to allow further covalent attachment of PEG-functionalised QDs. Subsequently, the system was covered by a poly(lactic-co-glycolic acid) (PLGA) layer (adapted with permission from Cho H. *et al.*, ACS Nano 2010, 4. Copyright 2016, American Chemical Society).

In a similar experiment, iron oxide NPs were coated with a fluorescent reporter by means of a silane derivative bearing primary amine groups (Figure 1-12) and then conjugated with folic acid. These types of nanosystem could be employed for specific imaging of cancer tissue thanks to their binding to folate receptors, which are up-regulated in several human cancers, thus allowing excellent tumour targeting capability[129]. Recently, it has been elucidated how folic acid interacts with its receptors[134,135]. These valuable findings can give a rationale for the design of novel drugs targeted to the folate receptors.
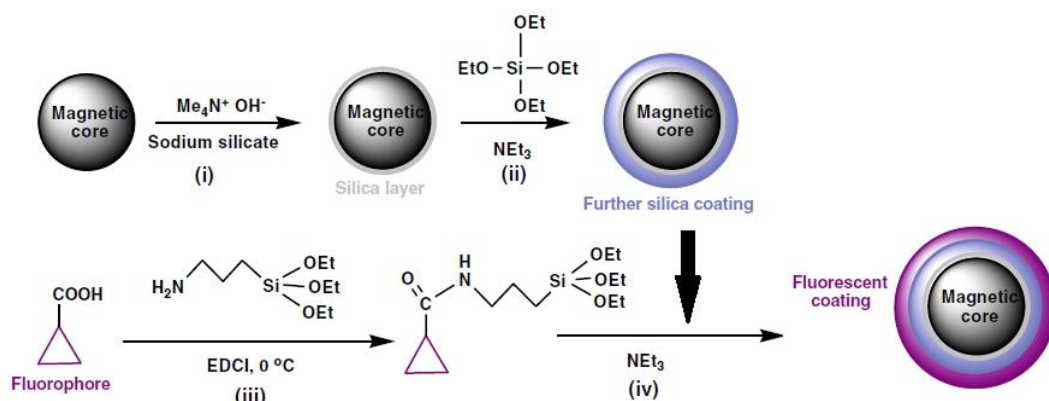
Figure 1-12. Synthesis of fluorescent silica-coated magnetic NPs (adapted with permission from Corr S. *et al.*, Nanoscale Research Letters 2008, 3).

Exploiting a similar approach, Lu and colleagues prepared multifunctional NPs endowed with upconverting properties. In upconverting materials, the absorption of several photons leads to emission at a shorter wavelength, since a single higher-energy photon is produced. An advantage of these upconverting materials is that they can be excited by NIR light, which show minimal background autofluorescence and can penetrate deep into tissues. Sodium yttrium fluoride co-doped with erbium and ytterbium were co-precipitated on the surface of iron oxide nanoparticles in the presence of EDTA. Protection of the crystals was assured by the deposition of a layer of silica which also allowed the covalent coupling with streptavidin[136]. This nanosystem is capable of emitting fluorescence upon excitation with a single NIR light source, and thanks to their excellent photostability, it was employed as single-molecule imaging probes[137].

The magnetic features of these multifunctional NPs are useful also for bioseparation. In one example, magnetic SNPs were first labelled with rhodamine and modified with PEG, and then incubated with cancer cells in culture. These NPs were capable of being internalised, allowing the cells to be both magnetically and fluorescently labelled. Furthermore, by applying an external magnetic field, such labelled cells could be actively moved (a process called "magnetic motor effect"), without any evident acute toxicity[138]. Besides simultaneous imaging and cell separation, this system may be employed for the magnetic delivery of drugs. More recently, a similar system has been used for cancer imaging. Multifunctional NPs based on rhodamine B and magnetic NPs demonstrated very low levels of toxicity in rats, with the ability to be imaged both by fluorescence microscopy and Magnetic Resonance Imaging (MRI) (Figure 1-13)[139]. Furthermore, once the particles were injected in the optic nerve, they were shown to remain at the injection site, thus opening the possibility to deliver drugs even to neurons. Composite nanosystems can be used also in anticancer phototherapy. A dual-colour system has been recently developed for cancer theranostics, exploiting the simultaneous generation of singlet oxygen and nitric oxygen triggered by light[140]. The synergistic effect of the produced species guarantees a better outcome, since both nitric oxygen radicals and $^1O_2$ possess promising anticancer effects.
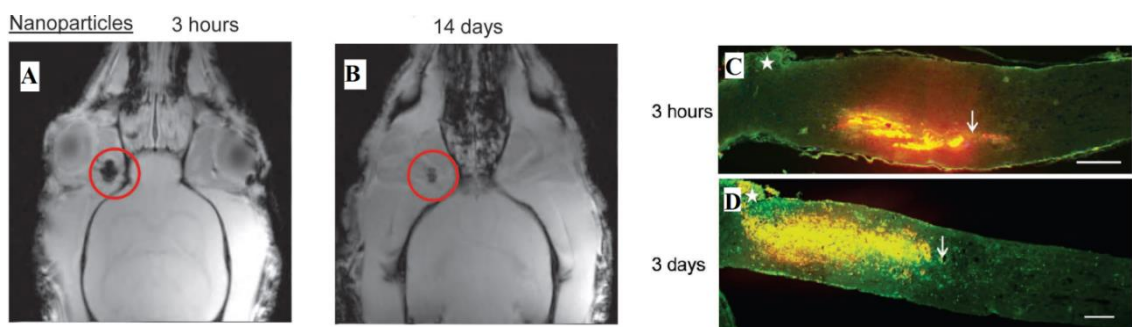
Figure 1-13. Magnetic resonance images of a rat's head after injection of composite nanoparticles, after 3h (a) and 14 days (b). Images captured by fluorescence microscopy of optical nerve sections from rats treated with particles (orange area) into the optical nerve, after 3 (c) hours and 3 days (d). The injection and the injury sites are indicated by an arrow and a ∗ respectively (adapted with permission from Harrison J. *et al.,* Small 2012, 8).

An interesting approach in theranostics relies on the use of degradable nanosystems which get metabolised upon exposure to the acidic microenvironment within the cells. Following this concept, fluorescent nanoparticles loaded with doxorubicin have been recently produced for targeted delivery to cancer cells[141]. The NPs were composed of acid-sensitive orthoesters which get cleaved in the acidic tumour microenvironment thus enhancing the drug release. Although this system showed excellent biocompatibility, good accumulation in the targeted area and inhibition of the tumour growth, no data were collected regarding the metabolites produced after degradation of the NPs.

In the next years, several other combinations of different moieties will be developed, for instance by incorporating enzymatic catalysis and electrochemical functionalities within the same system. By improving the "multifunctionality" of such nanocomposites, a wide choice of capabilities is envisioned for the realisation of functionalised nanoprobes, specifically designed for the intended bioanalytical application.

1.6 IN VIVO OPTICAL SENSING

Nanotechnology offers the unique possibility to tailor and manufacture systems with specific characteristics for *in vivo* applications, both for diagnostics and therapy. It is worth highlighting that for these applications the NPs used should possess an excellent biocompatibility and their biodistribution and elimination profile from the organism should be well known. Several materials employed in the manufacture of composite nanosystems (e.g. QDs) are potentially toxic, due to the presence of heavy metals. One way to reduce this risk relies in coating the source of the potential toxicity with an inert polymeric layer such as silica. Many review papers describing protocols for surface modifications of QDs for *in vivo* applications are available[142-144]. Thanks to their good biocompatibility, SNPs have been used as carriers of NIR reporters for *in vivo* imaging of mouse bladder[145], and also for specific tumour imaging[146]. However, SNPs may show a certain toxicity. Shape, porosity and surface characteristics are the main factors influencing their acute toxicity [147, 148]. These are also known to affect the colloidal stability of nanosystems *in vivo*, which may aggregate and lead an immune response.

Stabilisation against agglomeration can be obtained by coating the NP with hydrophilic polymers which create a physical barrier between particles, therefore sterically reducing the interactions among NPs.

The analytes which can require an *in vivo* detection or imaging vary from small molecules to whole cells. For instance, the excessive production of H_2O_2 is reported to be involved in the progression of various disorders, hence agents able to quantify hydrogen peroxide *in vivo* are of great use. Murthy and colleagues produced polymeric micelles embedding peroxalate ester groups[149], which generate an intermediate molecule (dioxetanedione) upon exposure to hydrogen peroxide, which in turn can excite a fluorescent reporter through a chemiluminescence mechanism, thus allowing H_2O_2 to be detected in living mice[150] (Figure 1-14). The limit of detection of the system was in the nanomolar range, even in the presence of other reactive oxygen species. Afterwards, the authors added a PEG corona around the particles in order to evade macrophage phagocytosis and the particle size was also reduced down to 33 nm to enhance extravasation[151].
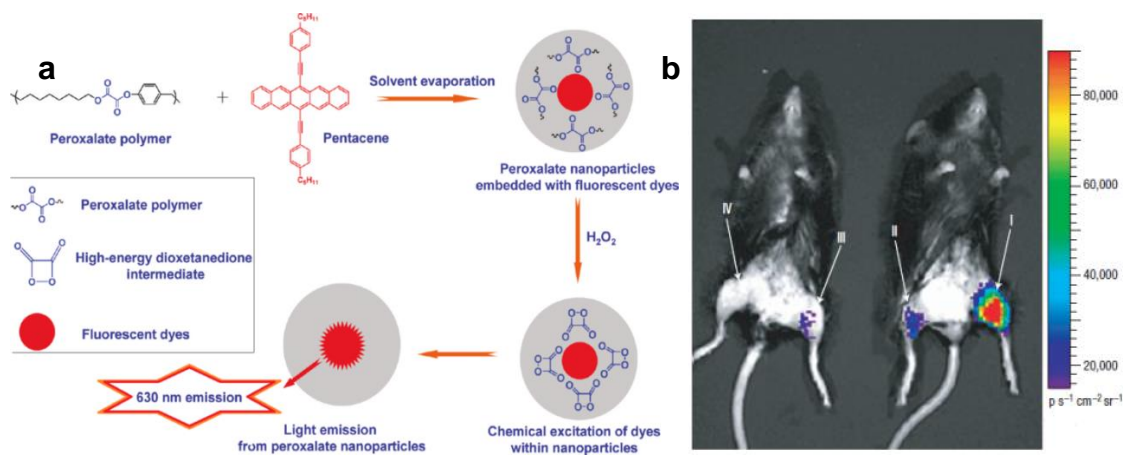
Figure 1-14. Peroxalate nanoparticles, incorporating pentacene as the fluorescent dye, used for *in vivo* H_2O_2 imaging (a). (adapted From Hu J.; Liu S., Macromolecules 2010, 43, 8315). *In vivo* H_2O_2 imaging using peroxalate NPs (b). (I) Peroxalate NPs +10 μM of hydrogen peroxide; (II) peroxalate NPs + 1 μM of hydrogen peroxide; (III) peroxalate NPs only; (IV) negative control (adapted with permission from Macmillan Publishers Ltd: Lee D. *et al.*, Nature Materials 2007, 6. Copyright 2016).

Another example of multimodal polymeric micelles is the one developed by Mulder and colleagues for imaging of cancer cells, which are known to overexpress a specific receptor. The proposed system was able to be imaged by both optical and nuclear techniques (Figure 1-15). The information provided by these nanoparticles may be useful for an early diagnosis of cancer and its angiogenesis[152]. To enhance active targeting, the NPs were derivatised with specific peptide sequences, thus increasing the specificity of tumour imaging[153].
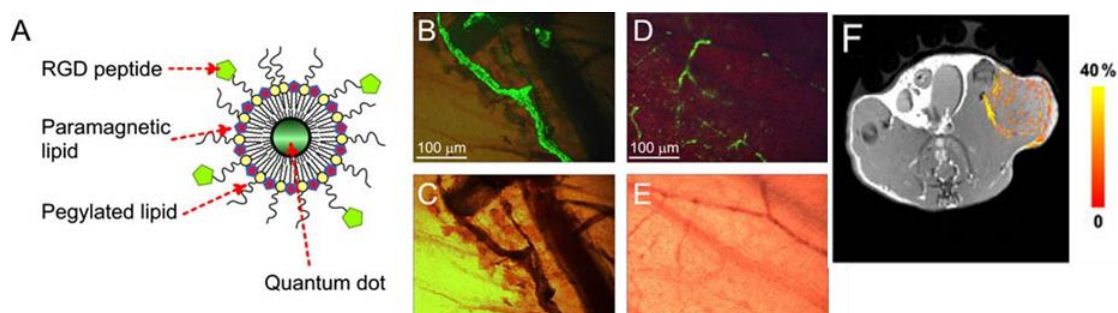
Figure 1-15. Composite magnetic-fluorescent nanosystem for angiogenesis imaging (a). Fluorescence images (b,d) and corresponding bright field images (c,e) of chorioallantoic membrane with topically growing LS174T human colon carcinoma tissue. MR imaging of the tumour region in mice (f) (adapted with permission from Mulder W. J. M. *et al*., Angiogenesis 2009, 12. Copyright 2016).

Specific targeting of NPs to the desired area has been achieved by both passive targeting, through Enhanced Permeability and Retention (EPR) effect[154], and active targeting[155-157]. In one example of passive targeting (EPR effect), NPs incorporating a fluorogenic dye and a quencher were synthesised, and coupled together using a cleavable peptide sensitive to matrix metalloproteinases (MMP)[158]. MMPs are proteins involved in inflammatory diseases and cancer progression. When the said nanosystem was exposed to the specific MMP, enzymatic cleavage of the peptide bond between Cy5.5 and the quencher occurs, this generating a fluorescence emission from Cy5.5. Specific active targeting in cancer is usually achieved by conjugating the nanosystem of interest with suitable antibodies. Other moieties used include folic acid[159-161], galactose[162], peptides[163, 164] and cell ligands[165]. Very recently a novel dipeptide (Ser-Glu) has been identified as a good targeting agent towards pancreatic cancer cells[166].

1.6.1 Biocompatibility and biodistribution

Generally, the toxicity of a nanosystem depends on whether or not it leads to cell death. However, further studies would be required in order to fully evaluate the biocompatibility of a given nanosystem (e.g. alterations in biochemical processes of the cell or its natural morphology) prior to their *in vivo* use. As mentioned above, for QD-based nanocomposites the biocompatibility may be negatively affected from a potential leaching of heavy metals[167, 168]. Furthermore, some capping reagents used for the synthesis of QDs, could also have cytotoxic effects[169]. However, sufficiently small polymer-coated QDs can be cleared from the body by excretion through the kidney[170]. Further studies have to be undertaken to fully elucidate the clearance mechanisms of QDs, before their clinical use in humans.

It should be noted that the potential for cytotoxicity depends mainly on the surface chemistry of the nanoparticle rather than on the embedded core. Some NPs, however, may not determine any acute toxicity, but could concentrate in specific organs. Hence, extensive analyses are to be performed to fully characterise the long-term effects of NPs. Besides the intrinsic properties of NPs, their biocompatibility is related also to dose and route of administration[171]. For instance, recent studies proved that particles around 300 nm show higher degrees of intestinal absorption compared to bigger particles (600 and 1000 nm)[172].

The particle shape and size are the two factors that mainly influence particle toxicity and internalisation in cells[173]. The latter depends also on the surface coating of the particle. In physiological conditions, nanomaterials are likely to undergo a covering process by the serum proteins, forming the so-called "corona". Such protein corona is the outmost layer and therefore it affects how the particle interacts with cells. Furthermore, this fact has been proved to be independent of the particle core, since both organic (polystyrene) and inorganic (QDs and gold NPs) nanosystems exhibited this corona effect[174]. Typically particles with diameter smaller than 100 nm are suitable for *in vivo* applications. However, for the blood–brain barrier (BBB) targeting, only

particles with molecular weight below 500 Da and hydrophobic coatings are suitable. It is still not clear how changes in particle size in the range from 20 to 100 nm may affect their biodistribution[175].

The surface properties of NPs influence also their biodistribution[176]. Ballu and colleagues investigated the role of the polymeric coating on circulation lifetime, by injecting PEG-coated QDs into mice. These endured in the blood circulation for several hours, whereas free organic dyes were cleared within minutes after their administration. Incredibly, it was possible to detect the fluorescence of these NPs even after four months *in vivo*[177]. This can be ascribed to the hydrophilic polymer coating, which lower opsonisation and reticuloendothelial uptake[178]. It should be mentioned that nanosystems for imaging applications should possess an enhanced blood circulation time and, in general, the choice of the suitable circulation halftime (t ½) of the NPs depends on the final application[179]. Typically imaging requires a t ½ of 2–6 h, whereas longer time is advisable in case of therapeutic application, in order to allow protracted permanence of the drug in the target area. By assessing the biodistribution and clearance of three types of surface-modified silica NPs (hydroxyl, carboxyl and PEGylated SNPs), it was proven that both organ deposition and clearance depend on the surface properties of NPs[180].

Once NPs are administered, they undergo various biological processes. Typically, NPs in the bloodstream are first opsonised and then sequestered in the reticuloendothelial system (RES), but if they are not biodegraded and cleared, they may accumulate in cells and tissues with potential toxic effects. One approach to attenuate cellular internalisation and enhance the biocompatibility is to modify the particle surface with hydrophilic polymers. PEG with MW > 2000 Da is a particular useful agent for increasing the blood circulation time of nanosystems, thanks to its ability to lower the adsorption of opsonins on the surface of NPs by steric repulsion forces[181, 182]. For bare (non-PEGylated) nanosystems, the RES sequestration is fast, typically a matter of minutes, with the majority of the NPs concentrated in spleen and liver. Notably, the addition of a PEG coating shifts the biodistribution towards the spleen[182]. To further extend the blood circulation time and enhance the biocompatibility, PEG has been combined with chitosan as agents for particle coating[183]. Interestingly, particles with

diameter >200 nm demonstrated a faster clearance compared to smaller particles, regardless of the presence of PEG. In general, other properties of the polymeric coating such as charge, functional groups, surface density and thickness influence the biodistribution of NPs, as they affect the way particles interact with opsonins[182].

Dextran is another polymer coating clinically approved for *in vivo* applications[179]. Other materials include hyaluronic acid and chitosan (both natural polymers), and polyethyleneimine and polyacrylic acid (both synthetic). In one original example, dextran-coated SNPs demonstrated excellent biocompatibility thanks to their ability to degrade into renally-clearable components, and hence reducing the *in vivo* toxicity in mice[184]. This represents the first type of polymeric nanosystem engineered to degrade *in vivo* into harmless components over specific timescales.

When a particle begins its "journey" in the body, it gets carried by the blood flow until it interacts either non-specifically (van der Waals, electrostatic and steric interactions) or specifically (through ligand-receptor bonds) with the walls of the blood vessel. NPs move in different ways from the core of the blood vessel towards its walls, (a process called "margination dynamics") according to their shape[185]. Spherical particles are inclined to follow the blood flow, moving parallel to the vessel walls; on the other hand, discoidal particles drift laterally from side to side of the vessels. Notably, if NPs are not driven by targeting forces (magnetic or antibody-epitope interactions), they tend to leave the bigger blood vessels in favour of smaller ones, hence accumulating in the microcirculation (Figure 1-16)[154]. Thus, coating and shape of NPs must be selected with care, to grant a suitable accumulation in the desired area. Furthermore, shape, size and surface coatings play a crucial role in the intracellular pathways of internalised NPs[186]. A theoretical model demonstrates that large round particles are more prone to cellular internalisation compared to small and elongated ones[187], thus proving that the internalisation process can be changed by varying the particle shape. Moreover, even the particle size affects the internalisation process: for particles smaller than 500 nm, receptor-mediated endocytosis is predominant, whereas larger particles (>1000 nm) are internalised by a phagocytic process[154].
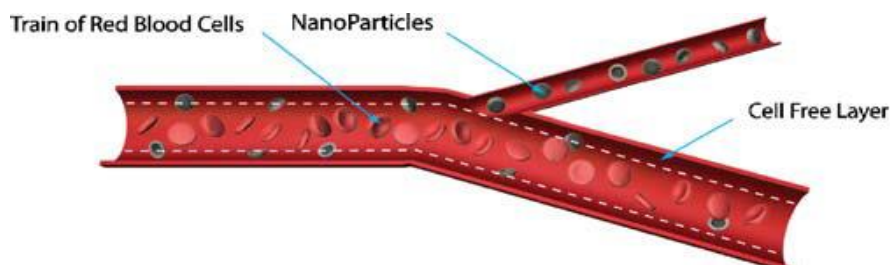
Figure 1-16. Nanoparticles tend to concentrate in proximity to the vessel walls and leave large vessels in favour of smaller ones (reproduced with permission from Decuzzi *et al.*, Pharmaceutical Research 2009, 26. Copyright 2016).

In conclusion, polymeric NPs offer great possibilities for *in vivo* diagnostics, and their adoption is expected to grow fast in the next years. Nevertheless, although toxicity studies are routinely carried out, a reliable protocol to assess the biocompatibility of different types of NPs is still missing. Furthermore, long-term biocompatibility studies at low concentrations are required, since many therapeutic protocols in humans necessitate only small amounts of NPs for prolonged times.

1.7 THE FUTURE OF NANOTECHNOLOGY IN MEDICINE AND DIAGNOSTICS

In the past two decades, nanotechnology has been widely employed as therapeutic and diagnostic tool and its use is expected to grow over the next 10 years, with estimates around $1 trillion as reported by the National Science Foundation[30]. This growth is also confirmed by the increase in the number of published patents in nanotechnology, which went from 531 patents in 1995 to 1976 patents in 2001. It is well recognised that nanotechnology will be a boon for *personalised medicine*, which aims to avoid prescribing standard doses of drugs to every patient, focusing rather onto a "customised" drug dose and targeting specific areas depending on the patient's physiology. This is particularly urgent in cancer treatment, where the nanoparticle's cargo would be specifically targeted towards cancer cells, thus reducing the serious side-effects of the powerful drugs usually employed.

Another potential application of nanotechnology in personalised medicine is the field of genetic analysis. It is well known that early stage detection is the key in the treatment of cancer. Epigenetics has been recognised to be chiefly involved in cancer genesis, in particular DNA methylation changes are frequently observed in many tumours at early stages[188]. Nanopore sensors can detect such alterations within dsDNA, thus allowing an earlier cancer detection[189]. These sensors have the potential to be developed in a high-throughput DNA sequencing assay-format, suitable for fast screening processes.

Nanotechnology is the basis for many lab-on-a-chip (LOC) technologies. These are typically made of a complex network of channels, chambers and valves, coupled with functionalised nanostructures (e.g. antibodies, enzymes, single-stranded DNA, etc.) which interact with the target analytes in the sample and provide an optical or electrical signal transduction. The advantages of these systems are the use of small sample volumes and fast turnaround times. However, detection at submicromolar levels is currently difficult to achieve and the manufacturing process is quite costly. Furthermore, it is still not simple to carry out assays in complex media (e.g. blood or urine) due to the presence of many interferents[190]. At present, QDs in FRET-based assays within microfluidic devices seem to be the next generation of LOC-based platforms for multiplexed assays[191].

Drug delivery is another field where nanotechnology is expected to play an important role in the near future. In this case, the final aim is to deliver the right dose in the right body area, thus reducing the dose needed to achieve the therapeutic effect (and therefore the side effects), as it happens when the drug is administered in a non-targeted manner. Moreover, a prolonged therapeutic effect provided by such drug delivery systems (DDS) is also desirable, since it would reduce the number of administrations required. Both organic and inorganic NPs have been recently developed, endowed with "smart" features (e.g. pH responsiveness) which allow the drug to be specifically received in the target area[192].

Despite the obtained achievements and the great potential of nanotechnology, many challenges remain. The need of a reliable and consistent production of polymeric NPs, together with their stability in biological media and some biocompatibility concerns

have slowed the actual market diffusion of many nanosystems. Specifically regarding *in vivo* applications, the biodistribution and clearance of several nanosystems remain still unclear. Furthermore, the sterilisation of nanoparticles might be an issue since there is not a single process that can be applied to all systems and hence a validation on a case-by-case basis is needed. In general, the sterilisation should not alter the physicochemical properties and functionality of the nanoparticles[193]. From a financial point of view, nanotechnology should be able to deliver products at a competitive price and reasonable shelf life. Solving problems related to long-term storage of nanoparticles (aggregation, bacterial contamination, reduction of fluorescence/binding capability, etc.) would surely contribute in increase their market diffusion.

Many of the examples discussed in this chapter are ideally expected to be developed in a lab-on-a-chip format, in which a portable diagnostic device would be capable of running tests quickly and with a small sample volume. Devices able to be remotely controlled by the GP will be soon widely employed (Figure 1-17).

Figure 1-17. Schematic diagram showing actual and potential applications of nanotechnology to medicine. Home-based tests (1), lab-on-a-chip platforms (2), and cantilever-based assays (3). Once the test is run at home, the patient could use a smartphone to send the test results to a computer for processing (4), and/or reporting the results to his physician (5) (reproduced with permission from Laroui *et al.*, Digestive and Liver Disease 2013, 45. Copyright 2016)

Real-time blood analysers are already commercially available (www.lantronix.com, www.medtronicdiabetes.com), and novel real-time monitoring devices based on nanotechnology are expected to be soon adopted. These cutting-edge devices are at the interface of several disciplines, ranging from engineering and bioinformatics to chemistry and physics. Although complex issues need to be addressed in developing such platforms, the final user will have to get a small device with a user-friendly software interface, possibly connected to personal mobile phones or computers, as already done by some blood analysers (www.dexcom.com).

1.8 POLYMERIC NANOPARTICLES IN DIAGNOSTICS: CONCLUSIONS AND OUTLOOK

Over the past years, polymeric nanoparticles have been widely employed in optical diagnostics, thanks to the advances in the tailoring of their properties. However, more studies are necessary to improve the controlled synthesis of nanoparticles, especially in relation to their long-term stability and size distribution. Furthermore, *in vivo* agglomeration, biodistribution and toxicity of NPs must be further examined. A fascinating alternative to reduce the particle toxicity involves the use of self-destructive components within the NPs, which would be degraded into safe products after the achievement of their purpose *in vivo*. Concerning the application of nanoMIPs, their routine use as a replacement of antibodies in diagnostics is still remote, although their potential is evident. It is without doubt, however, that innovative responsive nanosystems with multiplexing capabilities will be developed in coming years for improved diagnostic applications.

2 FLUORESCENT MONOMERS EMPLOYED FOR THE SYNTHESIS OF MIP NANOPARTICLES

2.1 INTRODUCTION – FLUORESCENCE: THE BRIGHT SIDE OF MOLECULES

Fluorescence is the emission of electromagnetic radiation by a molecule that absorbs at a certain wavelength and re-emits it at a longer wavelength. The absorption of light causes the transition of an electron (e⁻) from its ground state to one of its possible vibrational levels. This excited state lasts typically for 1-10 nanoseconds, after which the excited e⁻ comes back its ground state, re-emitting light. During this excitation process, the molecule undergoes conformational changes and interactions with its molecular environment which leads to dissipation of part of the energy previously absorbed. This internal "loss in energy" (called vibrational relaxation or internal conversion) is the reason why the emitted light is at longer wavelength (i.e. less energy). When a molecule is hit by light, an e⁻ is excited and it can be promoted to a singlet or a triplet state. If the e⁻ is promoted in the opposite spin orientation as it was in the ground state (paired), then the singlet state is formed (Figure 2-1). In a triplet excited stated instead, the promoted e⁻ has the same spin orientation (parallel) of the other e⁻ in the ground state. This latter transition causes phosphorescence and it is less likely to occur.
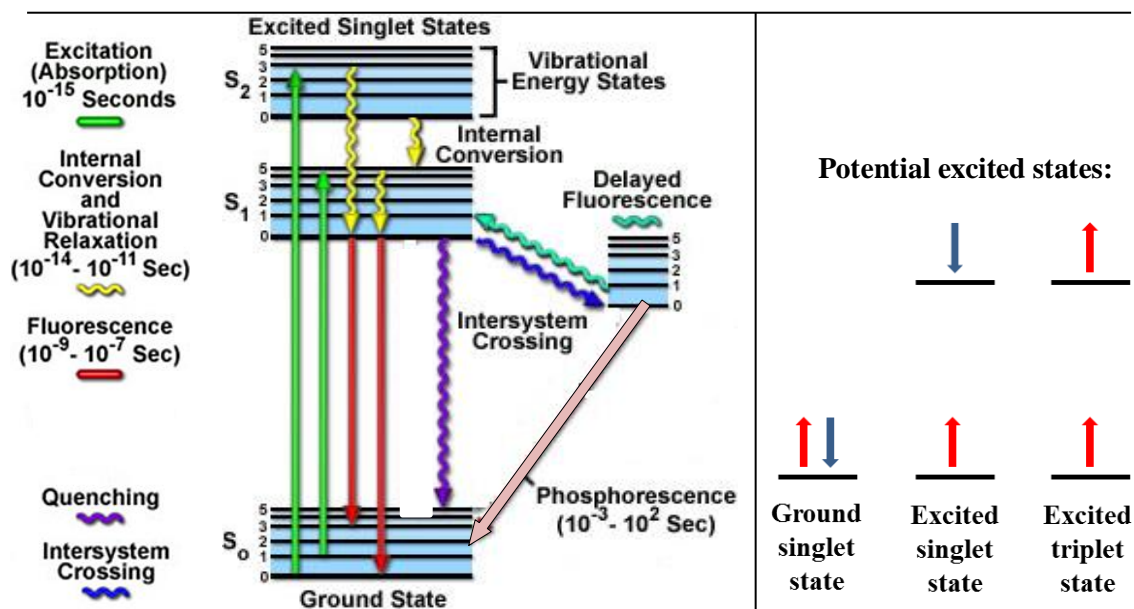
Figure 2-1. Jablonski energy diagram for a generic fluorophore (left). On the right, spin orientations of the electrons forming potential excited states in a molecule.

54

Depending on the dye, different fractions of photons absorbed are then re-emitted. Such fraction or percentage is the quantum yield of the fluorophore. A quantum yield of 1 (or 100%) is therefore the maximum achievable, although higher quantum yields are theoretically possible when photo-induced chain reactions are triggered. As mentioned above, the timeframe between excitation and emission is between 1-10 nanoseconds for most dyes. Such timeframe is called lifetime of the fluorophore and it can be useful in bioanalysis since it allows to get information about the molecular surrounding of the dye. The ideal fluorescent monomer should possess high quantum yield and high molar absorption coefficient, thus displaying a strong fluorescence emission. Furthermore, a large Stokes shift is highly desirable since it allows an easy detection of the fluorescent emission without issues related with the overlapping of excitation and emission spectra. Moreover, dyes should be photochemically and thermally stable. In this regard, novel dyes with superior performance (e.g. Alexa Fluor[®] dyes) in terms of both photostability and brightness are now available. However their main drawback is their price, in the range of £150-250 per mg.

The use of polymerisable dyes is advantageous because they allow a fast and straightforward labelling of polymer-based systems. However not many polymerisable dyes are currently commercially available (Table 3), and some of them have solubility issues in water or undergo hydrolysis in aqueous environment. For this reason, two novel polymerisable dyes were produced and other commercially available dyes were tested to assess their suitability to produce bright and stable fluorescent MIP NPs.

Table 3. List of polymerisable dyes commercially available.

Fluorescent monomer	Exc.-emission (nm)	Supplier	Price (£)	Note/comments
Fluorescein *O*-methacrylate/acrylate	492 - 515	Sigma-Aldrich	158 (1 g)	Poor solubility in water
Fluorescein *O,O'*-dimethacrylate	480 – 510	Sigma-Aldrich	410 (1 g)	Poor solubility in water. Can act as crosslinker
Acryloxyethyl thiocarbamoyl Rhodamine B	545 – 570	Polyscience	130 (100 mg)	Good solubility in water. Gives coloured solution
Nile Blue Acrylamide	635 – 675	Polyscience	130 (100 mg)	Good solubility in water
Vinyl anthracene	370 – 410	Sigma-Aldrich	50 (1 g)	Highly hydrophobic

9-Anthracenylmethyl methacrylate	360 – 407	Polyscience Sigma-Aldrich	150 (100 mg) 140 (100 mg)	Highly hydrophobic
Ethidium bromide-*N,N'*-bisacrylamide	420 – 510	Sigma-Aldrich	78 (100 mg)	Potentially cancerogenic
N-(1-Naphthyl)-*N*-phenyl acryl/methacrylamide	250 – 420	Sigma-Aldrich	Acryl: 93 (100 mg) Methacryl: 55 (100 mg)	Highly hydrophobic. Low quantum yield
2-Naphthyl acrylate/methacrylate	285 – 345	Sigma-Aldrich Polyscience	220 (1 g) 70 (1 g)	Hydrophobic
1-Pyrenylmethyl methacrylate	339 – 394	Polyscience Sigma-Aldrich	150 (100 mg) 74 (1 g)	Highly hydrophobic
O-Methacryloyl Hoechst 33258	355 – 495	Polyscience	260 (100 mg)	Poor solubility in water
7-[4-(Trifluoromethyl) coumarin] acrylamide	340 – 430	Sigma-Aldrich	46 (100 mg)	Hydrophobic. Low quantum yield

2.2 MATERIALS AND METHODS

2.2.1 Chemicals

Acryloyl chloride, eosin Y disodium salt, *N*-methyl-2-pyrrolidone (NMP), fluoresceinamine isomer I were purchased from Sigma-Aldrich, UK. Sand (40-100 mesh), Silica gel (35-70µm pore diameter), dichloromethane (DCM), acetone and Amicon Ultra-15 Centrifugal Filter Units (MWCO 30 kDa) were obtained from Fisher Scientific (UK). Molecular sieves (3 Angstrom), plates for TLC, paper filters and acetone was purchased from VWR (UK). Deionised water obtained from a Millipore (MilliQ) purification system at a resistivity of 18.2 MΩ cm was used for analysis. All chemicals were analytical or HPLC grade and were used without further purification.

2.2.2 NMR analysis

NMR spectra were recorded using a JEOL ECX-400 NMR spectrometer (Welwyn Garden City, UK). The deuterated solvents used for the NMR analysis were purchased from Goss Scientific Instruments Ltd. (Cheshire, UK).

2.2.3 Synthesis and characterisation of eosin O-acrylate

The synthetic procedure for the preparation of eosin *O*-acrylate is illustrated in Figure 2-2. In particular, 5 g of eosin Y disodium salt (7.23 mmol) were dissolved in 100 ml of

NMP. The solution was stirred, sonicated for 2 min and purged with N_2 for 10 min. Then 5.85 ml of acryloyl chloride (72.3 mmol) was added into the solution and the reaction mixture was stirred overnight in the dark. Salt, which was formed during the reaction, was filtrated and the product precipitated in deionised water. Further the solution was centrifuged to separate the precipitate and finally rinsed 5 times with deionised water. The precipitate was dissolved in DCM and extracted using liquid-liquid extraction. The organic phase including desired product was further purified on a silica column using DCM as mobile phase. All steps were followed by TLC. The powder product obtained after evaporation of the solvent was stored at -18 °C. The yield was 41 %.
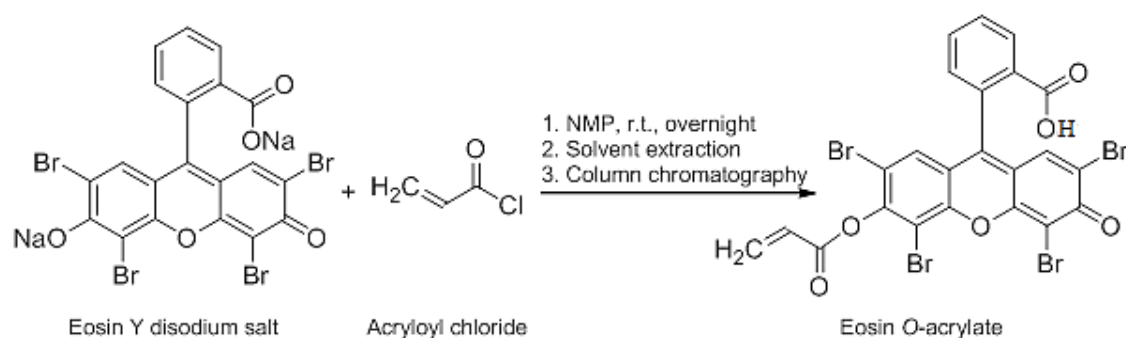
Figure 2-2. Schematic illustration of eosin O-acrylate synthesis.

Once the product was obtained, 15 mg of monomer were dissolved in DMSO-d_6. ^{1}H NMR analysis (Figure 2-3) proved the synthesis of the desired fluorescent monomer.
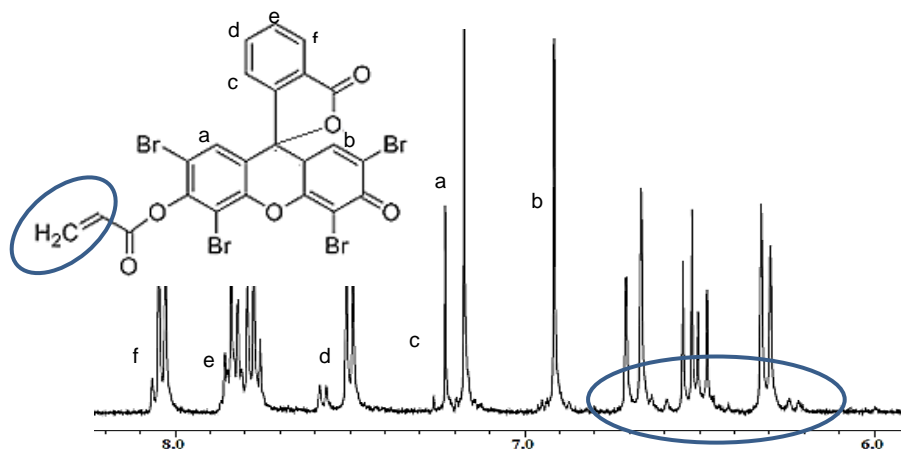
Figure 2-3. ^{1}H-NMR of the product eosin O-acrylate in DMSO-d6.

2.2.4 Synthesis and characterisation of *N*-fluoresceinylacrylamide

A water-stable polymerisable fluorescein-derivative was synthesised by reacting acryloyl chloride with fluoresceinamine (molar ratio 1.15 to 1) in dry acetone (Figure 2-4). This latter was obtained by means of molecular sieves (3 Angstrom), previously activated for 3 hours at 200 °C. The mixture was stirred under nitrogen for about 2 h. Afterwards, the flask was placed at 0°C in order to enhance the precipitation of the product. The precipitate obtained was collected by filtration and washed ten times with 20 mL aliquots of acetone. The product was dried under vacuum and stored in the dark at 4 °C. All steps were followed by TLC. Yield: 89 % w/w.
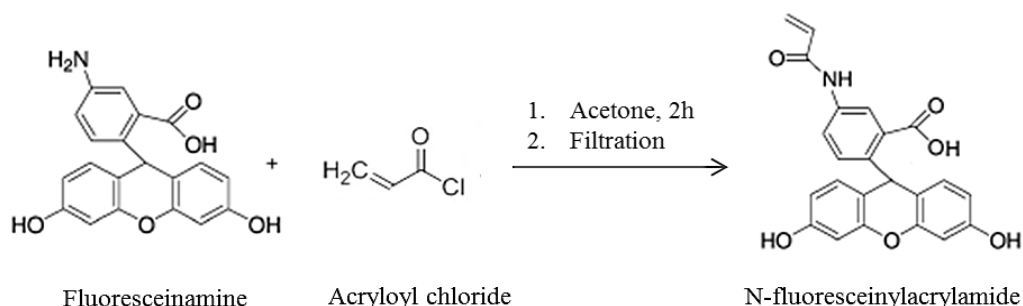
Figure 2-4. Schematic illustration of the synthesis of *N*-fluoresceinylacrylamide.

Once the product was obtained, 10 mg were dissolved in DMSO-d$_6$ ^{1}H and ^{13}C NMR analyses proved the presence of the polymerisable moiety within the dye structure.
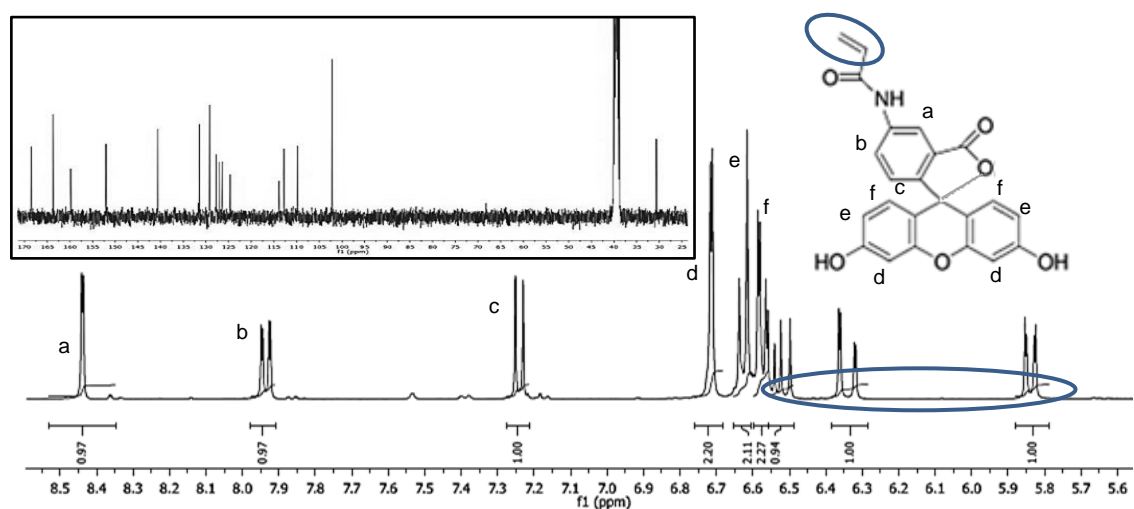
Figure 2-5. ^{1}H- and ^{13}C-NMR of the product *N*-fluoresceinyl-acrylamide in DMSO-d6.

58

2.3 RESULTS AND DISCUSSION

2.3.1 Fluorescence characterisation and stability in water

The produced eosin *O*-acrylate was then employed to produce core-shell fluorescent MIP NPs, by grafting the fluorescent monomer around the MIP core. After their synthesis, the nanoMIPs were washed and transferred to water by means of centrifugal cartridges (30 kDa MWCO). Thus, complete removal of unreacted dye was achieved. The fluorescence spectra of both monomer and NPs were evaluated in water after excitation at 535 nm (Figure 2-6). The small bathochromic shift in the emission wavelength (from 554 to 560 nm) observed after coating the nanoparticles with the fluorescent dye can be due to steric hindrance of the fluorophores, as reported for other dyes [194].
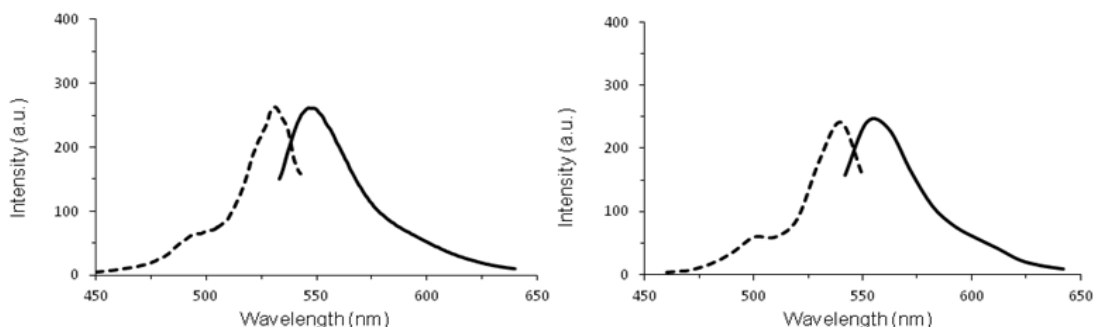
Figure 2-6. Excitation (---) and emission (—) spectra of eosin-acrylate monomer (left) and eosin-MIP NPs (right), respectively at a concentration of 0.0002 mg mL^{-1} and 0.1 mg mL^{-1} in water.

Similarly, the fluorescence properties of both free *N*-fluoresceinyl-acrylamide *(N*-fluo) and fluorescein-tagged MIP NPs were recorded in water, using an excitation wavelength of 492 nm. As previously, the nanoMIPs were washed by means of centrifugal cartridges (30 kDa MWCO) to remove any unreacted dye. The emission was detected at 512 nm (Figure 2-7), thus proving the incorporation of the fluorescent monomer in the polymer matrix.
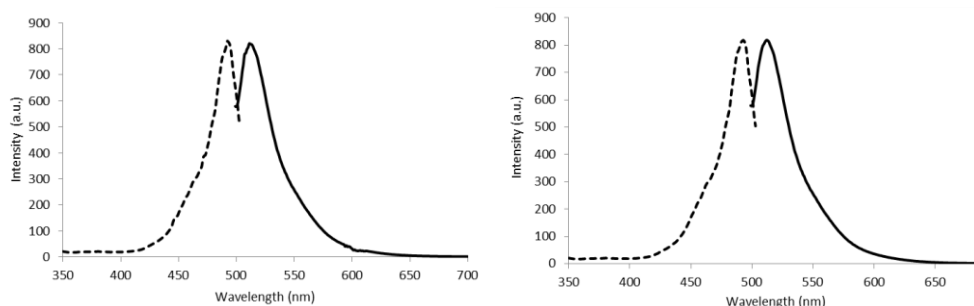
Figure 2-7. Excitation (---) and emission (—) spectra of *N*-fluoresceinyl-acrylamide (left) and *N*-fluorescein-MIP NPs (right), respectively at a concentration of 0.0001 mg mL^{-1} and 0.1 mg mL^{-1} in water.

Considering that many diagnostic assays are performed in aqueous environment, the photostability in water is a pivotal requirement. Therefore, stability studies in water on all dyes employed in this study were carried out.

2.3.2 Fluorescence stability of fluorescein *O*-methacrylate

The first fluorescent MIP NPs were synthesised employing the commercially available fluorescein *O*-methacrylate as fluorescent monomer. After their synthesis, the NPs were washed and transferred to water by means of centrifugation cartridges (30 kDa MWCO). Thus, complete removal of unreacted dye was achieved. Then, the NPs solution was analysed by spectrofluorimetric analysis for at least 5 days, and it displayed an increase in fluorescence emission intensity over the time (Figure 2-8).
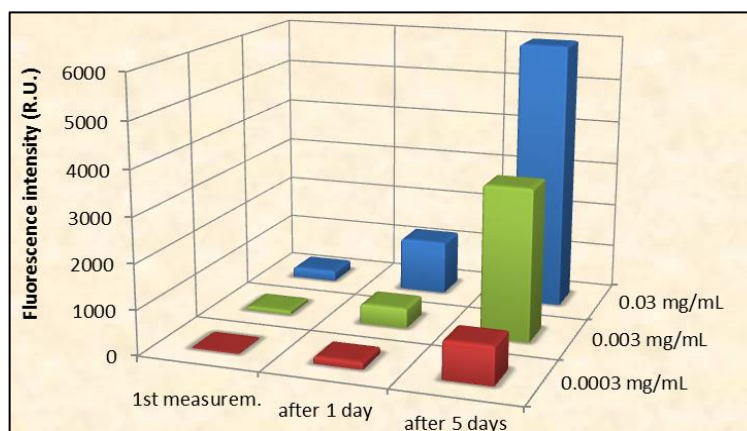
Figure 2-8. Diagram showing the increase in fluorescence emission intensity over the time.

Therefore, some kind of instability is present in the polymerisable dye. In order to verify this fact, several solutions of fluorescein *O*-methacrylate at different concentrations were compared with solutions of plain fluorescein (without any polymerisable portion) at the same concentrations. Interestingly, increase in fluorescence emission intensity (FEI) was reported only for the polymerisable form. This fact might be due to hydrolysis phenomena undergone by the ester bonds linking the polymerisable moiety to the plain dye structure (Figure 2-9). The reason of such an increase in FEI after hydrolysis can be found in the different FEI in water between the plain dye and its polymerisable derivative. In particular, it has been found that the FEI in water of plain fluorescein is about 200 folds higher compared to the polymerisable form. A possible explanation of this fact can be ascribed to two main factors: the presence of the methacrylate moiety and its water solubility. As shown in Figure 2-9, the presence of the polymerisable moiety affects the possibility for fluorescein to form its brightest form (dianion)[195, 196], therefore reducing the FEI of fluorescein *O*-methacrylate (flu-m).
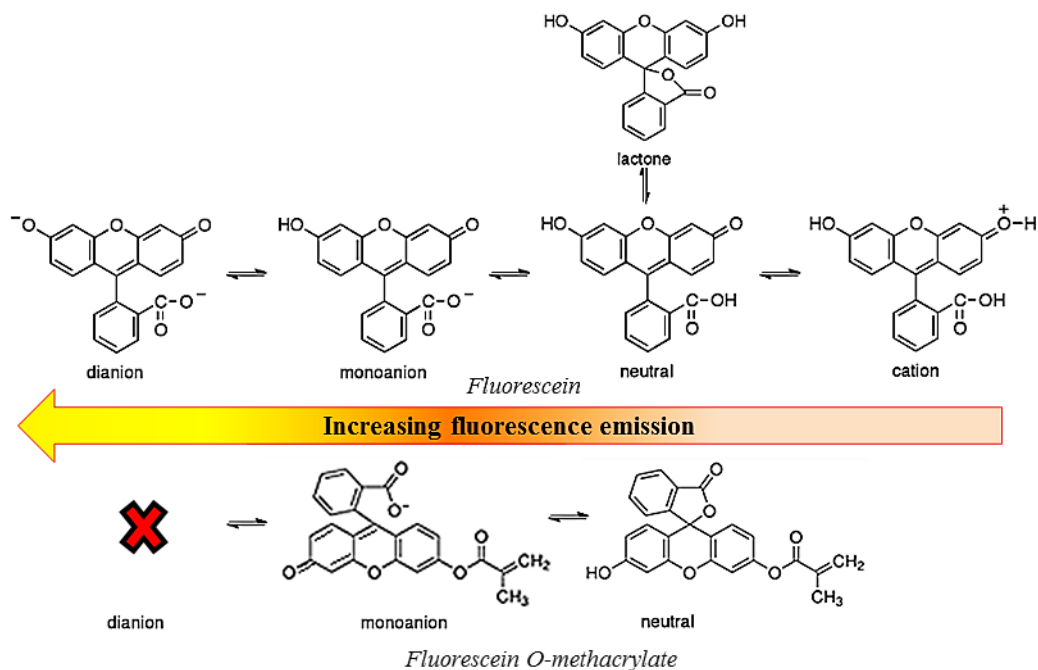
Figure 2-9. Comparison between the equilibrium of fluorescein (plain dye) and fluorescein *O*-methacrylate in water, related with their fluorescence emission.

The fact that the polymerisable moiety reduces the brightness of the monomer is indirectly proven (and exploited) in the so-called fluorescein diacetate (FDA) hydrolysis assay, used to assess the enzymatic activity in bacteria. FDA has two acetate groups linked to the two –OH of the xanthene ring (through an ester bond), just like fluorescein *O*-methacrylate. In this assay, the non-fluorescent FDA is taken up by bacteria and then hydrolysed to plain fluorescein (highly fluorescent)[196].

A simple experiment to prove this potential hydrolysis issue was carried out. A thin layer chromatography (TLC) of three dye solutions was performed. In particular, two fresh solutions of fluorescein (a) and flu-m (b), and a 24 hours-old solution of flu-m (c) were tested (Figure 2-10). The results showed the presence of two spots only in solution c, one due to flu-m and the other one due to the hydrolysed fluorescein.

○ Deposition point

● Fluorescein

● Fluorescein *O*-methacrylate
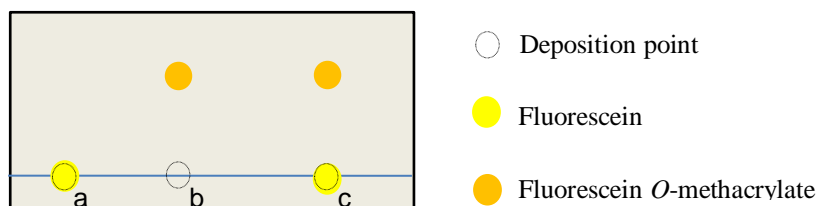
Figure 2-10. TLC representation of free fluorescein and fluorescein *O*-methacrylate in water.

2.3.3 Water-stable fluorescent monomers

Considering the aforementioned problems of photo-instability in water, other fluorescent monomers without any ester bonds were chosen. Another important parameter in the choice of the proper monomers was the position of the polymerisable moiety within the chemical structure of the dye. In particular, such a moiety should be linked to the fluorophore portion of the molecule without affecting the conjugation of the dye. Therefore, vinylanthracene, *N*-(1-Naphthyl)-*N*-phenylacrylamide and nile blue acrylamide were selected for further tests, together with the commercially available methacryloxyethyl thiocarbamoyl rhodamine b and the newly synthesised *N*-fluoresceinylacrylamide (Figure 2-11).

To test whether the aforementioned polymerisable dyes showed any increase in FEI, several solutions of each dye were tested. The results showed a stable fluorescence emission without any increase in FEI over the time. Therefore, vinylanthracene, nile

blue acrylamide, *N*-(1-Naphthyl)-*N*-phenylacrylamide, *N*-fluoresceinylacrylamide and methacryloxyethyl thiocarbamoyl rhodamine b were used as fluorescent monomers to produce MIP NPs with enhanced photostability.
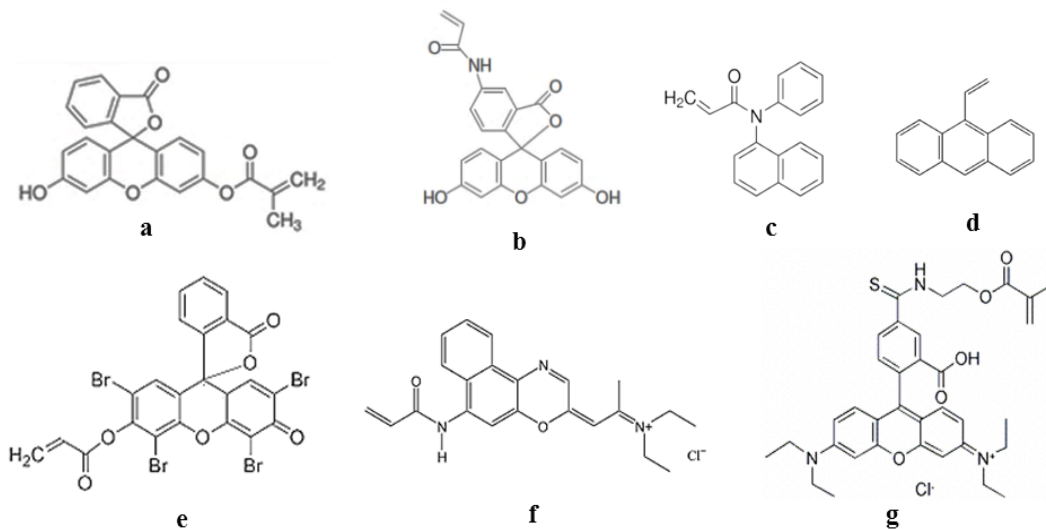
Figure 2-11. Structures of the fluorescent monomers tested. fluorescein *O*-methacrylate (a), *N*-fluoresceinylacrilamide (b), *N*-(1-naphthyl)-*N*-phenylacrylamide (c), vinylanthracene (d), eosin *O*-acrylate (e), nile blue acrylate (f) and methacryloxyethyl thiocarbamoyl rhodamine b (g).

To prove this, the synthesised NPs were first washed by means of centrifugal filter units (MWCO 30 kDa, Fisher) to remove any potential free dye, then placed in a dialysis membrane (MWCO 10 kDa, Pierce) at a concentration of 0.1 mg/ml in PBS. This dialysis cassette was placed in PBS under continuous stirring and incubated for 4 days. The release of free dye from the NPs through the dialysis membrane was then evaluated (Figure 2-12). The results showed an evident increase of FEI for MIPs based on fluorescein *O*-methacrylate, confirming what was previously observed with the free monomer. Although lower, also eosin-based MIPs showed an increase of FEI. On the other hand, MIPs based on vinylanthracene, nile blue acrylamide, *N*-(1-naphthyl)-*N*-phenylacrylamide, *N*-fluoresceinylacrylamide showed a low release rate.

It is worth mentioning that a certain amount free monomer (non-polymerised) might get included in the MIP matrix during the polymerisation. This portion of physically

embedded dye might be released during dialysis, thus contributing to increase the fluorescence of the solution especially during the first hours of incubation.
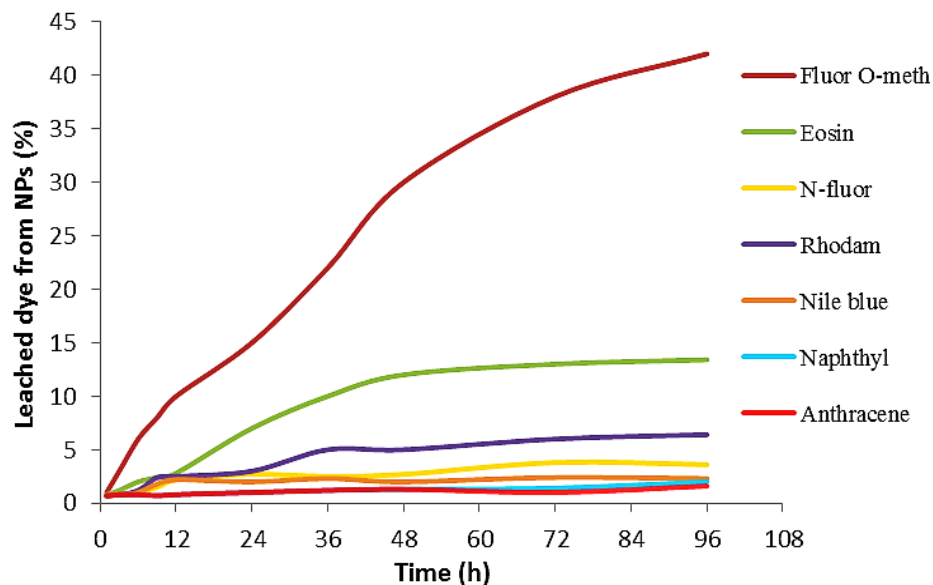
Figure 2-12. Leaching rate of the dyes out of the MIP NPs based on the respective fluorescent monomer.

It should be considered that, although *N*-naphthyl-*N*-phenylacrylamide- and anthracene-based MIPs showed no increase in FEI over the time, the respective fluorescent monomers are not soluble in water. Moreover, their excitation wavelengths are not ideal for biological applications (Table 4). For these reasons, such dyes were not chosen as a model for the further synthesis of MIPs. Although nile blue possesses fluorescent properties suitable for biological applications, its FEI is quite low, making difficult its use as labelling agent at low particle concentrations. For this reason, nile blue was rejected. It should be noted, however, that nile blue-based NPs showed a slight blue colour in solution at concentrations higher than 0.2 mg/ml. Hence, considering their fluorescent properties and performance in water, *N*-fluoresceinylacrylamide and methacryloxyethyl thiocarbamoyl rhodamine b were chosen as model monomers for the following synthesis of MIP NPs.

Table 4. List of fluorescent monomers tested and their properties.
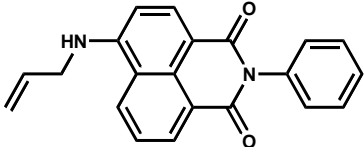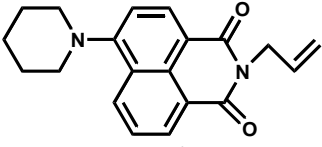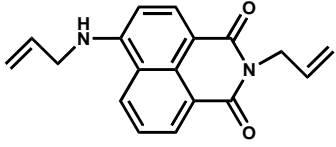
Fluorescent monomer	Fluor. intensity ratio*	Colour of the MIPs produced	Stability in water	Exc.-emis. (nm)	Notes
Fluorescein *O*-methacrylate	1	Slightly yellow solution with MIPs at conc.> 0.3 mg/ml	Poor	490-515	Poor water solubility
N-fluoresceinyl acrylamide	1.3	Slightly yellow solution with MIPs at conc.> 0.25mg/ml	Good	492-515	Poor water solubility. Not commercially available.
Methacr. rhodamine b	0.9	Slightly red solution with MIPs at conc.> 0.25mg/ml	Good	545-570	Good solubility in water
Eosin acrylate	0.7	None	Medium	535-554	Not commercially available
Nile blue acrylamide	0.3	Blue coloured MIPs at conc.> 0.2 mg/ml	Good	635-675	Good solubility in water. Poor fluorescence
Naphthyl phenyl-acrylamide	0.9	None	Excellent	250-420	Very poor water solubility
Vinyl anthracene	2.3	None	Excellent	370-410	Insoluble in water

*Fluorescence intensity ratio (compared to a solution of fluorescein *O*-methacrylate at the same concentration in water).

2.3.4 Novel fluorescent monomers

Three novel fluorescent monomers (Table 5), kindly provided by SETA Biomedicals, were tested to prove their suitability for producing water-stable fluorescent MIPs. MIP NPs based on these three monomers were produced as reported in Chapter 4, using vancomycin as model template. The obtained MIPs were concentrated and washed by means of the centrifugal filter units (MWCO 30 kDa, Fisher) generally employed to remove traces of free fluorescent monomers, and therefore assess the incorporation of the monomer within the MIP matrix.

Table 5. Chemical structures of the three fluorescent monomers tested, together with their excitation and emission wavelengths recorded in water.

K7-1	K7-2	K7-3
λ_{excit}: 420 nm	λ_{excit}: 396 nm	λ_{excit}: 450 nm
λ_{emiss}: 526 nm	λ_{emiss}: 502 nm	λ_{emiss}: 540 nm

To assess the performance of these three monomers, *N*-fluoresceinylacrylamide was used as a control. The same quantity (3.23 μmoles) of all fluorescent monomers was used to prepare the MIPs. Following their synthesis, the NPs were washed and their fluorescence intensity compared (Figure 2-13, insert). Considering that the number of moles of each monomer in the polymerisation mixture was kept constant, the higher fluorescence of the three novel dyes can be ascribed to their higher "brightness" compared to *N*-fluoresceinyl acrylamide. It is worth mentioning, however, that a different degree of fluorescence might be due to a non-equal degree of polymerisation, since K7-1, 2 and 3 are allyl-based monomers, whereas *N*-fluoresceinyl acrylamide is acrylamide-based. After synthesis, the fluorescence of the MIPs was monitored over the time by washing the particle solution by means of centrifugal filter units and recording the fluorescence in the supernatant. For all four monomers, the leaking rate profile is similar and reaches almost a steady state after 12 days (Figure 2-13). This confirms that these monomers are polymerisable and stable in aqueous environment and therefore suitable for further diagnostic applications. However, since these monomers are available as a custom synthesis only, their price is above £150/mg. Due to the fact that several mg of monomer are needed to produce MIP NPs, these three monomers were not used in further experiments.
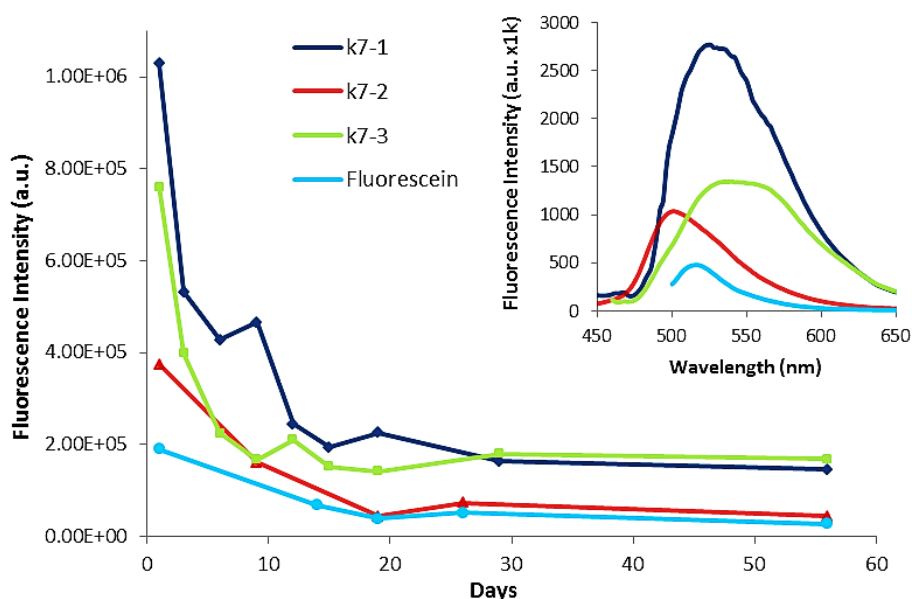
Figure 2-13. Fluorescence intensity of MIP NPs over 55 days. Insert: fluorescence intensity of NPs based on K7-1, 2 and 3 recorded after MIP synthesis.

2.4 CONCLUSIONS

Although several fluorescent monomers are commercially available, some of them may not possess the desired physicochemical properties. For instance, the commercially available fluorescein *O*-methacrylate initially employed to produce nanoMIPs showed poor fluorescence stability in water. For this reason, other two fluorescent monomers were synthesised (*N*-fluoresceinylacrylamide and eosin *O*-acrylate) and others, commercially available, were characterised. Some polymerisable dyes, such as vinyl anthracene and naphthyl phenyl-acrylamide, exhibited very poor water solubility and their excitation wavelength was not suitable for biological/*in vivo* applications. Conversely, the synthesised *N*-fluoresceinylacrylamide and the commercially available methacryloxy-ethyl thiocarbamoyl rhodamine b showed appropriate solubility and fluorescence properties to be employed for the synthesis of nanoMIPs for imaging applications. Novel fluorescent monomers suitable for imaging can be obtained as a custom synthesis, however their relative high cost may hamper their routine use.

3 SOLID-PHASE SYNTHESIS OF MIP NANOPARTICLES IN ACETONITRILE

3.1 INTRODUCTION

As outlined in paragraph 1.1, the application of MIP NPs in diagnostics is rapidly growing due to the improvements in their synthesis and performance in the recognition and quantification process of the analyte. However to date, despite all the aforementioned improvements, the synthesis of MIP NPs is neither simple nor fast. Most of the polymerisation techniques need a reaction time between 20 and 24 hours. Furthermore, generally the purification process of such MIP NPs from the imprinted template and unreacted monomers requires time-consuming procedures such as Soxhlet extraction[197] or dialysis[198].

Recently, an innovative approach for simultaneous synthesis and purification of MIP NPs has been developed[199]. It relies on the immobilisation of the template molecules onto a solid support which is later used both for synthesis and selection/purification by an affinity chromatography step. In particular, the template is covalently immobilised at the surface glass beads (75 μm mean diameter). This support is placed in contact with monomer mixture and polymerisation is initiated either chemically or by UV, under conditions leading to formation of polymer nanoparticles. Post-synthesis, the solid support functions as an affinity matrix for separation of MIP NPs from remaining monomers and low affinity polymer. This process (synthesis and subsequent affinity purification) can easily be automated and can produce robust imprinted nanoparticles in about 2-3 hours. Thanks to the affinity purification step, MIP NPs possess high affinity/specificity to their target and have a homogeneous distribution of binding site affinities, much like monoclonal antibodies. The MIPs obtained are virtually free from template, a common issue with traditional approaches, requiring lengthy (up to a week) dialysis of the nanoparticles for its removal. This approach is generic in nature and can be used both in water (persulfate-initiated polymerisation) and in organics (UV-triggered process). The polymerisation in water was successfully employed to produce hydrophilic MIP nanoparticles imprinted against peptides and proteins[77, 200, 201] (and

further discussed in chapter 4), whereas the polymerisation in organics proved to be advantageous for imprinting of small molecules[76, 202, 203] (Mw < 500 Da). Furthermore, this method allows for the solid-phase to be reused several times thus saving template molecules, and it is fully scalable and automatable as described in paragraph 4.4. Moreover, this method allows for the production of core-shell MIP NPs (paragraph 3.4), endowed with "multifunctional" features and therefore applicable in a broad range of diagnostics as direct replacement for natural antibodies. In this work, melamine was used as a model template to produce fluorescent MIP NPs.

3.2 MATERIALS AND METHODS

3.2.1 Chemicals

Melamine (MEL), methacrylic acid (MAA), ethylene glycol dimethacrylate (EGDMA), trimethylolpropane trimethacrylate (TRIM), phosphate buffered saline (PBS), pentaerythritol-tetrakis-(3-mercaptopropionate) (PETMP), *N*-methyl-2-pyrrolidone (NMP), 3-aminopropyltrimethyloxysilane (APTMS), toluene, glutaraldehyde (GA), dimethylsulfoxide (DMSO) and poly(ethylene glycol) methyl ether methacrylate (PEG) (Mw = 1100 and 4000 g/mol) were purchased from Sigma-Aldrich, UK. Acetonitrile (ACN), ethanol and Amicon Ultra-15 Centrifugal Filter Units (MWCO 30 kDa) were obtained from Fisher Scientific (UK). Methanol and acetone were purchased from VWR (UK). *N,N*-diethyldithiocarbamic acid benzyl ester was bought from TCI Europe (Belgium). Glass beads (Spheriglass® 2429, 53 mm < diameter < 106 mm) were purchased from Blagden Chemicals, UK. Deionised water obtained from a Millipore (MilliQ) purification system at a resistivity of 18.2 MΩ cm was used for analysis. All chemicals were analytical or HPLC grade and were used without further purification.

3.2.2 Preparation of template-derivatised solid-phase for synthesis of MIP nanoparticles

Glass beads with diameter ranging from 70-100 μm (Potters, Spheriglass A-Glass cat. no. 2429 CP 00 or Sigma Aldrich cat. no. 59200-U) are first activated by boiling them in a 2M NaOH solution for 15 min, then rinsed with deionised water and acetone, desiccated at 80 °C and incubated overnight in 2 % v/v APTMS/toluene solution. This last step leads to beads bearing $-NH_2$ groups. Following this step, template molecules are immobilised in different ways depending on their chemistry. Scheme 3-1 depicts the procedures used with commonly occurring functionalities, which enable immobilisation of templates on amine-derivatised beads. In particular:

(i) Templates bearing –COOH group can be linked to the solid phase by standard *N*-(3-Dimethylaminopropyl)-*N*′-ethylcarbodiimide (EDC)/*N*-Hydroxysuccinimide (NHS) coupling.

(ii) Templates bearing $-NH_2$ groups can be immobilised through the formation of a Schiff base using glutaraldehyde (GA).

(iii) templates bearing –SH groups (e.g., peptides bearing a cysteine residue for oriented immobilisation) can be immobilised via *N*-succinimidyl iodoacetate (SIA) thanks to the reactivity of thiols towards haloacetyl groups.

After silanisation the beads are incubated with the template in an appropriate solution to enable the coupling reaction to occur, depending on the immobilisation chemistry. The concentration of template was 5 mg/ml for melamine and 0.5 mg/ml for peptides or proteins. This procedure is estimated to lead to 2.55×10^{13} templates per square centimetre[204].

In particular, for melamine-derivatised solid-phase, silanised beads were rinsed with acetone and then incubated for 2 h in 7 % v/v GA solution in PBS at pH 7.2 and followed by washing with deionised water. The immobilisation of melamine onto the beads was performed overnight at 4 °C, by placing the beads in a 5 mg/ml solution of

melamine in PBS pH 7.2 containing 10 % v/v of NMP as co-solvent. Eventually, the beads were washed with deionised water, dried in vacuum and stored at 4 °C.
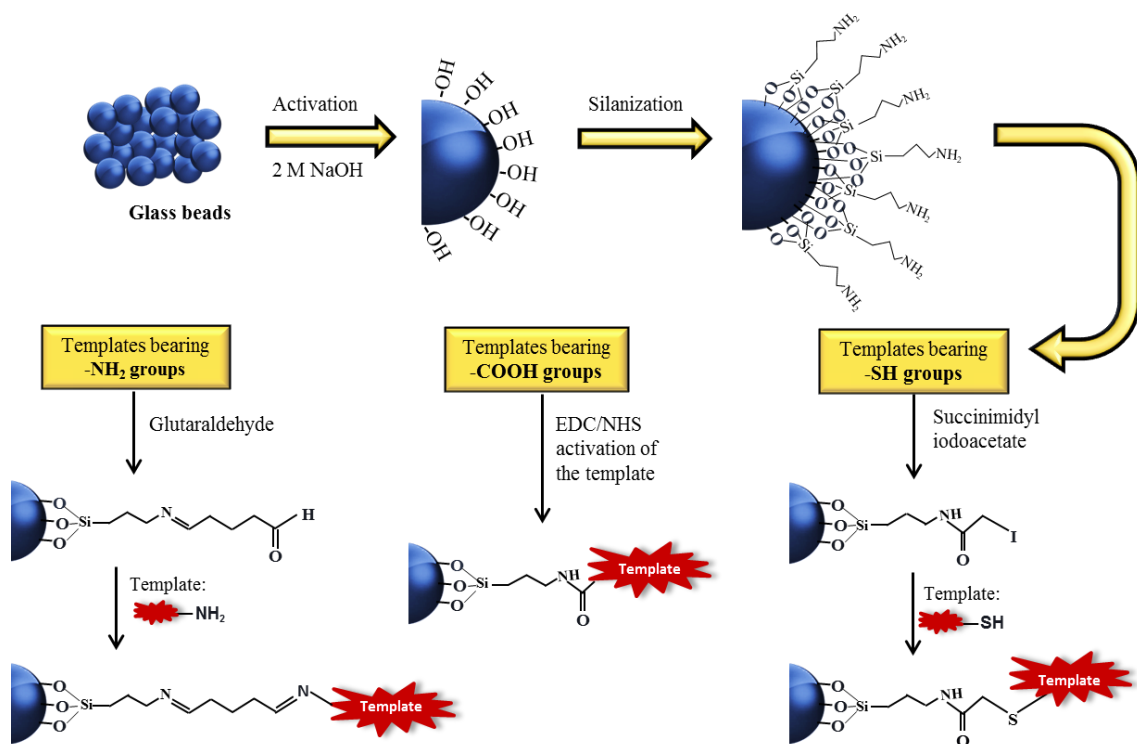
Figure 3-1. Scheme of the protocol employed for immobilising melamine onto glass beads for three common functional groups (reproduced from Canfarotta *et al.*, Nature Protocols 2016).

3.2.3 Synthesis of fluorescent melamine-MIP NPs by photopolymerisation

The composition of the polymerisation mixture for the synthesis of core MIP NPs for melamine detection was adapted from [199]. It was performed by mixing 0.96 g MAA (1.12×10^{-2} mol, Mw = 86.06 g/mol) as functional monomer, 1.08 g TRIM (3.18×10^{-3} mol, Mw = 338.40 g/mol) and 1.08 g EGDMA (5.46×10^{-3} mol, Mw = 198.22 g/mol) as cross-linkers, 0.261 g *N,N*-diethyldithiocarbamic acid benzyl ester (1.09×10^{-3} mol, Mw = 239.40 g/mol) as iniferter and 0.06 g pentaerythritol tetrakis(3-mercaptopropionate) (1.23×10^{-4} mol, Mw = 488.66 g/mol) as chain transfer agent (CTA) in 3.51 g ACN. In order to obtain fluorescent MIPs, 0.5% or 1% in mol of either

fluorescein *O*-methacrylate, eosin acrylate, vinyl anthracene, nile blue methacrylate or *N*-fluoresceinylacrylamide were added as fluorescent monomers.

The mixture was poured in a glass vial where nitrogen was purged for 20 minutes. 30 g of melamine-derivatised glass beads was placed in 200 mL flat glass beaker and degassed in vacuum for 20 min. The polymerisation mixture was poured onto the glass beads layer in the vessel and placed between two UV light sources (Philips HB/171/A with 4×15 W lamps) for different irradiation times (1, 1.5 or 2 min depending on the final size required) under continuous stream of nitrogen. After polymerisation, all the content was transferred into SPE cartridge fitted with polyethylene frit (20 μm porosity) in order to perform the temperature-based affinity separation of MIP NPs. SPE cartridge was first placed in an ice bath (0 °C) for 7 min and the supernatant was drained by means of a syringe piston. Washing steps were carried out in low temperature by washing with 10 bed volumes of ACN at 0 °C. Low temperature washings were performed in order to remove non-polymerised monomers and low affinity MIP NPs. The efficiency of elution/washing process was assessed by UV spectrophotometric analysis of the column eluate. After low temperature washings, temperature of incubation and ACN was increased to 60 °C. This allowed an elution of high affinity MIP NPs from the solid phase. ACN was poured into the cartridge and incubated for 4 min at 60 °C. This procedure was performed 6 times. The total collected volume of high affinity fraction of MIP NPs in ACN was about 150 mL. A simplified scheme of this solid-phase synthesis is reported in Figure 3-2.

3.2.4 Core-shell approach

The synthetic protocol has been slightly modified to allow the formation of the polymeric shell around the MIP core. In particular, post-derivatisation of melamine-MIP NPs was performed on the glass beads having the high-affinity MIP NPs attached (on material prepared as described in section 3.2.3 after washing at low temperature but before the high temperature elution phase). For this either two types of poly(ethylene glycol) methacrylate (Mw 1100 g/mol, 75 mg and Mw 4000 g/mol, 272 mg) or eosin

acrylate (45 mg) were dissolved in ACN (15 mL) added to a 200 mL capacity sealed glass vessel, along with the glass beads with attached MIP NPs recovered from the SPE cartridge. The mixture was bubbled with N_2 for 5 min and irradiated with UV for 1 min 30 s using the same arrangement of lamps as described above. Following irradiation, the contents of the vessel were transferred into a new SPE cartridge and washing performed 8 times following the same protocol as described in the preceding section. The washing process was monitored by UV spectroscopy, in order to ensure complete removal of all unreacted monomers from the glass beads. After the washing, the hot elution step was also carried out as described in section 3.2.3.

3.2.5 Size and concentration analysis of MIP NPs

Dynamic Light Scattering (DLS). Particles sizes were measured with a Zetasizer Nano (Nano-S) particle-size analyser from Malvern Instruments Ltd (UK). An aliquot of the dispersion of NPs in ACN (10 mL) was sonicated for 2 min, washed and the solvent exchanged to water by means of an Amicon Centrifugal Filter Unit (MWCO 30 kDa). The dispersion was analysed by DLS at 25 °C in a 3 cm^3 disposable polystyrene cuvette. Attenuator position, measurement duration and number of runs were automatically chosen by the instrument. The values are reported as an average of 5 measurements.

NanoSight®. Size analysis was also carried out using a NanoSight® LM20 device (NanoSight Ltd., Ames-bury, UK) equipped with a NanoSight® NTA 2.2 software. Samples were first washed by means of an Amicon Centrifugal Filter Unit (MWCO 30 kDa) and then diluted in milli-Q water down to a concentration around 10^8 particles/mL prior to injection into the aforementioned device at room temperature. Three independent analyses were performed recording 60s videos. Then NPs were tracked by the NTA software which evaluates their Brownian motions in solution. These latter depend on the particle size, allowing the software to calculate the particle size. Moreover, the software also calculated the particle concentration. The reported value is

the average of 6 measurements (two different positions of the digital camera in the chamber for three independent analyses).

Transmission electron microscopy (*TEM*). TEM images of MIP NPs were taken using a Philips CM20 Transmission Electron Microscope. Samples were prepared by placing 10 µL of the MIP NPs dispersion, previously sonicated for 2 min and filtered through a 1.2 µm glass fibre syringe filters (Cronus, Jaytee, UK), onto a carbon coated copper grid. Then the sample was left to dry overnight under a hood.

3.2.6 Grafting of PEG and fluorescent monomers around the MIP core

MIP NPs were post-functionalised with poly(ethylene glycol) (PEG) methacrylate (Mw 1100 and 4000 g/mol) in ACN at 4 °C whilst still bound to the glass beads. The presence of a PEG layer in the MIP NPs produced by solid phase synthesis was previously confirmed by NMR analysis[203, 205]. To further confirm this, hyperspectral microscopy analysis was used. In particular, all samples were vortexed prior to imaging and 1.5 µL of each sample (1 nM) was aliquoted onto an ultrasonically cleaned slide and hyperspectrally imaged at 100x magnification using the CytoViva enhanced darkfield illuminator. The respective spectra of the MIPs were averaged and compared to examine the varying spectral responses of coated and uncoated particles.

3.2.7 Fluorescence spectroscopy analysis

Measurements of fluorescence intensity were performed using a Cary Eclipse spectrofluorometer (Varian Australia Pty Ltd) at 25 °C. Excitation and emission wavelengths were chosen depending on the fluorescent monomer employed. In particular, λ_{exc} and λ_{em} for fluorescein *O*-methacrylate were 490 nm and 515 nm respectively; for eosin acrylate they were 535 nm and 554 nm; for vinyl anthracene 370 nm and 410 nm; for *N*-fluoresceinylacrylamide 492 nm and 515 nm; for nile blue methacrylate 635 nm and 675 nm. The fluorescence measurements were performed using 1 mL quartz cuvettes of 10 mm path length. It should be noted that before

measuring fluorescence, the absorbance of each sample at the excitation wavelength should be checked and be below 0.1 Au, in order to minimize inner filtering effects.

3.2.8 Preparation of melamine-derivatised BIAcore chips

Au-coated chips (SIA Kit Au, Biacore, purchased from GE Healthcare, UK) were cleaned by immersion in Piranha solution (H_2SO_4/H_2O_2, 3:1 v/v) for 5 min, then thoroughly washed with deionised water and placed in ethanol overnight. The immobilisation of the template molecule (melamine) was carried out by incubating the chips in a solution of cysteamine (0.2 mg/mL in ethanol) at 4 °C for 24 h, after which they were rinsed with ethanol and incubated in a 7 % v/v solution of GA in PBS pH 7.4 for 2 h. Afterwards, the chips were washed with PBS and placed in a solution of melamine or DA (1.2 mg/mL) in PBS pH 7.4 containing 20 % v/v of methanol as co-solvent for 24 h at 4 °C. After this step, the chips were rinsed with methanol and dried in a stream of N_2. Once the immobilisation was completed, the chips were assembled on their holders and stored under inert atmosphere (Ar) at 4 °C until used.

3.2.9 Surface plasmon resonance analysis (SPR) of MIPs

SPR experiments were carried out using a Biacore 3000 SPR system (GE Healthcare, UK). A volume of nanoparticle solution in ACN (10 mL) was first diluted with water then concentrated down to 2 mL using centrifugation cartridges (Amicon ultracentrifugal polypropylene, Ultracel membrane, 30 kDa MWCO, 15 mL, Millipore) purchased from Fisher Scientific (UK). The filtration was carried out according to the manufacturer's specification on a Sigma 3-16P bench-top centrifuge fitted with a swing-bucket rotor, using first deionised water and then PBS pH 7.4. For immobilisation of core-shell NPs on Biacore chips (Fig. 4a) a solution of 0.05 mg mL^{-1} NP was injected sequentially onto a bare gold chip. Each solution was sonicated for 10 min, adjusted to a concentration of 0.05 mg mL^{-1}. Three consecutive injections of 100 µL were made and the sensor response was followed for 2 min after each injection. All experiments were

performed using a flow rate of 35 μL min⁻¹ at a temperature of 25 °C. Data were processed using BIAEvaluation Software v4.1.

3.3 RESULTS AND DISCUSSION

3.3.1 Synthesis of fluorescent MIP nanoparticles

The solid phase synthesis of MIP NPs was adapted from Poma et al.[206] . The glass beads activation in boiling sodium hydroxide allows to increase the amount of silanol groups (-Si-OH) on their surface, thus promoting the following silanisation reaction with APTMS[207]. Once that the primary amino groups cover the bead surface, GA is used to link these groups with the other $-NH_2$ groups present in the melamine structure, generating a Schiff base bond (Figure 3-1). Both APTMS and GA allow the reduction of potential steric hindrance issues during the polymerisation, arising from the overcrowding of the template on the bead surface[208]. It is noteworthy that the immobilised template allows first the imprinting process and then operates as particle ligand in the following temperature-based affinity separation, where high-affinity NPs are selectively separated from both low-affinity NPs and unreacted materials. In a standard affinity chromatography technique, a column is packed with a material bearing specific affinity ligands on its surface. Once that a raw sample is loaded in the system, only the molecules which recognise the aforementioned ligands are retained, whereas the other compounds are removed by using proper elution conditions. Hence, the desired molecules can be collected by employing stronger elution conditions, for instance increasing the ionic strength of the solvent or adding surfactants. The temperature-based affinity separation used for the synthesis of MIP NPs exploits the same principle. The initial washings at low temperature (0 °C) allow the elution of only the low-affinity materials, whereas by increasing the temperature (60 °C) the stronger interactions between high-affinity NPs and template can be disrupted, thus making possible the particle collection. This method allows both the purification of the final product by most of the unreacted materials, and selection of the high-affinity particles.

NMP was used as co-solvent to increase the water-solubility of melamine. Considering the good fluorescent properties of fluorescein and its low cost, its polymerisable derivative (fluorescein *O*-methacrylate) was chosen as preliminary fluorescent monomer. However, due to its poor fluorescence stability in water, the fluorescent monomer used afterwards as a model was *N*-fluoresceinylacrylate. The UV-irradiation time employed, between 1.5 and 3.5 minutes, should avoid an excessive heating of the polymerisation mixture which would reduce the particle affinity for the template[209, 210].
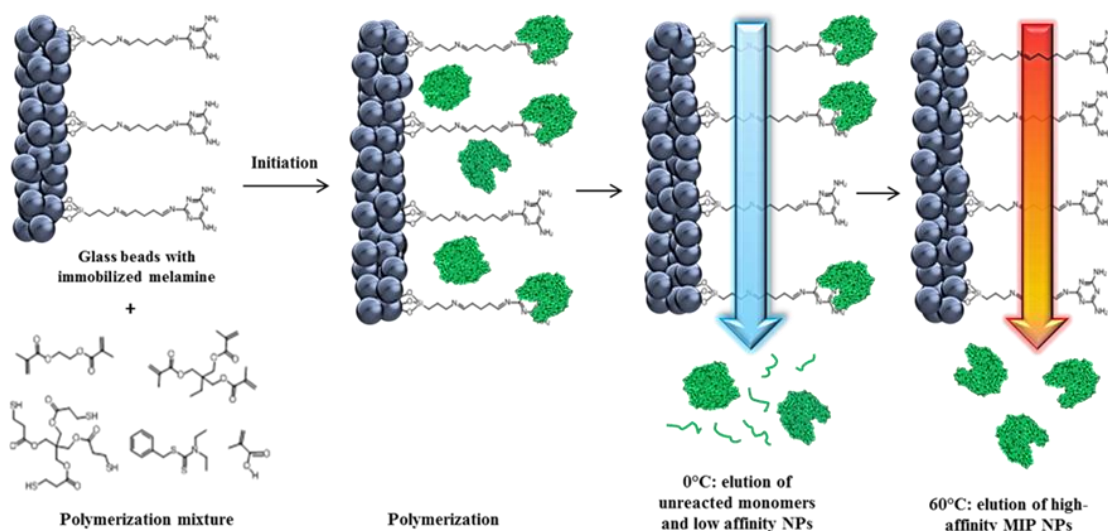
Figure 3-2. Scheme of the synthesis and separation process of MIP NPs by using melamine-derivatised glass beads (reproduced from Canfarotta *et al.*, Nature Protocols 2016).

In this work we employed iniferter (*N,N′*-diethyldithiocarbamic acid benzyl ester) as initiator. This kind of initiator is capable of acting as initiators, transfer agents and terminators. In particular, iniferters generate one radical (dithiocarbamyl) after the decomposition step which is capable of terminating the growth of the polymer chains in solution, forming again the initial C-S bond. Therefore, the product formed after termination can further generate a new propagating radical upon application of the stimulus triggering the polymerisation[90]. In this way, sequential polymerisations with other monomers can be re-initiated, in order to tailor properties or functionalities of the synthesised particles[199, 211, 212]. Moreover, in contrast to conventional radical polymerisation, the iniferter-based living polymerisation proceeds at low rate and

without autoacceleration phenomena, allowing a better control over some parameters such as the polymer chain length and the particle size[213].

3.3.2 Synthesis of core-shell MIP nanoparticles

As mentioned before, iniferters allow sequential grafting of several layers around the particle core, thus modifying the particle surface with the functionality of interest (Figure 3-3). An advantage of this method is that only the surface of the nanoMIPs is modified, without affecting the functionalities within the active sites. In fact, the process relies on the production of the imprinted NPs in the presence of template-derivatised beads as previously described. In the core-shell approach, the difference is that, after washing at low temperature, the beads bearing high affinity MIPs are used for a second polymerisation process. Therefore, since the nanoMIPs remain attached to the solid-phase through their interaction with the template, only their surface is left exposed for derivatisation, thus protecting the binding sites during the grafting process. By raising the temperature, the rate of exchange of particles with the template increases and the strength of association is reduced, allowing the MIPs to be eluted from the solid-phase. However, since it is a polymerisation-based process, only monomers can be employed and therefore not all functionalities might be available in such a format.
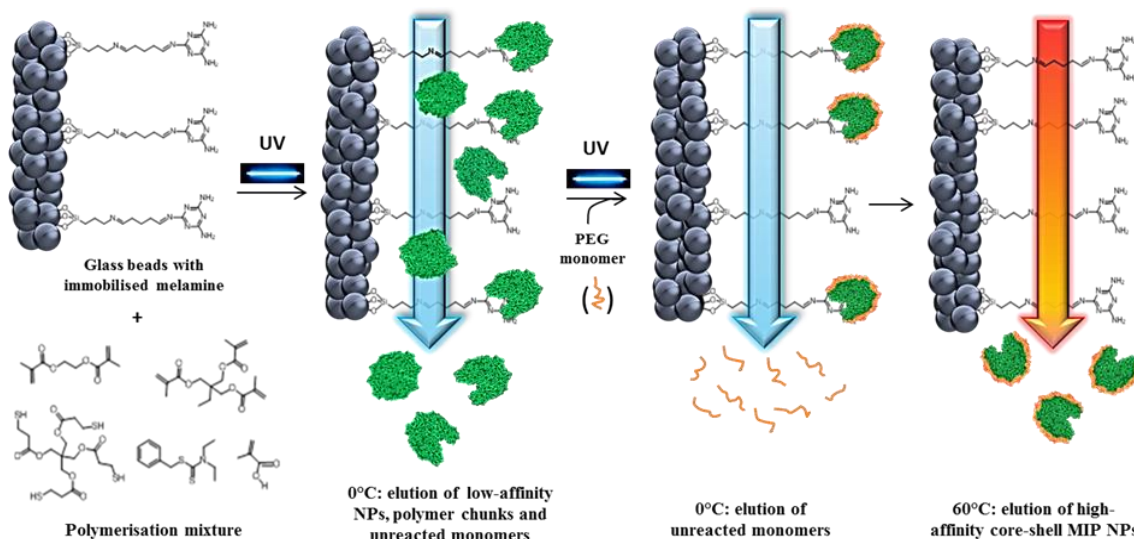
Figure 3-3. Scheme of the synthesis of core-shell MIP NPs by using melamine-derivatised glass beads and a PEG-based monomer to produce PEGylated MIPs.

3.3.3 Size analysis by Dynamic Light Scattering (DLS), NanoSight™, Scanning and Transmission Electron Microscopy (SEM/TEM)

DLS analysis

Dynamic Light Scattering (DLS), or photon correlation spectroscopy (PCS), measures the intensity of the light scattered by particles in a sample. When light hits a particle, the light is scattered in all directions (so called Rayleigh scattering). If the particles was stationary, then the light scattered would be constant. However, since nanoparticles randomly undergo Brownian motions in solution, interference (constructive or destructive) occurs thus causing a change in light intensity, due to the fact that the distance between the scatterers (i.e. the particles) in the solution and the detector changes constantly. By monitoring the time of such fluctuations in light intensity, DLS measures the diffusion coefficient of the particles, which can be converted into a size using the Stokes-Einstein equation:

$$d(H) = \frac{kT}{3\pi\eta D}$$

Where: dH = hydrodynamic diameter; k = Boltzmann's constant; T = absolute temperature; η = viscosity and D = diffusion coefficient.

Three types of bare NPs, synthesised using 1 (A), 1.5 (B) and 2.5 (C) min of UV-irradiation time, were tested. The samples were first washed by means of a dialysis tube to remove unreacted monomers and polymeric chains, then sonicated one minute to avoid potential agglomeration issues and filtered through 1.2 micrometer syringe filter. As expected, by increasing the polymerisation time, bigger particles are obtained. In particular, the particle size of sample A, B and C in ACN were respectively 140, 160 and 260 nm. It should be noted, however, that once the NPs are transferred to water their measured size reduces to about half. This might be due to the fact that MIPs

synthesised in organics are quite hydrophobic, and therefore they tend to shrink once in water.

Concerning core-shell nanoMIPs, as shown in Moczko et al.[203], the successful functionalisation of the MIP NPs was proven by grafting fluorescent or PEG-based monomers. In particular, two PEG methacrylates having different molecular weights (1100 and 4000 g/mol) were used, thus producing MIPs with reduced agglomeration tendency without affecting negatively their recognition properties. PEG is an FDA approved hydrophilic polymer which has been successfully used to stabilise nanosystems against aggregation and improve their drug delivery efficiency[214, 215]. Figure 3-4 shows a comparison between bare and PEGylated MIP NPs, analysed by DLS in distilled water. An increase of the hydrodynamic size of bare nanoMIPs over the time is evident, whereas such a trend is not observed in PEGylated MIP NPs.
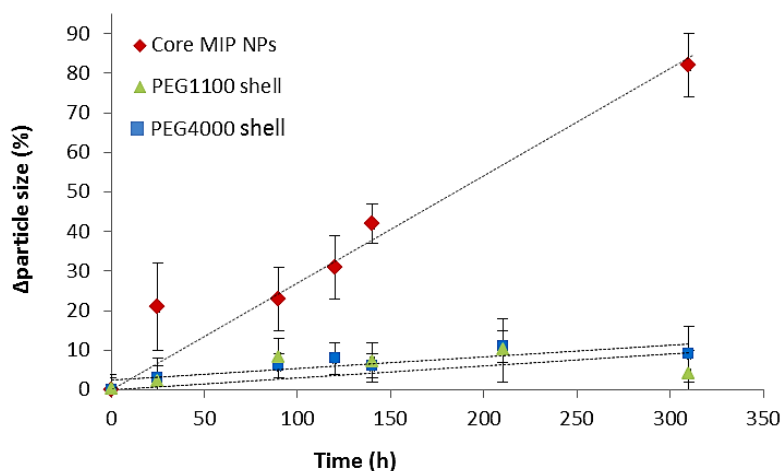
Figure 3-4. Aggregation tendency of bare and PEGylated core-shell MIP NPs. Experiments were performed in Milli-Q water, in four replicates. Dashed lines (—) indicate linear fits to the data points.

However, it is worth mentioning that DLS measures the light scattered from each nanoparticles in the sample as a whole, hence giving an average measurement[216]. It should be noted that smaller particles scatter less light than larger particles (intensity of the scattering proportional to the sixth power of the particle diameter), therefore the scattered light of these latter can cover the signal from smaller particles. Hence the apparent particle size distribution measured by DLS can be shifted towards bigger sizes[217]. For example, as reported by Malvern (www.malvern.com), a mixture of 60 and

200 nm latex particles with a mass composition of 70% and 30% respectively would produce a higher response in the region of the 200 nm particles, although the latter composes only 30% of the total sample. Another parameter to be considered is the effect of ions in solution. These latter may affect the speed of the particle diffusion by altering the thickness of the electric double layer around the NPs (called Debye length). In fact MIPs measured in PBS show an apparent larger hydrodynamic diameter. For this reason, in this work measurements of the MIP size were performed in water.

Nanosight analysis

NanoSight's nanoparticle tracking analysis (NTA) exploits the Brownian motions of individual nanoparticles and, by analysing their diffusion, particle size distribution and concentration can be calculated. NTA was proven to accurately size different nanosystems and is it is a more accurate technique compared to DLS especially when polydisperse samples are analysed, since individual nanoparticles are tracked rather than measuring the overall scattered light[218]. Nanosight analysis was employed to differentiate between bare and PEGylated MIPs. These particles were used as models to test the biocompatibility and internalisation of nanoMIPs in cells (Chapter 5).
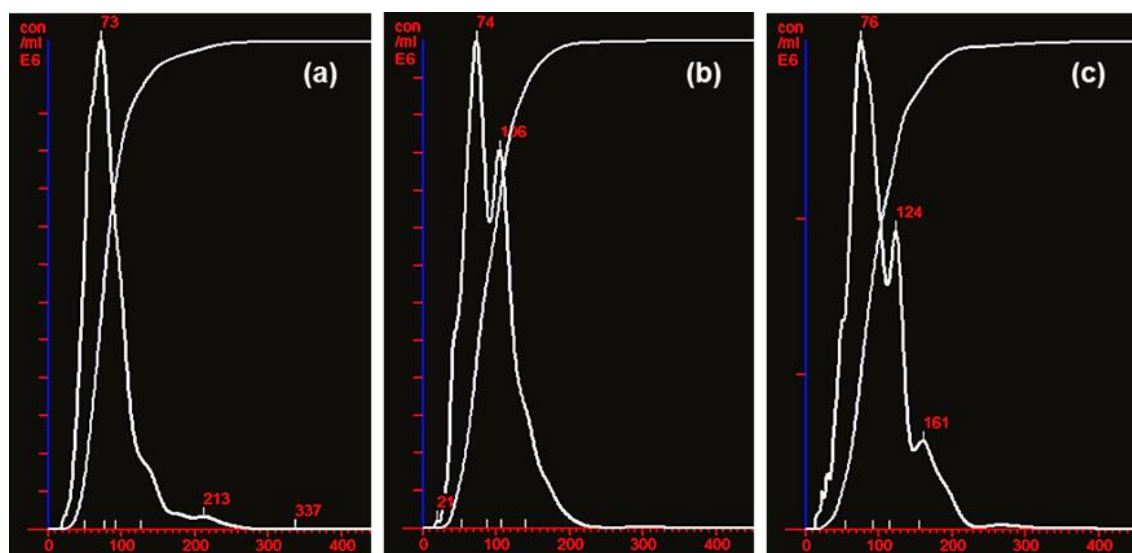
Figure 3-5. Nanosight size analysis of bare (a), PEG1100-coated (b) and PEG4000-coated (c) MIPs in water at 37°C, obtained considering at least 1000 tracks in 3 analyses of each nanoparticle type (60 seconds videos).

Both DLS and NTA analyses showed no significant difference in particle size between fluorescent and non-fluorescent MIPs.

TEM analysis

TEM analysis showed two size populations of NPs for the particles synthesised using 2 min of irradiation time (Figure 3-6). It should be noted that the size of the particles by TEM differs from the results of DLS and Nanosight, since the latter techniques measure the hydrodynamic size and therefore solvatation effects tend to increase the particles' apparent size.
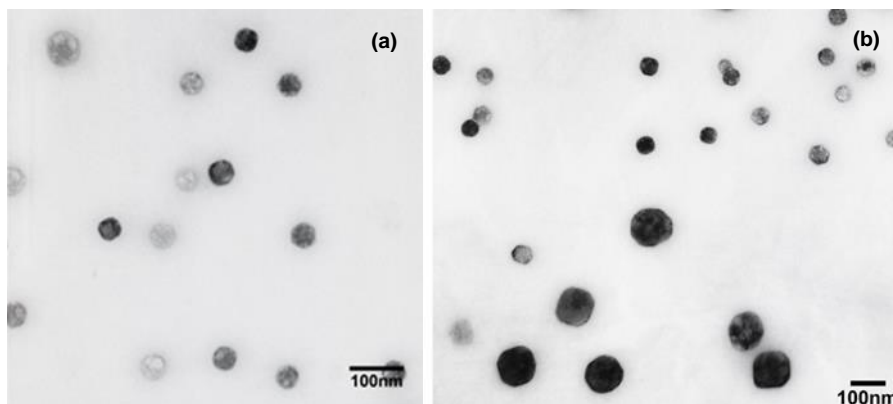
Figure 3-6. TEM image of fluorescein-based MIP NPs after 1 (a) and 2 (b) min of irradiation.

3.3.4 Fluorescence properties of fluorescent MIP NPs

As mentioned above, fluorescence is the emission of light by a molecule that absorbs at a certain wavelength and re-emits it at a longer wavelength. It should be noted that this process depends on several factors such as temperature, pH, concentration and solvent. Furthermore, if small particles (e.g. dust/debris) are present in the sample, part of the incident radiation may be scattered rather than absorbed (a process called Tyndall scattering), thus giving rise to an incorrect fluorescence reading. In some cases, the molecule itself may scatter the incident light (Rayleigh scattering). This latter, however, is an elastic scattering of light and therefore the light is diffused at the same wavelength

than the incident one. Both Rayleigh and Tyndall scattering can be a hurdle especially when excitation and emission wavelength are very close. On the other hand, Raman scattering consists in an inelastic diffusion of photons, hence photons are scattered at a frequency different from the incident light. However, only a small fraction of photons (about 1 in 10 millions) is diffused by Raman scattering. In general, molecules containing aromatic/conjugated moieties exhibit fluorescence properties, due to the high number of electrons which can potentially absorb a photon and get promoted to the excited state, thus initiating the fluorescence process.

In this work, several fluorescent monomers were employed to synthesise fluorescent MIP NPs. In particular, fluorescein *O*-methacrylate, eosin acrylate, *N*-fluoresceinyl acrylamide, methacryloxyethyl thiocarbamoyl rhodamine B, *N*-naphthyl phenyl-acrylamide and vinyl anthracene were tested. Depending on the fluorescent properties of the obtained NPs (Figure 3-7), some fluorescent monomers were then used as models in cell experiments, others were not employed further. As mentioned before, MIPs based on fluorescein *O*-methacrylate and eosin acrylate showed poor fluorescence stability and for this reason were dropped. *N*-fluoresceinyl acrylamide ($\lambda_{exc.}$ 492 – $\lambda_{em.}$515 nm) and methacryloxyethyl thiocarbamoyl rhodamine B ($\lambda_{exc.}$ 545 – $\lambda_{em.}$570 nm) were the monomers of choice for application in cells (optimum excitation/emission spectra). On the other hand, due to their short excitation wavelength, *N*-naphthyl phenyl-acrylamide ($\lambda_{exc.}$ 250 – $\lambda_{em.}$420 nm) and vinyl anthracene ($\lambda_{exc.}$ 370 – $\lambda_{em.}$410 nm) are not recommended in cells.

The modification of bare MIP NPs to obtain core-shell MIPs is possible thanks to the presence of iniferter moieties around the MIP core. As mentioned before, such moieties are capable or reinitiating the polymerisation upon exposure to UV light, while the core MIP NPs are still bound to the solid-phase. The successful grafting of this secondary monomer around the MIP core was assessed by checking whether such fluorescent properties were retained after complete removal of any unreacted dye. In particular, bare MIP NPs were post-irradiated for 1 min in the presence of a solution of the fluorescent monomer in ACN. The obtained core-shell MIPs were then washed by means of the Amicon centrifugal units (30kDa as MWCO) and their fluorescence properties checked.

The excitation and emission spectra of fluorescent core-shell MIP NPs were similar to the spectra of the respective monomers, thus confirming the efficiency of the grafting procedure.
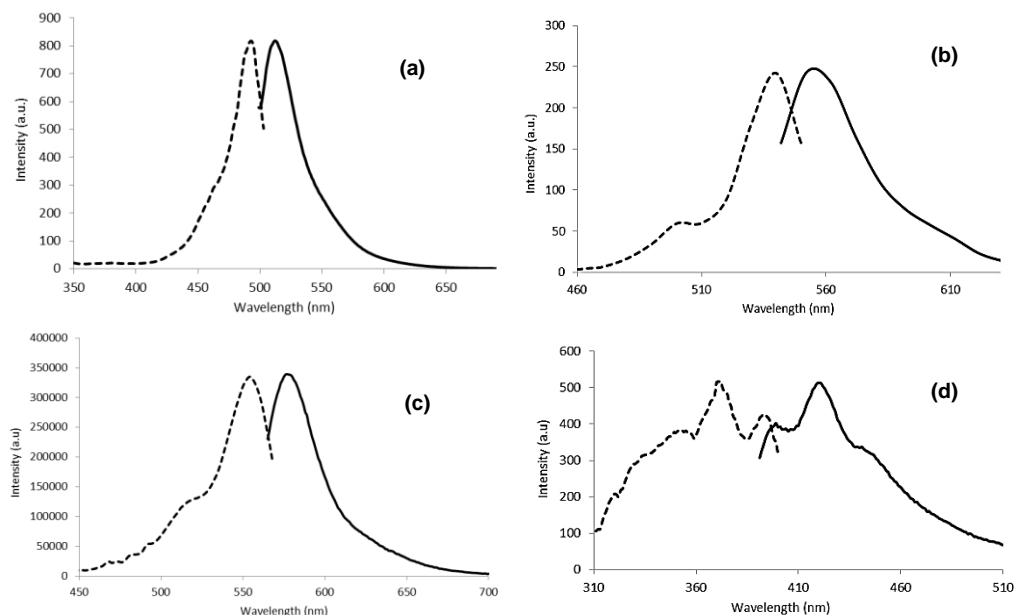
Figure 3-7. Excitation (---) and emission (—) spectra of *N*-fluorescein-MIP NPs (a), eosin-MIP NPs (b), rhodamine-MIP NPs (c) and anthracene-MIP NPs (d), at a concentration of 0.05 mg mL^{-1} in water.

3.3.5 Grafting of PEG – CytoViva analysis

The grafting of the PEG shell around the MIPs was assessed by a novel label-free technique called hyperspectral microscopy, integrated in a system called CytoViva®. Such hyperspectral imaging feature enables this instrument to spectrally characterize the sample by mapping its spectral emission. Different surface chemistries result in different spectral emission, each one being a unique spectral "fingerprint"[219]. In fact, the hyperspectral imaging feature records these spectral signatures within pixels associated with distinct areas in the image[220]. The advantage of this technique is that it allows unlabelled samples to be analysed and also spatially located (i.e. a nanoparticle within a cells). In this work, CytoViva instrument was employed to prove the surface modification of MIPs by analysing the spectral emissions of bare, PEG1100- and PEG4000-coated MIP NPs, each one having its own spectral fingerprint (Figure 3-8), as

recently done by other authors[221]. It should be noted that the CytoViva spectral resolution is 2 nanometers. Therefore, any peak shift higher than 2 nm is considered significant. Moreover, also the peak shape and width are used to distinguish between different coatings. Considering the three samples analysed, bare MIPs have a peak location at 468 nm and a half width spanning about 70nm. MIPs modified with PEG_{1100} have a peak location at 454 nm and a half width of 50nm. MIPs modified with PEG_{4000} have a peak location at 446nm and a half width of about 25nm. The consistent shape of the curves indicates that there is a common component, in this case, the bare nanoparticle. The peak shifting suggests that the coating obstructs the original spectral profile, meaning that the particle surface is different.
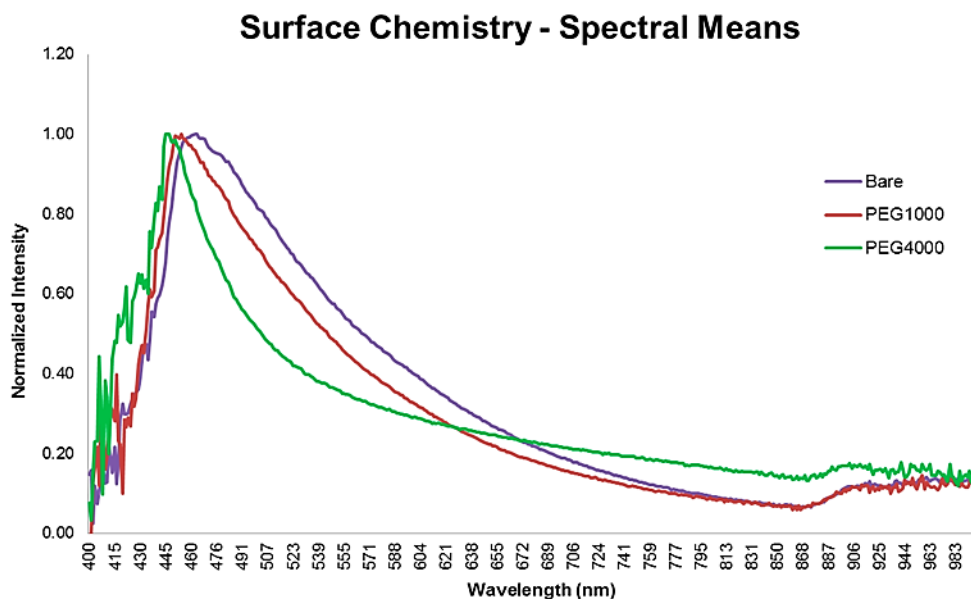
Figure 3-8. Spectral emission of bare MIPs (violet), PEG_{1100}-coated (red) and PEG_{4000}-coated (green) MIPs.

3.3.6 Biacore analysis

Biacore is a system based on the surface plasmon resonance (SPR) technique, capable of monitoring the binding properties of a given binder. In this system, one binding partner is immobilised on the sensor surface (a gold chip) and the other is injected and passes over the gold surface. The variation in mass on the gold surface due to the

binding event is detected and registered in a sensorgram, whose typical shape is shown in Figure 3-9. This binding event can be detected down to changes in mass of a few picograms/mm^2 on the chip, which corresponds to pico/nanomolar concentrations. This capability to detect such low concentrations is possible thanks to the SPR phenomenon, which occurs at the interface between two media with different refractive index (RI). In Biacore's case, the glass layer of the chip and the sample solution possess different RI. For the SPR to occur, a conducting film (gold in Biacore systems) is necessary between the two media. The light incident on the glass generates an electric field called evanescent wave. In fact, at a specific angle, this incident light generates electron charge oscillations (called plasmons) in the gold layer and such absorption of energy is registered as a drop in intensity of the reflected light. Such plasmons are non-radiative electromagnetic surface waves travelling on the boundary of the conductor (gold) and the external medium (sample).
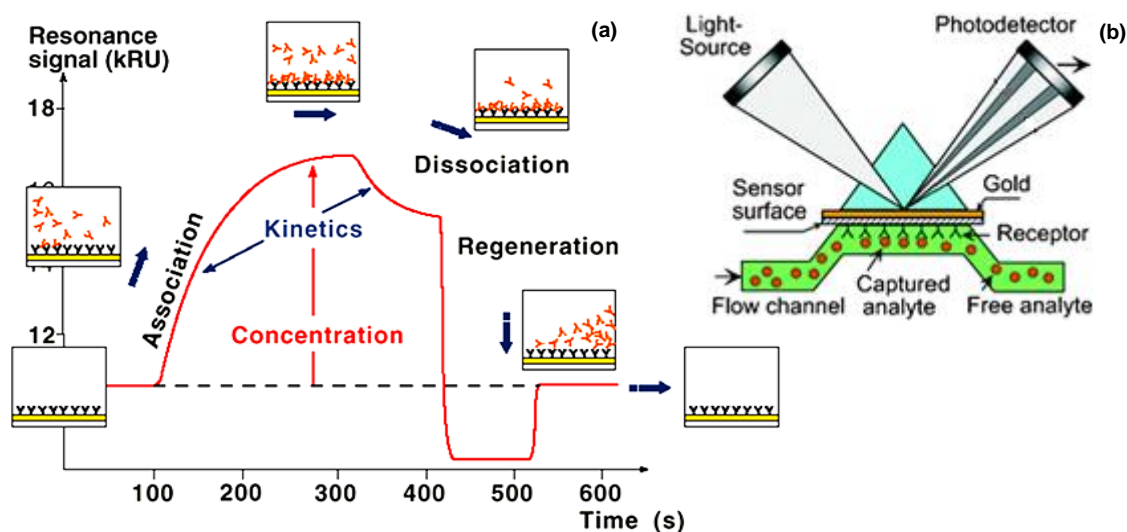
Figure 3-9. A typical Biacore sensorgram (a). Mechanism of detection based on the SPR effect (b).

Biacore analysis was employed to confirm that affinity and specificity of the core-shell MIPs was not affected by the grafting process. The template used in MIP synthesis, melamine, and its structural-analogue desisopropyl atrazine were then immobilised onto the surfaces of gold chips. The immobilisation procedure employed a spacer (GA) to

reduce steric hindrance issues. Afterwards, the core-shell MIPs were injected and analysed. As can be seen from Figure 3-10, the MIPs retained their specificity for the template. Both bare (a) and MIP NPs that were post-irradiated in the absence of any shell-forming monomer (b) exhibited specific binding to melamine, confirming that the post-irradiation process does not negatively affect the recognition properties of the particles. Furthermore, fluorescent core-shell MIPs show preferential binding to melamine over its analogue (d). Although the magnitude of the sensor response is different in each case, we can confirm that the grafting process did not adversely affect the rebinding properties of the NPs, thus proving that the template acts as a "protecting group" for the binding site during the derivatisation process. Interestingly, the surface modification with PEG methacrylate (MW 1100) increased the apparent response to both melamine and its analogue (c). It is possible that this may be an effect of the enhanced molecular weight and/or the change in the refractive index of the particle surface after PEGylation. Another contribution may come from the enhanced hydrophobic interactions potentially arising from the apolar carbon-carbon backbone created after PEG polymerisation. The hydrophobic interactions result from the association of two nonpolar moieties in water. This should be distinguished from the hydrophobic effect, which refers to the ordering of water molecules in proximity of a free (non-associated) hydrophobic compound. This effect determines a decrease in entropy, which is then offset when hydrophobic molecules associate since this leads to an increase in entropy. These hydrophobic interactions can be confirmed by the significant reduction in binding of the PEGylated NPs to desisopropyl atrazine when a surfactant (Tween 20) was injected in the system. However, such addition of Tween did affect significantly the binding of the NPs to melamine, thus proving the specificity of the particles. Similarly, fluorescent core-shell MIPs (d) showed specific binding.
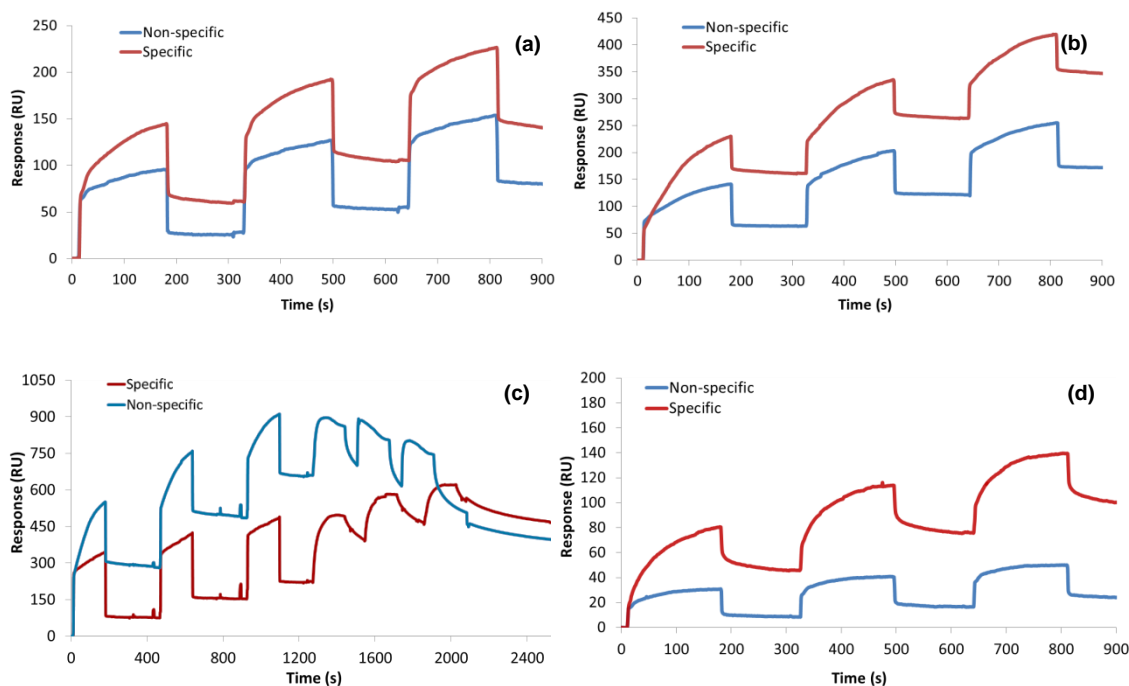
Figure 3-10. SPR sensorgrams of MEL MIP NPs: core MIP NPs (a), post-irradiated core MIP NPs (b) MIP NPs with PEG shell (c), MIP NPs with eosin shell (d). Analysis was performed using melamine (red lines) and desisopropyl atrazine (blue line) immobilised on gold chips, for specific and non-specific binding respectively. In the case of PEG-modified particles, MIP NPs were injected (first three injections), followed by a solution of Tween 20 0.005 % v/v (last three injections).

3.4 PERFORMANCE OF MIPs NPs IN PSEUDO ENZYME-LINKED IMMUNOSORBENT ASSAYS (ELISA)

3.4.1 Introduction

The enzyme-linked immunosorbent assay (ELISA) is one of the most widely employed tests in diagnostics. It relies on the use of antibodies to detect and quantify the target molecule. ELISA tests can be performed in different formats: direct, indirect, competitive and sandwich assays. In the direct format, either the antigen or the antibodies are immobilised on the surface of microplate wells. The binding of the counterpart (Ab or antigen) produces the analytical signal. In the indirect format, the antigen is first immobilised in the microplate and then

followed by the binding of the antibodies. Subsequently these are bound by a labelled anti-species antibody which generates the analytical signal. In the competitive format, the antibodies are first immobilised and then competition between the free analyte and the analyte conjugated with an enzyme occurs. In the sandwich format, a capture antibody is first immobilised on the surface of the wells and, after binding with the antigen, a detection antibody usually labelled with an enzyme is employed to quantify the target molecule. Typically the detection Ab is able to bind a different epitope of the antigen compared with the capture Ab.

Despite some advantages (high sensitivity and selectivity, easy operation), ELISAs exhibit several drawbacks mainly related to their high costs (due to the price of the antibodies) and poor stability of the reagents involved. In this regard, nanoMIPs thanks to their stability, cost efficiency and easy production, can be a promising alternative to antibodies in pseudo-ELISAs. However to date, a simple and reproducible method for coating the microplate well with MIPs is still missing. Although several papers demonstrated the applicability of MIPs in ELISAs[222-225], their use as Ab replacement in routine tests has not occurred yet. Some authors employed a MIP film to bind the target analyte, achieving a sensitivity in the micromolar region[226]. The use of nanoMIPs prepared by solid-phase approach as Ab-replacement can guarantee higher levels of sensitivity compared to "classical" MIPs due to the pseudo-monoclonal binding properties of the nanoMIPs themselves since, as described above, they exhibit a more uniform distribution binding site affinities. Recently our group described the use of nanoMIPs synthesised by solid-phase approach in a pseudo-ELISA assay for the quantification of vancomycin (1449.3 g mol^{-1})[77]. Encouraged by these results, we decided to investigate whether nanoMIPs imprinted for smaller analytes such as melamine could be successfully used in pseudo-ELISAs.

3.4.2 Materials and methods

Chemicals

Bovine serum albumin (BSA), horseradish peroxidase (HRP), 3,3′,5,5′-tetramethylbenzidine (TMB liquid substrate for ELISA), Tween 20, phosphate buffered saline (PBS) tablets, sodium dodecyl sulfate (SDS), 2-[morpholino]ethanesulfonic acid (MES), *N*-hydroxy-succinimide (NHS) and 1-ethyl-3-(3-dimethylaminopropyl)-carbodiimide hydrochloride (EDC) were obtained from Sigma-Aldrich, UK. Amicon Ultra-15 Centrifugal Filter Units (MWCO 30 kDa) and Nunclon 96 microwell plates were obtained from Fisher Scientific (UK). In all experiments double-distilled ultrapure (DI) water (Millipore, UK) was used. All chemicals and solvents were of analytical or HPLC grade and used without further purification.

Preparation of HRP-Melamine (HRP-M)

HRP (10 mg) was dissolved in 0.1 M MES buffer at pH 6 (1 mL). Ten times molar excess of EDC (0.4 mg) followed by NHS (0.6 mg) was then added. The reaction was allowed to proceed for 15 min at room temperature. Afterwards, the buffer was removed by using Amicon Ultra centrifugal filter units (30 kDa MWCO). The activated HRP was collected from the Amicon unit and incubated with melamine (1 mg/mL) in PBS at pH 7.4 for 2 h. Subsequently, the HRP−melamine conjugate (HRP−M) was washed by means of the previous centrifugal filter unit to remove free melamine. In particular, 10 washes with PBS (10 mL) were performed. Afterwards, the conjugate was dissolved in deionised water (2 mL) and stored at −18 °C until further use. This conjugate solution was employed as a stock solution.

Immobilisation of MIPs in microplate wells

40 μL of each type of MIPs (0.056 mg/mL) were dispensed into the wells of a 96-well microplate and the solvent was left evaporating overnight at room temperature.

Competitve assay using melamine-HRP conjugate

After the MIPs were immobilised in the microplate wells, these latter were conditioned by washing with PBS (2 × 250 μL), followed by blocking by incubation with PBS (300 μL) containing BSA (0.1%) and Tween 20 (1%) for 1 h. Wells were then washed with PBS (3 × 250 μL). A solution of HRP−Melamine (100 μL, 1:800 dilution from stock) was added to each well; this solution contained also different amounts of free analyte at a final concentration in the range of 0.001 and 6000 nM. Plates were incubated in the dark at room temperature for 1 h. Wells were then washed with PBS (3 × 300 μL), containing BSA (0.1%) and Tween 20 (1%), followed by addition of the TMB reagent (100 μL). After a 10 min incubation, the enzymatic reaction was stopped by the addition of H2SO4 (0.5 M, 100 μL). Colour development was determined by measuring the absorbance of each well at 450 nm using a UV−vis microplate reader (Dynex, UK).

3.4.3 Results and discussion

Once immobilised, the nanoMIPs were used in a competitive pseudo-ELISA to quantify melamine, exploiting the competition between HRP-Melamine conjugate and free melamine. The assay was carried out using the same conditions as in the assay developed for vancomycin[77]. Interestingly, nanoMIPs imprinted for melamine prepared in water by a persulfate-initiated polymerisation did not show specific binding to the HRP-Melamine conjugate. This could be due to the fact that, since melamine is a small molecule, it cannot form strong bonds with MIP in water due to competition with water molecules themselves. On the other hand, nanoMIPs prepared in organics by photopolymerisation showed affinity for the conjugate (Figure 3-11 a). Therefore only the nanoMIPs prepared by photopolymerisation were further assessed.

In order to evaluate their specificity, the nanoMIPs were incubated with the conjugate (3.1 μg mL^{-1}) for 1 hour. After a washing step, the substrate TMB was added and incubated for 10 minutes. The enzymatic reaction was quenched with H_2SO_4, and then

the colour produced in the wells was read at 450 nm using a UV/visible microplate reader. As shown in Figure 3-11 a, the nanoMIPs produced in organics showed specific binding to the conjugate, as there is a significant difference in signal between wells with and without nanoMIPs. It should be noted, however, that bare nanoMIPs imprinted for melamine by polymerisation in organic solvent also did not show good performance in ELISA (Figure 3-11b) due to the fact that they do not stick to the surface of the microplate (relatively hydrophilic) because of their hydrophobicity. For this reason core-shell nanoMIPs based on PEG were produced. This would increase their surface hydrophilicity, protecting at the same time the particle binding sites. PEG coated nanoMIPs were prepared as described in the experimental above.

The competitive pseudo-ELISA was performed using concentrations of free melamine between 10 and 6000 nM, added to the microplates at the same time as the conjugate. Competition was achieved over 3 orders of magnitude, with linearity from 10 nM to 6000 nM and a limit of detection of 25 nM, calculated as the concentration value obtained from 3 times the standard deviation of the control (in absence of enzymes). The assay showed saturation at concentrations of analyte higher than 6000 nM.
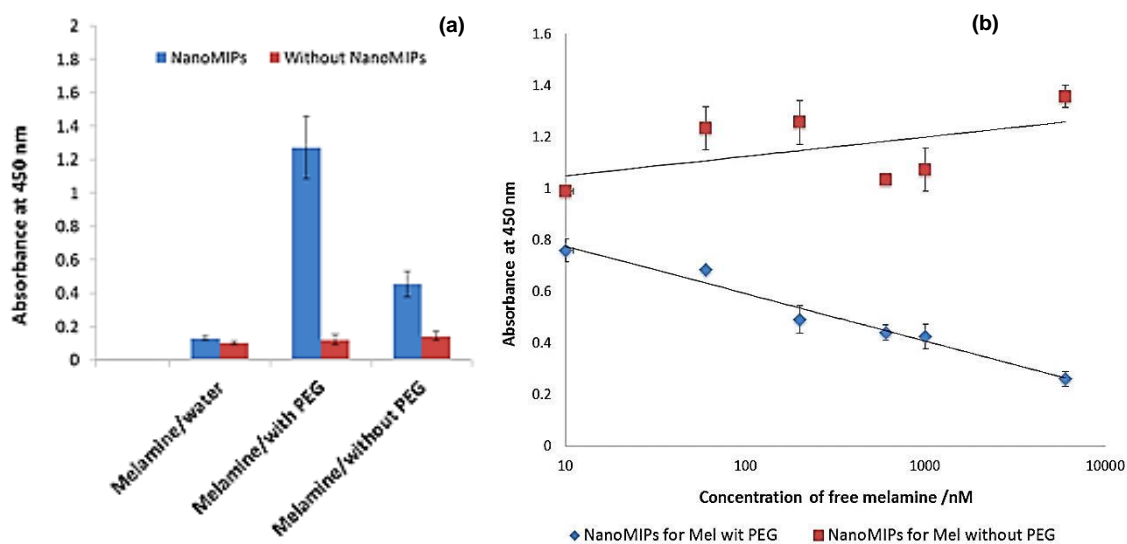
Figure 3-11. Binding of the HRP-Melamine conjugate to melamine-imprinted nanoMIPs (a). Bare microplates wells (blocked and washed) were used as controls. Calibration curves obtained with nanoMIPs imprinted for melamine with and without PEG shell (b) (adapted with permission from Caceres *et al.*, Analyst 2016. Copyright 2016, The Royal Society of Chemistry).

Therefore the presence of the PEG shell is pivotal to ensure a good performance in pseudo-ELISAs using nanoMIPs imprinted for melamine (and possibly other small molecules), since in the case of nanoMIPs without PEG shell successful competition was not achieved.

3.5 CONCLUSIONS

Fluorescent NPs imprinted against melamine were synthesised employing an innovative solid-phase synthetic approach, which involves the immobilisation of the template molecules onto micro-sized glass beads. This method allows both synthesis and purification of high-affinity MIP NPs. Furthermore, both bare and core-shell imprinted NPs were produced. In the latter case, the method is very useful for performing surface functionalisation of MIP NPs, being capable of potentially addressing the requirements in a wide range of applications. Since the particle's surface is modified while the nanoMIPs still interact with the templates on the solid-phase, their binding sites are protected and thus their recognition properties remain unaffected.

PEGylated MIPs exhibited improved colloidal stability in water thanks to the steric effect of the PEG chains which reduces the agglomeration tendency of the nanoMIPs over the time. Furthermore, the surface modification of nanoMIPs with such hydrophilic shell allows them to be employed in ELISA-like assays, since bare nanoMIPs are too hydrophobic to interact with the surface of the microwell plates.

4 SOLID-PHASE SYNTHESIS OF MIP NANOPARTICLES IN WATER

4.1 INTRODUCTION

Considering the poor stability of biomacromolecules such as proteins and enzymes in organic solvents, imprinting in aqueous environment is the method of choice for these targets, as aqueous conditions are appropriate to maintain the protein structure as close as possible to its native state. As previously demonstrated by Hoshino *et al.*, nanoMIPs based on acrylates and obtained through a persulfate initiated polymerisation performed well as recognition tools against proteins and peptides[115, 224]. The presence of both basic and acidic monomers in the polymerisation mixture allows virtually all residues within a protein or a peptide to be targeted. On the other hand, as demonstrated in chapter 3, the polymerisation in organic solvents has proven to be advantageous for imprinting of small molecules (Mw < 500 Da), avoiding the disruptive effects of water (due to its hydrogen-bonding capacity) in relation with imprinting of molecules which possess a limited number of interaction points with the monomer (as opposed to larger molecules such as peptides or proteins). Polymerisation in water is advantageous because of it is environmental friendly and easy to handle, especially when further purifications (e.g dialysis) are required.

As previously demonstrated by other authors, however, persulfate-initiated polymerisation may lead to oxidation of methionine and tryptophan residues[227]. The oxidation of these residues is inhibited in the presence of TEMED, suggesting that the persulfate anion is the oxidative specie. In fact, it was proven that TEMED accelerates the homolytic scission of the persulfate anion, producing the bisulfate free radical $(HSO_4^•)$[228]. The level of such oxidation can be minimised by pre-incubation of the persulfate with TEMED (1 h), by reducing the polymerisation time or the persulfate concentration, or by increasing the concentration of TEMED[227]. However, very recently, it has been demonstrated that the TEMED radical can induce methylenation on proteins or peptides when lysine is next to arginine, cysteine, proline, glutamine, aspargine, histidine, tryptophan, tyrosine, and aspartic acid residues[229]. When TEMEC

was replaced with sodium bisulfite, such modification did not take place. These findings demonstrate that the choice of the initiator/catalyst pair plays an important role in the integrity of the protein or peptide used as a template in the polymerisation process.

4.2 MATERIALS AND METHODS

4.2.1 Chemicals

N-isopropylacrylamide (NIPAm), *N,N,N′,N′*-tetramethylethylenediamine (TEMED), ammonium persulphate (APS), acrylic acid (AAc), *N,N′*-methylenebisacrylamide (BIS), *N*-tertbutylacrylamide (TBAm), PBS, tris(hydroxymethyl)aminomethane (TRIS), 3-aminopropyltrimethyloxysilane (APTMS), glutaraldehyde (GA), calcium chloride, cysteamine, α-amylase, pepsin A, ethanol, toluene and acetone were purchased from Sigma-Aldrich (UK). Trypsin was purchased from Thermo Fisher Scientific (UK). Sodium hydroxide was obtained from Fisher Scientific (UK). Double-distilled ultrapure water (Millipore) was used for analysis. All chemicals and solvents were analytical or HPLC grade and were used without further purification.

4.2.2 Preparation of template-derivatised solid-phase

The solid-phase used for the synthesis of nanoMIPs in water was prepared as described in 3.2.2. For the immobilisation of peptides through the –SH group, 60 g of glass beads were placed in a solution of SIA linker (0.2 mg/ml) in acetonitrile for 2 h in the dark. The succinic moiety allows the linker to react with the solid-phase, and the haloacetyl group enables coupling with the thiol group intentionally added on the N-terminus of the peptide sequence of interest.

In case of templates bearing a –COOH group, the beads after being silanised were placed in a solution of the template in PBS pH 7.2 with 10 fold molar excess of EDC and 15 molar excess of NHS, to allow activation of the carboxyl groups for the subsequent reaction with the $–NH_2$ groups on the solid-phase.

4.2.3 Solid-phase synthesis of fluorescent MIP NPs

The procedure has been adapted from Hoshino *et al.*[115]. The following monomers were dissolved in H_2O (100 mL): NIPAm (39 mg), BIS (2 mg), TBAm (33 mg), *N*-(3-aminopropyl)methacrylamide hydrochloride (AMPA, 5.8 mg) and AAc (2.2 µL). TBAm was previously dissolved in EtOH (1 mL) and then added to the aqueous solution. The total monomer concentration was 6.5 mM. When fluorescent MIPs were required, either 2.6 mg of *N*-fluoresceinylacrylamide (*N*-fluo) or 2.36 mg of methacryloxyethyl thiocarbamoyl rhodamine b (RHOD) where used, according to the final requirements in terms of excitation/emission properties. The solution was degassed and sonicated for 5 min, and then purged with N_2 for 20 min. The polymerisation was started by adding an APS aqueous solution (800 µL, 60 mg/mL) and TEMED (24 µL). The polymerisation was then performed at room temperature for 1 h. Subsequently, the content of the polymerisation vessel was poured into a SPE cartridge (60 ml) equipped with a frit (20 microns porosity). 9 washings with 20 ml of distilled water at room temperature were carried out to remove low affinity MIPs and polymer chunks. Afterwards, the SPE cartridge containing the solid-phase was placed in a water bath at 65°C for 15 min. 20 ml of distilled water pre-warmed at 65°C were poured into the SPE to collect the high affinity MIPs. This action was repeated 5 times, until about 100 ml of a solution of high affinity MIPs in water were collected.

4.2.4 Size, concentration and fluorescence analyses

DLS, SEM and fluorescence analyses were carried out as described in Chapter 3. It was not possible to perform NanoSight analysis because of the low refractive index (probably due to a low cross-linking degree) of the MIPs produced in water. This results in the MIPs being "invisible" to the instrument, because of the low amount of scattered light.

4.2.5 Affinity analysis

In a typical MicroScale Thermophoresis (MST) experiment a dilution series of 16 dilutions was prepared. The concentration of the fluorescently labelled partner (the MIP NPs) was kept constant and the concentration of the ligand was varied. Serial dilutions of the non-labelled ligand (trypsin and vancomycin) were prepared using phosphate buffer 0.1 M. The samples were mixed and then loaded into glass capillaries, followed by MST analysis performed using the Monolith NT-115. Because of the specific requirements from the MST manufacturer, the MIP NPs were previously labelled with a proprietary dye (NT-647) suitable for analysis with the Monolith NT-115. In particular, 20 ml of vancomycin and trypsin MIP NPs bearing $-NH_2$ groups (coming from the AMPA monomer) were first washed 4 times with 15 ml of distilled water, by means of the Amicon centrifugal units (50kDa MWCO), to remove excess of unreacted monomers. Then the MIP NPs were placed in a vial to react with 6.7 µg of the NT-647 NHS-derivative (previously solubilised in 20 µl of DMSO) for 1 h. The excess of unreacted dye was removed by filtration through Amicon centrifugal units (50kDa MWCO, 5 washes with 15 ml), until about 1 ml of NT-647-labelled MIP NPs was collected and used for the MST analysis.

4.3 RESULTS AND DISCUSSION

4.3.1 Synthesis of fluorescent MIP nanoparticles in water

The synthesis of MIP nanoparticles by persulfate-initiated polymerisation was performed using water-soluble acrylate monomers. The presence of AMPA and AAc in the polymerisation mixture ensures that both acidic and basic residues in the peptide sequence can take part in the formation of the binding sites. In contrast with the UV-synthesis in organics, the polymerisation in water does not allow sequential polymerisations, however, it is the only option for the imprinting of proteins, since an organics-based synthesis would lead to denaturation of the protein itself. The non-living character of this polymerisation gives less control over the particle size and size distribution compared to iniferter-based methods. Depending on the final application,

the nanoMIPs were fluorescently tagged by using either *N*-fluo or RHOD. These two monomers are suitable for most of the cell-based analyses (flow cytometry and confocal microscopy).

Biotin, vancomycin and trypsin (respectively small, medium and large molecules) were used as model templates to prove the synthesis of fluorescent MIPs. Biotin and vancomycin were used to produce fluorescent control MIPs in the experiments with cancer cells. An epitope for Epidermal Growth Factor Receptor (EGFR) targeting (CSLNITSLGLRSLKEISDG) and another (CEYASRVNHVTLSQPKIVKW) for targeting an overexpressed protein present on the surface of senescent cells were employed to produce fluorescent MIPs for imaging purposes (Chapter 7). The synthetic protocol employed relies on the incubation of the template-derivatised beads with the polymerisation mixture for 1-2 h, in the presence of ammonium persulfate as initiator and TEMED as catalyst. The subsequent temperature-based affinity separation was performed first at room temperature to remove low-affinity MIP NPs, followed by elution of the high affinity MIPs at 65°C, similarly to what was performed for the imprinted particles produced in acetonitrile (Figure 4-1).
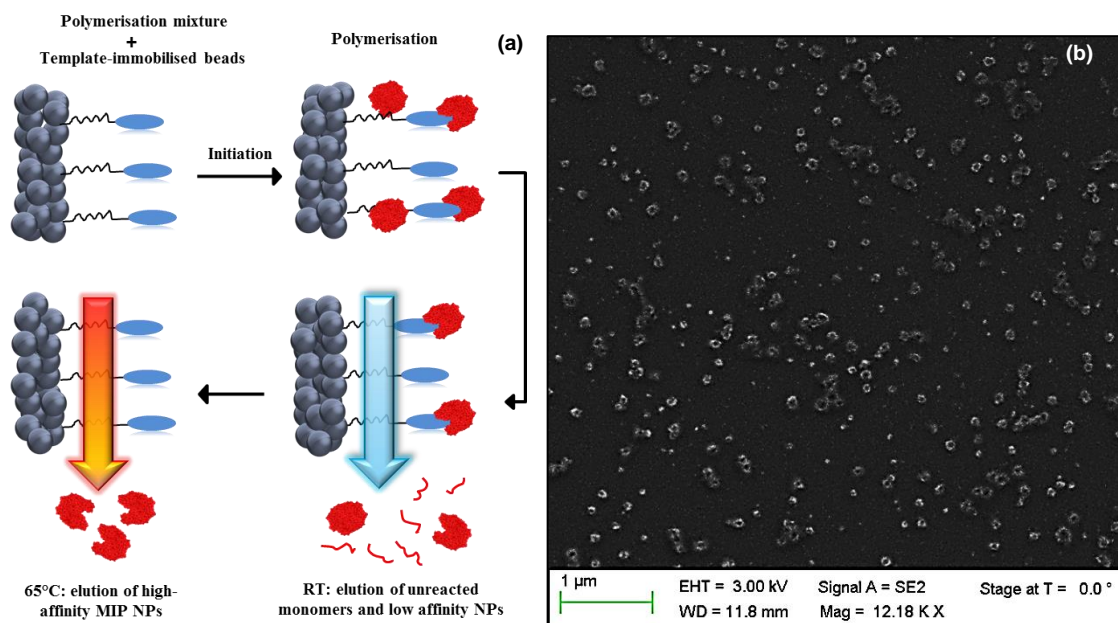
Figure 4-1. Scheme of the solid-phase synthesis in water (a). Representative SEM image of fluorescent MIPs imprinted for vancomycin (b).

4.3.2 Affinity analysis

A novel technique, called MicroScale Thermophoresis (MST), was used to assess the binding of vancomycin and trypsin MIP NPs. MST is a rapid and easy technique to quantify biomolecular interactions between a given pair (two proteins, or a protein and a nanoparticle). It detects changes in the charge, hydration shell, or size of molecules by measuring variations of the mobility of molecules in microscopic temperature gradients, an effect termed "thermophoresis"[230]. The mobility of a fluorescently label partner in a buffer solution is followed over the time and, as the binding of a non-fluorescent ligand changes one of the aforementioned properties, the binding is quantified by measuring the variation in thermophoresis at different ligand concentrations.

MST allows to work under conditions close to the natural ones (e.g. both interacting partners free in solution), without any need to immobilise one of the partners as done in SPR. Another advantage is the low sample consumption (4 µl per sample at nM concentration) and the possibility to detect K_d in the pM to mM range. Moreover the instrument is virtually maintenance-free, only needing capillaries to load the sample.

The thermophoretic mobility of the fluorescent partner is measured by monitoring the fluorescence distribution (F) within a capillary (Figure 4-2A). An IR laser (1480 nm) produces a microscopic temperature gradient, raising the temperature of the aqueous solution in the laser spot by 2-6°C. Prior the activation of the IR laser, a homogenous distribution of the partners (both the fluorescent and the non-tagged ones) is observed in the capillary. When the laser is then switched on, two effects are observed. Initially, the fluorescence of the dye changes due to its intrinsic temperature dependence. As a second response, the fluorescent partner diffuse from the locally heated region to the outer cold region, and therefore the concentration of partners in the heated area decreases (until it reaches a steady state after typically 10-30 s)[231] (Figure 4-2B).
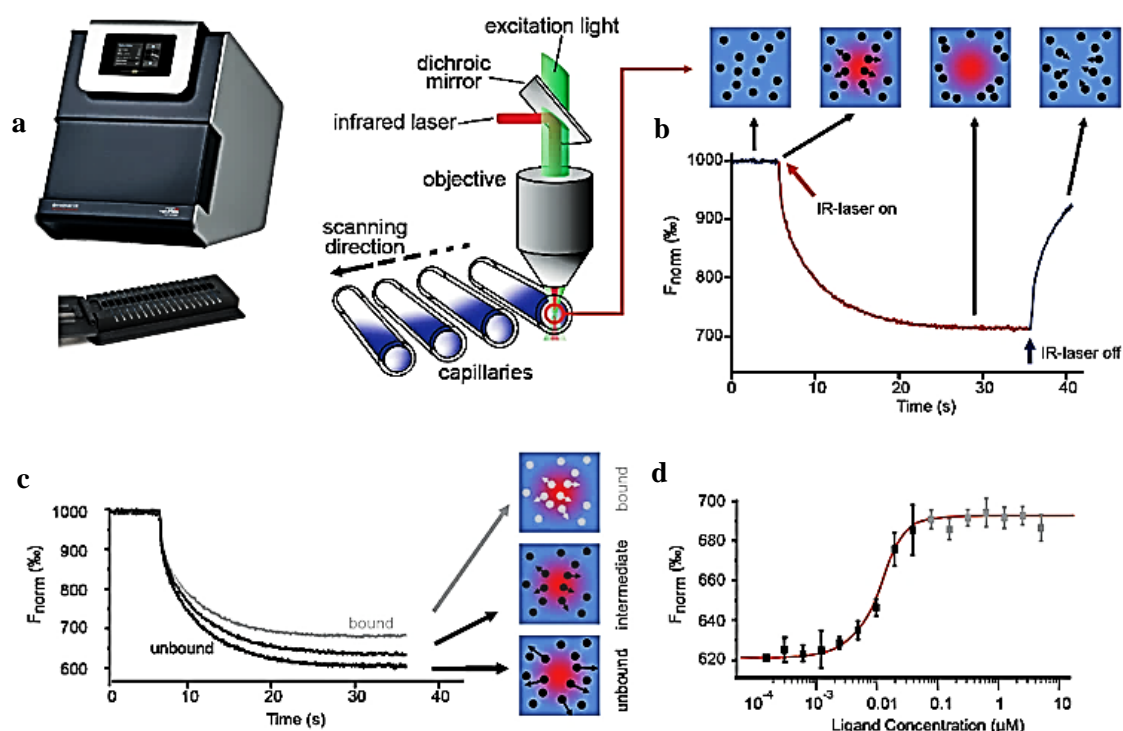
Figure 4-2. MST instrument and schematics of its optics (a). Schematic representation of MST optics. Typical signal of an MST experiment (b). Example of binding experiment (c) used to derive a binding curve (d): the thermophoretic movement of the fluorescent partner (''unbound'', black trace) changes upon interaction with a non-fluorescent partner (''bound'', grey trace). The changes in fluorescence are plotted to obtain a dissociation constant (reproduced with permission from Jerabek-Willemsen *et al.*, Journal of Molecular Structure 2014).

In a typical experiment, the concentration of fluorescent partner [P] is kept constant, whereas the concentration of ligand [L] is varied in a dilution series. For the calculation of binding constants, several capillaries with constant concentrations of the fluorescent partner and increasing amounts of ligand are scanned. Within the titration experiment, F changes according to:

F = (1-x) F[P]+ x F [PL]

The fluorescent signal obtained from the above equation directly corresponds to the ratio of fluorescent partners that formed the complex x = [PL]/[P] which then can be used to obtain K_d.

After the instrument has recorded the MST curves for each capillary, the software plots them on a graph. The software then calculates automatically the binding by plotting the ratio between the fluorescence of the partner when the laser is on and the fluorescence before the laser is turned off. Since each curve represents a different concentration of binding partner, the software can automatically fit the data and give a K_d.

Trypsin MIP NPs were previously functionalised with amine groups, by adding the AMPA monomer in the polymerisation mixture, and then coupled to an NHS derivative of the fluorescent dye NT-647. The concentration of NT-647 labelled MIPs was kept constant, while the concentration of the non-labeled trypsin was varied between 5 μM – 0.15 nM. Raw thermophoresis traces from each concentration of trypsin are reported in Figure 4-3a. The MST traces are bumpy (highlighted in black) indicating aggregation of the MIPs. To remove aggregates, the MIPs were filtered through a 0.45 μm filter (Figure 4-3b). These experiments demonstrate the speed and ease of optimisation in MST and the fact that a visualisation of particle aggregation can be clearly obtained.
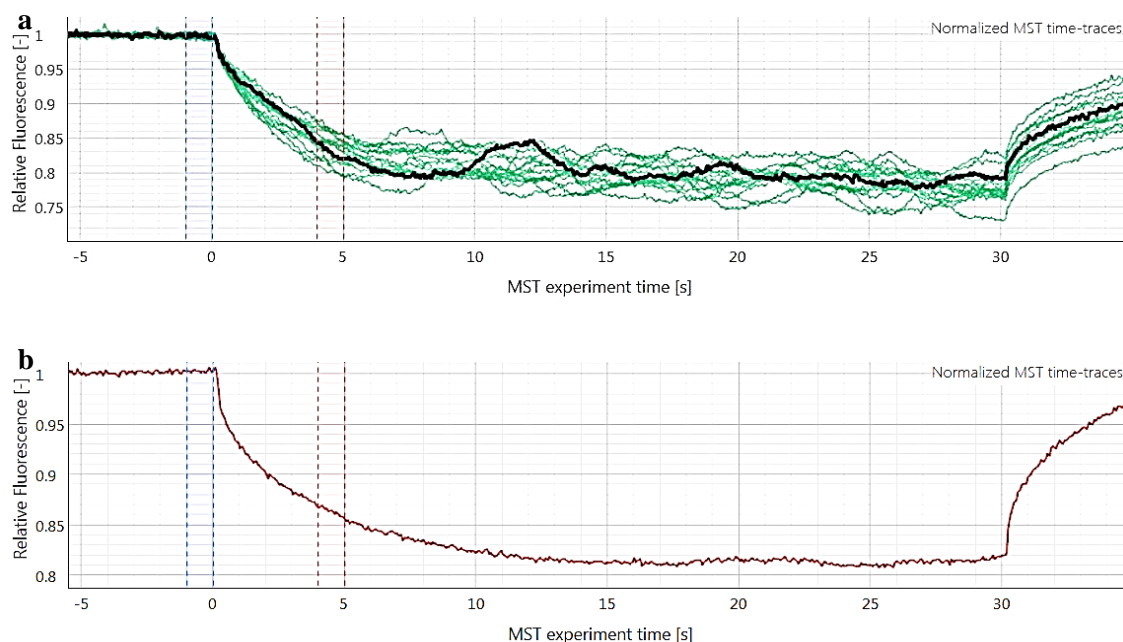
Figure 4-3. Raw thermophoresis traces of trypsin MIP NPs (a), showing high level of aggregation (ongoing or already occurred). Representative trace after 0.45 μm filtration (b).

A K_d of 85 nM was determined for this interaction (Figure 4-4). Unfortunately, the high level of aggregation of vancomycin MIP NPs, albeit reduced after 0.45 μm filtration, determined high noise which did not allow a neat calculation of the K_d. However, the K_d values calculated for trypsin MIPs were not in agreement with those previously calculated by SPR (5.5 pM)[232]. This could be explained by the potential conjugation of the NHS-dye with –NH_2 groups coming from AMPA possibly present in the active sites of the MIPs, thus altering the recognition properties of those binding sites affected by the such conjugation. Interestingly, when melamine was used as a template (iniferter-mediated polymerisation) and the –NH_2 groups for the conjugation with the NHS-dye were grafted around the MIP core (as a shell, thus not affecting the binding sites), the K_d values obtained for melamine MIP NPs from MST (20 nM) were in good agreement with those from Biacore (63 nM)[202]. This can be explained by the fact that by grafting a shell around the MIP core (iniferter-based polymerisations) the conjugation with the dye is limited to the outer part of the MIP, with no disruption of the binding sites. Furthermore, the amine shell helps in reducing the aggregation tendency of the MIP NPs, as shown by "cleaner" thermophoresis traces.
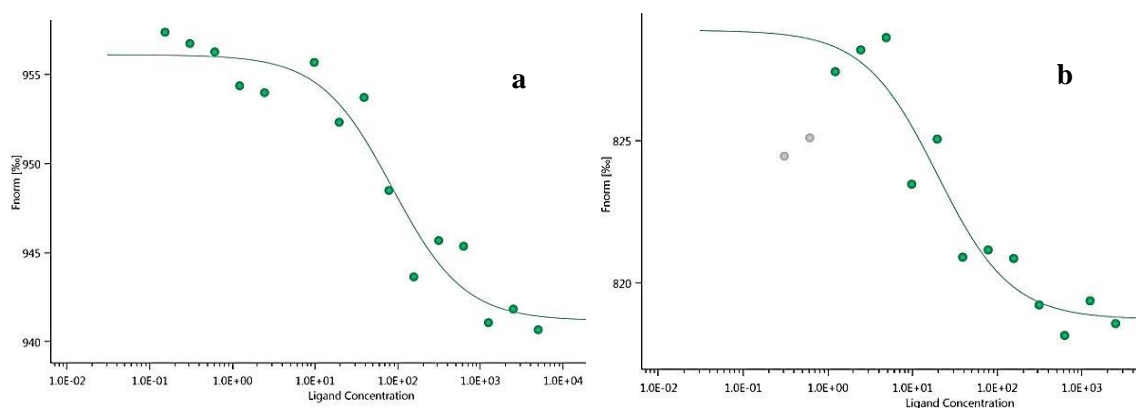
Figure 4-4. Binding curves for trypsin (a) and melamine (b) MIP NPs. Ligand concentration is in nM.

4.3.3 Automatic synthesis of MIP NPs

One of the advantages of this solid-phase synthesis is the possibility to automate the synthetic process, thus reducing the labour required. In the last two years, 3 prototypes

have been developed in Cranfield Health and assembled by HEL Ltd. (UK). The first model was designed for a UV-based polymerisation in organics and employed in this work for preliminary synthesis of fluorescent MIP NPs. As shown in figure 4-5, the equipment is composed of multiple liquid supplies (4 independent lines), a UV-light source (2×8 W lamps), a reaction column containing the template-immobilised beads (6.6 mm diameter $\times$ 150 mm), a temperature controller for the column, a 6-ways valve for the separation of waste from product and a computer control system which allows the control of some reaction parameters.
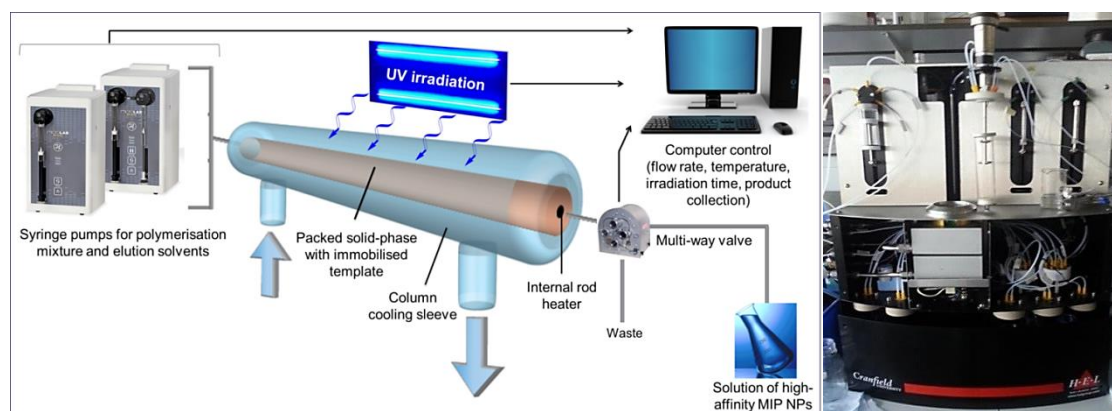
Figure 4-5. Scheme of the automated reactor for the solid-phase synthesis of MIP NPs (left). Image of the last module developed for both polymerisations in water and organics.

The second automatic model was adapted for a persulfate-initiated synthesis in aqueous environment. The chamber containing the solid-phase is capable of shaking to allow the homogenisation of the content, whilst an inert-gas line inlet removes the oxygen. Eventually the last model, delivered by HEL last year, was further developed for both photopolymerisation in organics and persulfate-initiated polymerisation in water (Figure 4-5 on the right). In this last model, the shaking is performed by a rotating stirrer present inside the chamber and the UV-light source is a LED-type.

4.4 CONCLUSIONS

The same solid-phase approach employed for the synthesis of MIP NPs in organics proved to be successful for the production of water-soluble fluorescent nanoMIPs. Fluorescent MIP NPs imprinted against biotin, vancomycin and trypsin (respectively small, medium and large molecules), as well as against two peptides for targeting cancer and senescent cells were produced. The last two templates were used to produce fluorescent MIP NPs for imaging purposes, further described in chapter 7. Interestingly, it was possible to assess the rebinding properties of trypsin MIPs by means of a novel technology called Microscale Thermophoresis. This method requires one of the interacting partners to be fluorescently labelled and allows working under conditions close to the natural ones (both interacting partners are free in solution). However, the presence of agglomerates in vancomycin MIP NPs interfered with the binding events, thus preventing the calculation of a K_d. Overall, this technology showed potential for the characterisation of binding event between nanoMIPs and the respective ligand in solution, although some optimisation is required to minimise the effect of agglomeration.

5 STABILITY AND BIOCOMPATIBILITY EVALUATION OF IMPRINTED NANOPARTICLES

5.1 INTRODUCTION

Although nanotechnology holds immense promise for diagnostics, not many nanoparticulate systems are currently employed in routine practice, mainly due to the lack of a complete toxicological assessment[233]. MIP NPs represent an innovative, cheap and robust alternative to their natural counterparts such as antibodies. Despite several successful applications of MIP NPs within sensors or assays[76, 200, 234], such nanoparticles have not been applied for *in vivo* diagnosis/therapy, besides the two works reported in Chapter 1. However, no comprehensive biocompatibility studies have been carried out so far. Even the inflammatory response of MIP NPs is still unknown, thus preventing them from being considered for any clinical *in vivo* applications. To better understand how MIP NPs would behave *in vivo*, their cytotoxicity evaluation, including viability and cytokine release assays, was carried out. Using the aforementioned solid-phase synthesis, potentially biocompatible core-shell imprinted NPs were produced, by employing two poly(ethylene glycol) (PEG) monomers with different molecular weights (Mw), 1100 and 4000 Da. PEG_{1100} was chosen initially since it has been shown to successfully increase the stability of MIPs in solution during storage, without affecting their rebinding properties[203]. Despite the extensive use of PEG in the last two decades, there is no general consensus on the optimum molecular weight and coverage-density of PEG for a certain nanosystem/application[214].

In this chapter, the effects of surface modifications on stability and cytotoxicity of MIP nanoparticles are analysed, together with an assessment of the cell metabolism and the cytokine release in the presence of said MIPs (performed in collaboration with Cork University and GlaxoSmithKline respectively). We demonstrate that toxicological evaluations based only on viability tests might be misleading, since cells are able to compensate to some extent for the effect of particle exposure and, in general, adapt their metabolism under external adverse factors, as demonstrated with other nanosystems[235, 236]. Considering that both biocompatibility and uptake depend on the polymer

composition and surface chemistry (regardless of the imprinting process), herein we will focus on the effect of surface modifications on the cytotoxicity and internalisation of NPs within cells.

5.2 MATERIALS AND METHODS

5.2.1 Chemicals

Paraformaldehyde (PFA), Dulbecco's Modified Eagle's medium (DMEM), D-glucose, DiO (3,3'-Dioctadecyloxacarbocyanine Perchlorate), D-galactose, L-glutamine, sodium pyruvate, antimycin A, cell lysis agent (CelLyticTM) and toluene were purchased from Sigma-Aldrich, UK. Acetonitrile (ACN), ethanol and Amicon Ultra-15 Centrifugal Filter Units (MWCO 30 kDa), coverslips and microscope slides were obtained from Fisher Scientific (UK). Methanol and acetone were purchased from VWR (UK). *N,N*-diethyldithiocarbamic acid benzyl ester was bought from TCI Europe (Belgium). Methacryloxyethyl thiocarbamoyl rhodamine B was obtained from Polysciences Europe. Mouse embryonic fibroblasts (MEFs), HT1080, NR8383 macrophages and human keratinocytes (HaCaT) were purchased from American Tissue Culture Collections (ATCC, Manassas, VA). O_2-sensitive probes MitoXpress37 and pH-sensitive probe pH-Xtra were from Luxcel Biosciences (Cork, Ireland). CellTiter-Glo® ATP Assay was from Promega (Madison, WI). Ham's F12 medium, heat inactivated FBS, sodium bicarbonate and penicillin/streptomycin solutions were purchased from Invitrogen. The LDH assay kit was obtained from Roche. Mineral oil was from Cargille Laboratories (Cedar Grove, NJ). Deionised water obtained from a Millipore (MilliQ) purification system at a resistivity of 18.2 MΩ cm was used for analysis. All chemicals were analytical or HPLC grade and were used without further purification.

5.2.2 Size and concentration analysis of MIP nanoparticles

DLS and Nanosight analyses were performed according to chapter 3.2.5.

5.2.3 Cell culture and experimental conditions

HT1080 and MEFs cells were grown in DMEM medium supplemented with 15 mM HEPES (pH 7.2), 2 mM L-Gln, 10% fetal bovine serum (FBS), 100 U/ml penicillin/100 µg/ml streptomycin (P/S) in humidified atmosphere of 5% CO_2 and 95% air at 37°C. MEFs were seeded at 4×10^5 cells/well on 96-well plates (Greiner) coated with 0.01% collagen IV, grown for 1 days prior to NP addition. The NPs were made up in plain DMEM containing HEPES, 2mM L-Gln, 10mM glucose and 1mM pyruvate. The experiments were conducted in this medium. The NR8383 macrophages were grown in Kaighn's modification of Ham's F12 medium (F12K) with 2 mM glutamine and 1.5g/L sodium bicarbonate. It was also supplemented with 15% heat inactivated FBS and 100units/ml penicillin/100µg/ml streptomycin. In all tests, exposure time ranged between 24-72 h. For the viability and cytokine endpoints, cells were seeded into 48-well tissue culture plates at a density of 4.8 x 10^5 cells/ml (6 x 10^4 cells/well) and incubated at 37ºC with 5% CO_2, in a humidified atmosphere for 1-2 h. Media containing the test compound treatment was then added at twice the final concentration required and incubated for 72 h. 10 min before the end of the 72 h treatment period, Triton X-100 solution was added to the LDH positive control cells.

Macrophages were routinely maintained in T75cm^2 tissue culture flasks (20mL) or T175cm^2 tissue culture flasks (50mL) as both floating and attached cell populations. Media was changed twice per week, which involves resuspending cells into fresh media on the first occasion and diluting the cell population into fresh T75cm^2 or T175cm^2 flasks on the second occasion. The procedure used for maintaining the cultures involves removing nearly all the culture medium but leaving enough to cover the loosely attached population on the bottom of the flask (this loosely attached population of cells does not spread on the surface of the plastic). The removed medium is centrifuged at 340g for 5mins at room temperature and the medium discarded. The pellet is gently resuspended back into ~20mL or ~50mL (T75 or T175 respectively) of fresh culture medium and put back into the same flask.

Diluting the cell population was carried out by gently scraping the loosely attached cells into the existing culture media when near confluency is reached. The resultant cell

suspension was collected and centrifuged at 340g for 5 mins at room temperature and the supernatant discarded. The pellet was gently resuspended into a suitable volume of fresh medium (equilibrated at 37°C and 5% CO_2), aspirated to a single cell suspension, and a cell count taken using a haemocytometer. Cells were seeded back into T75cm^2 flasks at ~2×10^5 cells/mL in 20mL (4×10^6 total) and ~3.5×10^5 cells/mL in 40mL in T175cm^2 flasks (~14×10^6 total). Approximately 50% of these cells would attach and 50% would become a floating population. All flasks were incubated at 37°C with 5% CO_2, in a humidified atmosphere. In all tests, exposure time ranged between 24-72 hours.

5.2.4 MTT test

The cytotoxicity of imprinted NPs was evaluated by MTT colorimetric assay. HaCaT cells were seeded onto 96-well microplates at a density of 5×10^4 cells/well and treated separately with three concentrations of MIP NPs for 24 h. A density of 8×10^3 cells/well was employed for 48 h exposure to allow sufficient room for the cells to grow. Cells incubated in NP-free media were used as a control. The number of cells in each well was chosen in order to obtain an absorbance value between 0.8 and 1.2, so that both inhibition and stimulation of cell proliferation can be evaluated. 20 μl of MTT working solution (5 mg/ml in PBS) was added to each well and incubated at 37°C for 4 h in the darkness. The medium was then removed and washed with PBS solution. The produced formazan salts were dissolved using 150 μl of DMSO. The assay was run according to the official procedure of the manufacturer (MTT Cell Proliferation Assay). Afterwards, the absorbance was measured at 570 nm by means of a microplate reader (MRX DYNEX®, Magellan Biosciences, Chelmsford, MA, USA).

5.2.5 LDH assay on macrophages

Each MIP suspension was treated to 3 rounds of 10 min stirring and 1 min sonication before being diluted. A serial dilution was carried out in complete culture media to obtain the concentration range required before diluting 1 in 2 directly into the wells containing cells and media only. These dilutions were mixed before adding to cells. The

48-well plates were centrifuged at 805g for 10 min. 50µl of the supernatant were then transferred to flat bottom 96 well plates for leaked LDH measurements, the remaining supernatant was transferred to a V bottom 96 well plate for cytokine assessment. 250µl of the cell lysis agent (CelLytic^{TM}) were added to the 48 well plates for incubation at RT for 15 min whilst shaking. After lysis, the plates were centrifuged at 805g for 10 min. 50µl were removed to another flat bottom 96 well plate for lysed LDH measurements.

Directly following preparation of the leaked and lysed 96 well plates, the LDH reaction mix was prepared as described in the protocol supplied with the LDH assay kit (Roche 11 644 793 001) and 50µl added to each well. Plates were incubated for 30 min at RT protected from light (without shaking). The absorbance was read at 490 nm on a Spectromax absorbance plate reader, with a wavelength correction at 650 nm. The % leaked LDH of total LDH (leaked + lysed) was calculated.

5.2.6 ATP assay

ATP was quantified using CellTiterGlo® assay, the assay was conducted according to the manufacturer's specifications. After the NP exposure was complete, 100 µl of CellTiterGlo® reagent was added to each well. Intensive shaking of the plate for 2 min was done using Victor 2 reader (PerkinElmer). Samples were transferred into wells in a white 96-well plate and read on a Victor 2 plate under normal luminescence settings.

5.2.7 O$_2$ consumption rate (OCR) assay

OCR measurements were conducted in 100 µl of air-equilibrated plain DMEM supplemented with 200 nM MitoXpress-Xtra probe as described[237]. Sample wells were sealed with 150 µl of pre-warmed mineral oil to 37ºC and the plate was monitored on a TR-F reader Victor 2 (PerkinElmer Life Sciences) at 37ºC with excitation/emission at 340/642 nm. Each sample well was measured repeatedly every 3-5 min over a 60-90 min time period, by taking two intensity readings at delay times of 30 and 70 µs and gate time 100 µs. Intensity signals were converted into phosphorescence lifetime (τ) values: $\tau = (t_2-t_1)/\ln(F_1/F_2)$, where F_1, F_2 are the TR-F intensity signals at delay times t_1

and t_2. Average O_2 levels across the samples were calculated from τ values[238], and then the OCR for each WM was calculated as O_2 consumed in 1 min by 10^6 cells in 1 ml or the medium ($\mu M/min*ml*10^6$ cells)[237].

5.2.8 Lactate-specific extracellular acidification assay (L-ECA)

The ECA was measured as described[237]. Growth medium was replaced with 150 µl plain DMEM containing 10 mM HEPES and placed into CO_2-free conditions at 37°C for 2 h to release absorbed CO_2. The medium was then replaced with unbuffered plain DMEM (without HEPES) and put back into CO_2 free conditions for a further 1 h. After that, 100 µl of unbuffered plain DMEM medium containing 1 µM pH-Xtra probe were added to experimental wells and the plate was measured on the Victor 2 plate reader at 37°C for 60-90 min in the TR-F mode with excitation/emission at 340/615 nm. Two TR-F intensity signals were measured at delay times of 100 and 300 µs and a measurement window of 30 µs. The emission lifetime τ was calculated as described for the OCR and converted into pH values, which were then used to calculate the amount of protons extruded in 1 minute by 10^6 cells in 1 ml or the medium ($[H^+]/min*ml*10^6$ cells).

5.2.9 Cytokine and chemokine assessment on macrophages

The supernatants obtained as described in the LDH assay sections were centrifuged again at 340 g for 5 min to remove any debris. These can be stored at -80°C prior to quantification using the multiplex Meso Scale Discovery (MSD) protocol supplied with kit N75CA-1, which measures IL-1α, IL-1β, TNFα, CXCL-1/rKC and MCP-1.

5.3 RESULTS AND DISCUSSION

5.3.1 Agglomeration tendency of bare and core-shell MIP nanoparticles

Since biocompatibility and internalisation experiments are generally performed in media enriched with FBS, it is important to take into account the effect of the "protein corona" generated from the adsorption of proteins onto the nanoparticles. Such a corona

evokes different responses in cells and also *in vivo*, since the interfacial composition of the nanomaterial is changed. Previous studies reported that albumin is the most common protein absorbed onto the nanoparticles and that PEGylated particles have less proteins adsorbed onto their surface[239, 240].

Our results show that bare MIPs have a higher increase in the particle hydrodynamic size (34%) in cell medium compared to PEG4000-coated MIPs (5%), since proteins are more prone to be adsorbed onto an hydrophobic surface rather than a hydrophilic one (PEG shell)[241]. Furthermore, PEG steric repulsion forces might contribute to lower protein adsorption. More importantly, the presence of the protein corona stabilises nanoparticles against agglomeration. Furthermore, Figure 5-1 shows that bare MIPs in plain DMEM (without FBS) undergo evident agglomeration, probably due to the high ionic strength of the solvent[242], whereas in the presence of FBS the particle aggregation is limited. This "protective" effect has been previously reported and described as ubiquitous and independent of the particle's surface composition[241]. On the other hand, PEGylated MIPs in plain DMEM showed a lower level of aggregation due to steric effects of the PEG shell, confirming that the latter is a deterrent against particle agglomeration. Furthermore, Figure 5-1 shows that the reduction in the protein corona thickness is more evident when high Mw PEGs are employed, confirming what was previously reported for other nanosystems[243]. Interestingly, PEGylated particles showed 30% higher solubility in water compared to bare MIPs, due to the presence of hydrophilic ethylene glycol repeating units.

Table 6. Average size of MIP NPs in water, Dulbecco's Modified Eagle Medium (DMEM) and DMEM supplemented with 10% fetal bovine serum (FBS) by Nanosight® and DLS at 37°C.

Type of MIPs	Size [nm] by Nanosight[a] in water	Size [nm] by DLS in water[b]	Size [nm] by DLS in DMEM	Size [nm] by DLS in DMEM+FBS
Bare	86	126 ± 2	152 ± 14	196 ± 4
PEG$_{1100}$ shell	94	137 ± 14	184 ± 11	203 ± 5
PEG$_{4000}$ shell	108	131 ± 9	189 ± 6	206 ± 3

(a), mean diameter assessed by Nanosight equipped with NTA software and considering at least 1000 tracks. (b) z-average hydrodynamic diameter extracted by cumulant analysis of the data. The error bars represent the standard deviation of at least four measurements.

Generally, the cell uptake is mediated by nonspecific interactions of the nanomaterials with serum proteins[244]. Therefore, the protein corona effect might reduce the performance of particles coated with active targeting moieties. PEGylated nanoparticles which interact less with serum proteins represent an important advancement for the development of nanosystems with enhanced active targeting capabilities. The aforementioned protein corona is not a static layer, and its composition is determined by different kinetics rates of adsorption/desorption of the proteins[245, 246] (the so-called Vroman effect). Such behaviour must be taken into account especially when nanomaterials are designed for cellular or *in vivo* applications.
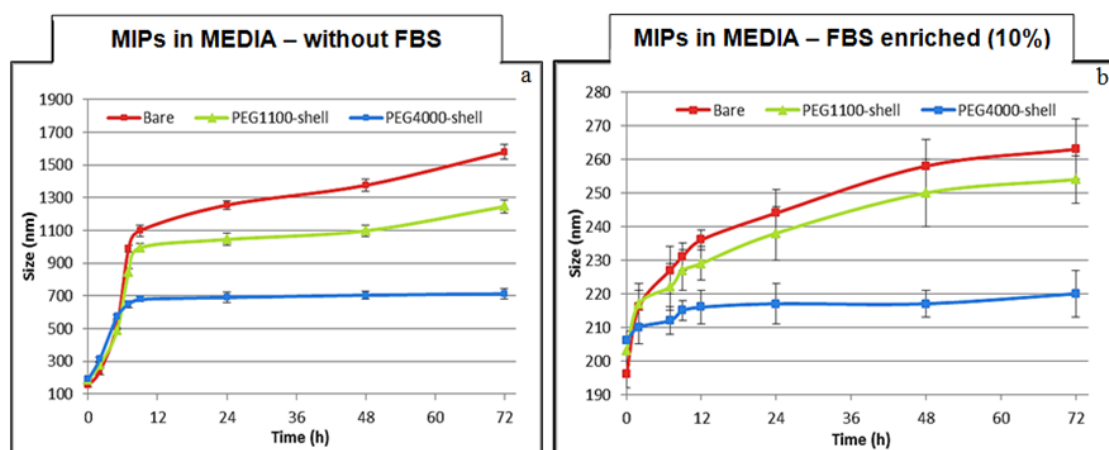
Figure 5-1. MIPs in cell culture media (DMEM), without (a) and enriched (b) with FBS 10% v/v.

5.3.2 Viability tests

The biocompatibility of an unknown material depends on different factors, such as the cell lines employed, the exposure times, the mechanism of interaction with cells, together with size, shape, functionality and concentration of the nanosystem tested. In light of this, a complete toxicological assessment should take into account all the

aforementioned aspects to fully characterise a novel material. For this reason, several viability tests were performed on different cell lines and exposure times.

Firstly, MIP NPs were analysed by the MTT assay (Figure 5-2), which relies on the measurement of the purple formazan product formed after reduction of the yellow compound 3-(4,5-dimethylthiazol-2-yl)-2,5-diphenyltetrazolium bromide (MTT). Such a reduction is performed by the mitochondrial succinate/dehydrogenase, active only in living cells. The resulting purple formazan produced can be quantified by spectrophotometric means (Figure 5-3 a). Therefore, the assay allows for the evaluation of the cellular metabolic activity and, hence, if cell viability is affected by the presence of foreign material in the cellular media. This method is widely employed and now accepted as a reliable assay to assess cell death.

In this work, three concentrations of each type of imprinted NPs were tested (50, 25, 10 μg/ml) and cells incubated in NP-free media were used as a control. The number of cells seeded in each well was appropriately chosen to give an absorbance value between 0.75 and 1.25, in this way both inhibition and stimulation of cell growth could be measured. In order to remove any background signal, the plate was divided in three sections: (1) blank wells containing medium only, (2) untreated control cells, (3) MIP NPs in medium only and (4) cells treated with MIP NPs. As shown in Figure 5-2, the imprinted NPs showed no appreciable cytotoxicity after 24 h incubation with HaCaT and HT1080 cells.
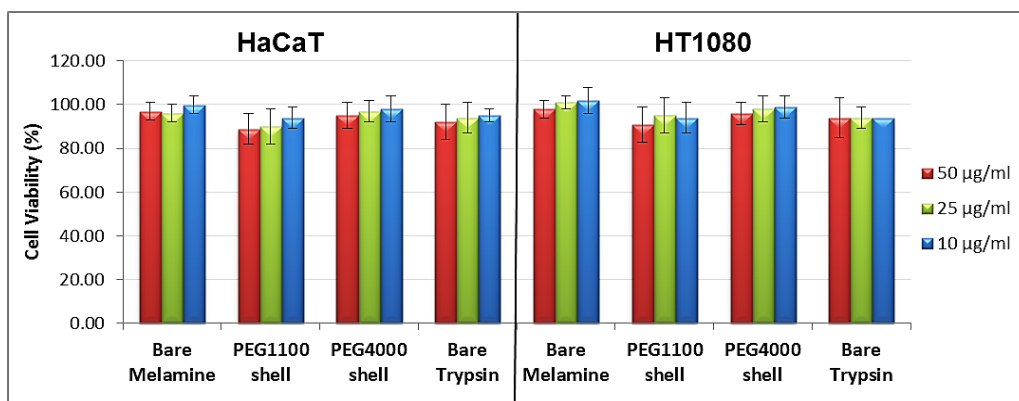
Figure 5-2. MTT test performed on both HaCaT and HT1080 cells after 24 h incubation.

Moreover, the presence of the fluorescent rhodamine monomer in the MIP matrix does not affect the biocompatibility of the particles, since fluorescent and non-fluorescent

MIPs showed the same cytocompatibilty profile (bars omitted for clarity). Concluding, this assay showed that MIPs are biocompatible in the range of concentrations needed for fluorescence studies by confocal microscope.

To further assess the particle biocompatibility and confirm the previous results obtained from the MTT test, the lactose dehydrogenase (LDH) assay was employed on a different cell line (R8383 rat macrophages) and for longer incubation time. This assay is another method widely employed to assess the cell viability (Figure 5-3 b).
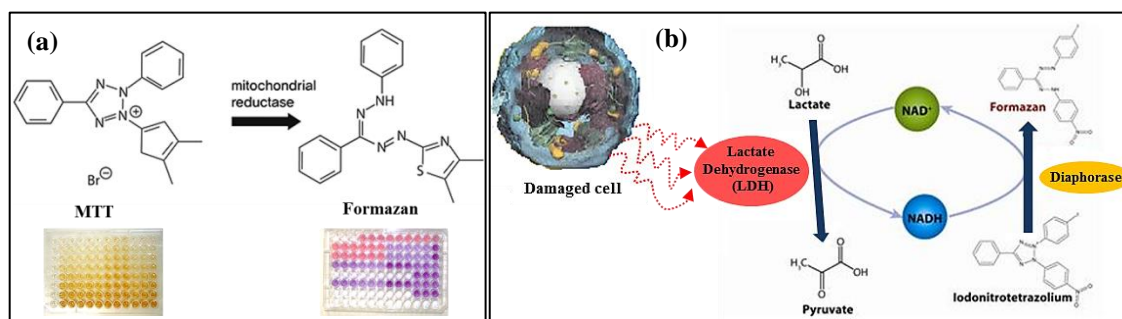
Figure 5-3. Schemes of MTT (a) and LDH (b) assays.

This method relies on the measurement of the LDH (a cytosolic enzyme) released into the media from damaged cells as a marker for cellular cytotoxicity. Cells release LDH when damaged and so the level of leaked LDH increases as a result of toxicity. The LDH assay on R8383 rat macrophages confirmed that the cell viability is only marginally affected by the presence of the MIPs (Figure 5-4).
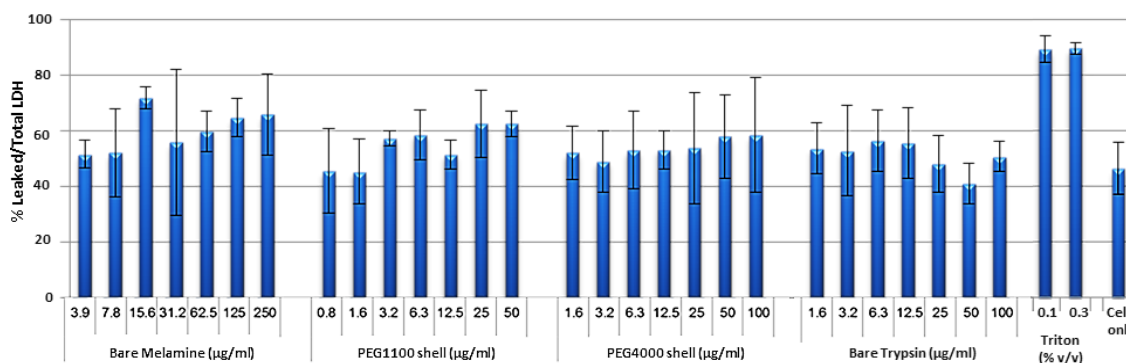
Figure 5-4. LDH assay on macrophages after 72 h exposure to different concentrations of MIP nanoparticles. Triton was used as a positive control.

Viability results, however, might be misleading since cells are able to adapt and compensate to some extent for the effects of external adverse factors[236, 247]. A deeper understanding of the metabolic effects of nanoparticulate systems can be given by a combination of other assays, such as the Oxygen Consumption Rate (OCR) and the Extracellular Acidification Assay (ECA). These are more sensitive to assess toxicity as they provide information about the metabolic effects of nanoparticles and their targets within the cell. In contrast, conventional tests such as total ATP, LDH release and MTT assay could overlook toxic effects, especially if these are masked by compensatory pathways inside the cell.

MEF cells were chosen as a model to assess whether their oxidative phosphorylation is affected by the presence of nanoparticles. Toxicity tests revealed that ATP levels (Figure 5-5) remain unchanged upon exposure to Bare NPs, PEG_{1100}- or PEG_{4000}-coated MIPs, confirming that the cell viability is not negatively affected. However, MEF cells treated with PEG_{1100}-coated MIPs showed a 57% reduction in oxygen consumption rate along with a 38% increase in extracellular pH, which indicates a certain level of mitochondrial toxicity. A reduction in the level of oxidative phosphorylation along with a compensatory increase in the glycolytic activity is observed. This also occurs, although not to the same extent, in MEF cells treated with PEG_{4000}-coated MIPs, in which a 21% reduction in oxygen consumption rate is present but without the associated increase in extracellular acidification. Interestingly, there is no change in metabolic function in the cells exposed to Bare NPs. This proves that toxicological assessments should in general involve more than a single cell line analysis, since viability tests might not be exhaustive and also different particle coatings might evoke diverse effects in different cell lines.
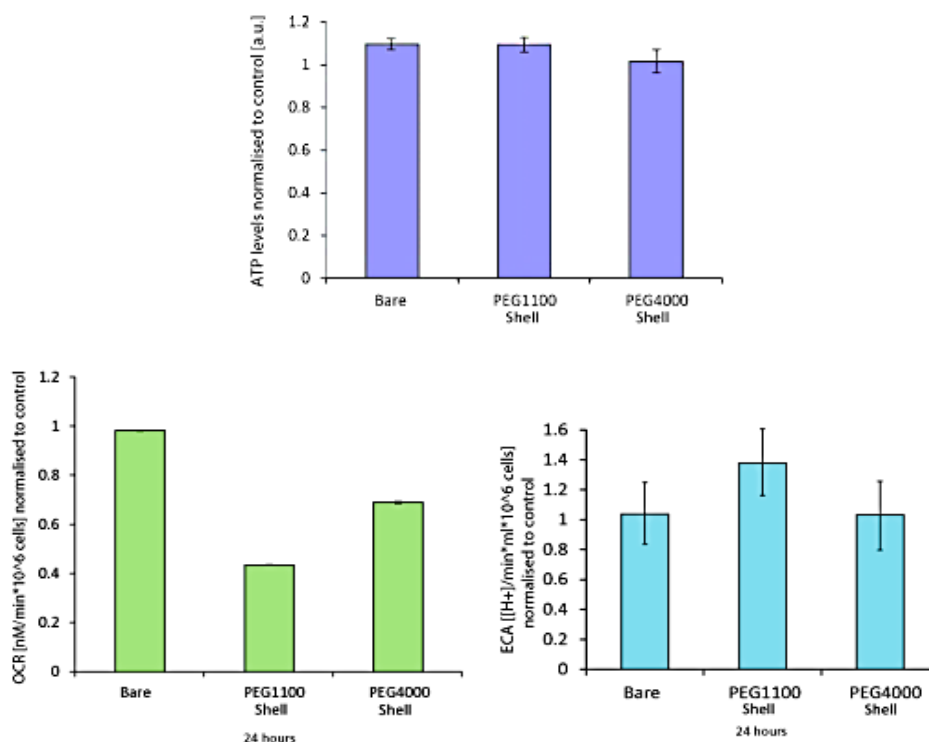
Figure 5-5. At the top, ATP levels in MEF cells after 24 h exposure to a 50 μg/ml solution of Bare Melamine (bare) and core-shell MIPs bearing a shell of PEG_{1100} or PEG_{4000} (PEG1100 and PEG4000 Shell). OCR (bottom left) and ECA (bottom right) assays performed on the same sample.

5.3.3 Inflammatory response in macrophages

In light of the promising biocompatibility data previously obtained and considering the potential applicability of MIP nanoparticles *in vivo*, the cytokine release from macrophages upon MIP exposure was assessed. In particular, IL1a, IL1b, MCP-1, TNFα and rKC after 72 h treatment were measured, since they are good indicators of the M1 phenotype[248]. In fact, it is recognised that M1 macrophages are involved in various chronic inflammatory and autoimmune diseases[249]. The assay aims to flag the potential of a compound for generating an inflammatory response *in vivo*. Although this assay is not predictive of inflammation, assessing the cytokine release profile is pivotal for any preparation that has to be administered intravenously, since massive release of cytokines might lead to the cytokine release syndrome (CRS) which causes serious systemic symptoms (fever, hypotension, organ failure)[250].
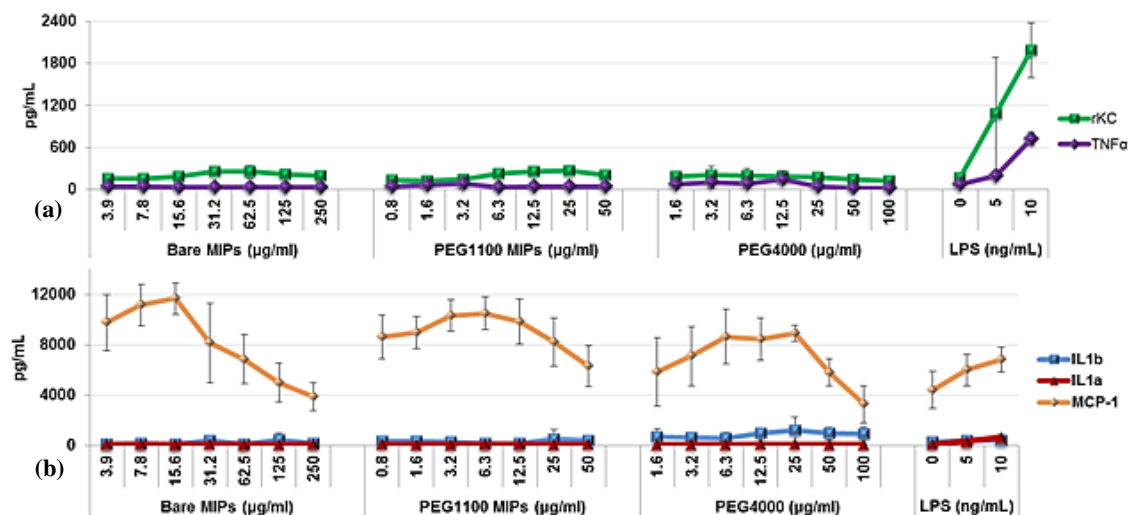
Figure 5-6. Cytokine release profile of macrophages exposed to MIPs for 72 h. Chemokine (C-X-C motif) ligand 1, here referred to as rKC in green and tumour necrosis factor α in purple (a). Interleukin-1 alpha in red, interleukin-1 beta in blue and monocyte chemotactic protein 1 (MCP-1) in orange (b).

However, this type of assay is far from being standardised, therefore it is not possible to set a threshold after which cytokine release may be considered dangerous. Nevertheless, such an assay can identify compounds that might lead to a potentially severe pro-inflammatory response. The MCP-1 profiles were bell shaped over the dosing ranges, 'hinting' at a response to all three MIPs, however the absence of a response observed for the other cytokines measured suggests a low probability that any of these MIPs will induce an inflammatory response. Therefore MIP nanoparticles seem to be suitable for *in vivo* administration. However, considering the increase in MCP-1, it would be recommended to monitor the neutrophil and monocyte activity.

5.4 CONCLUSIONS

The biocompatibility assessment of a given nanosystem is a pivotal step towards its actual applicability in clinical/diagnostic practice. In light of the potential of nanoMIPs for both *in vitro* and *in vivo* diagnostics, herein we evaluated the biocompatibility of nanoMIPs produced by solid-phase synthesis. In particular, nanoMIPs produced by

persulfate-initiated polymerisation, together with both bare and core-shell nanoMIPs produced by UV polymerisation were assessed. Our results suggest that PEGylation of MIPs improves the particle stability in solution against agglomeration. Both bare and PEG-coated MIPs obtained by UV polymerisation, as well as trypsin nanoMIPs produced in water, did not decrease significantly the cell viability in four different cell lines at the concentrations tested. However, more comprehensive tests on the cell metabolism showed that a certain level of mitochondria toxicity was detected for PEG_{1100}-coated MIPs in MEF cells. Nevertheless, no signs of mitochondria toxicity were detected in macrophages, suggesting that the same nanosytem can have diverse responses in different cell lines, and therefore the *in vivo* fate is much more complex than a single cell line analysis. However, conflicting data exist about the role of PEG coating on the biocompatibility of nanoparticles. Such opposing results might be due to a lack of standardised internalisation protocols, since different cell lines, particle compositions, sizes and concentrations are usually tested. The low cytokine release showed by MIPs suggests that this novel type of nanosystem endowed with targeting capabilities holds great potential also for *in vivo* uses although, due to the increase in MCP-1 release, it would be recommended to monitor the neutrophil and monocyte activity.

6 INTERNALISATION STUDIES

6.1 INTRODUCTION

One possible field of application for imprinted nanoparticles is the intracellular delivery of drugs. In particular, in the case the drug of interest is not able to cross the cell membrane (charged or poorly soluble molecules in water) and/or when a targeted delivery of large quantities of drug is desired. A single nanoparticle, in fact, can deliver several drug molecules, thus improving the therapeutic effect. Another potential application of MIP NPs is cellular imaging: detection and localisation of a given cell populations overexpressing a specific protein can be theoretically achievable by using fluorescently-tagged MIP NPs. If MIPs are intended to be used for this purpose, an assessment of their internalisation is needed. In this chapter, the uptake of nanoMIPs imprinted by UV or persulfate-initiated polymerisation will be evaluated, thus opening the possibility of their use as intracellular drug delivery systems. It should be noted, however, that particle agglomeration affects their internalisation. In some cases, agglomeration of nanoparticles may lead to an enhancement of their uptake because they can rapidly reach the cell by sedimentation. However, if the agglomerate size is close to the one of the cell itself, uptake is reduced[251]. Several authors developed systems such as flow models or inverted cultures where the effect of sedimentation is reduced. In the inverted culture method, cells are grown on an insert facing downwards so that potential agglomerates would settle at the bottom of the chamber/well without interacting with the cells[252]. On the other hand, flow systems allow a more homogeneous particle distribution and are closer to *in vivo* conditions[253].

In general, current *in vitro* methods to assess biocompatibility and internalisation of nanomaterials face the following issues: (1) a non-complete characterisation of the nanosystem, (2) the lack of standardised biocompatibility and internalisation protocols, (3) the lack of consistency on the dose metric to be used and (4) the intrinsic limitations of the classical 2D monocultures. It is important to highlight that most authors express the particle concentration in terms of mass per volume (mg/ml) which, however, is not always the best option and does not allow a comparison between nanosystems with

different compositions. In fact, for instance, a solution of gold nanoparticles at 1 mg/ml would not contain the same quantity of particles compared to a sample of polymeric nanoparticles at the same concentration. Furthermore, if we consider two samples of the same type of nanoparticles having different sizes (e.g. 60 nm and 300 nm) at the same mg/ml concentration, they would contain a different number of particles/ml and therefore their biocompatibility cannot be directly compared since the toxic effect is mainly due to the number of nanoparticles (and their surface area) rather than their weight. We believe that the best way to express the particle concentration (which would also allow to compare different nanosystems) is in terms of particle/ml (or molarity) and always specifying their size. However, because of an apparent reluctance by other authors in accepting this principle and switching towards molar concentrations, both mg/ml and molar concentrations will be here employed.

6.2 MATERIALS AND METHODS

6.2.1 Chemicals

Poly(ethylene glycol) methyl ether methacrylate (PEG) (Mw = 1100 and 4000 g mol-1), dimethylsulfoxide (DMSO), D-galactose, paraformaldehyde (PFA), DiO (3,3'-Dioctadecyloxacarbocyanine Perchlorate), Dulbecco's Modified Eagle's medium (DMEM), D-glucose, L-glutamine, sodium pyruvate, were purchased from Sigma-Aldrich, UK. Ethanol and Amicon Ultra-15 Centrifugal Filter Units (MWCO 30 kDa), coverslips and microscope slides were obtained from Fisher Scientific (UK). Methanol and acetone were purchased from VWR (UK). Methacryloxyethyl thiocarbamoyl rhodamine B was obtained from Polysciences Europe. NR8383 macrophages and human keratinocytes (HaCaT) were purchased from American Tissue Culture Collections (ATCC, Manassas, VA). Ham's F12 medium, heat inactivated FBS, sodium bicarbonate and penicillin/streptomycin solutions were purchased from Invitrogen. Mineral oil was from Cargille Laboratories (Cedar Grove, NJ). Deionised water obtained from a Millipore (MilliQ) purification system at a resistivity of 18.2 MΩ cm was used for analysis. All chemicals were analytical or HPLC grade and were used

without further purification. Cell culture and experimental conditions as reported in 5.2.3.

6.2.2 Flow cytometry

Following 24 h incubation time with the nanoparticles of interest at a concentration of 10 μg/ml (0.05 nM), plates were washed three times with PBS and cells were collected by trypsinisation. Cells were then centrifuged (200 g for 5 min at 4 °C) and the supernatant discarded. Cells were suspended in 5 ml of PBS and then centrifuged again. This was repeated three times, to remove any free nanoparticles from the solution to be analysed. Finally the cell pellets were resuspended in in 0.5 ml cold PBS, and then kept on ice until analysis.

6.2.3 Confocal microscopy

Aliquots of 150 μl of a dispersion of HaCaT cells (4×10^5 cells) were seeded on each round coverslip, previously washed with 70% ethanol, and put in a 12-well plate which was incubated for 4 h at 37°C. After that, 2 ml of DMEM + 1% FBS were added in each well and incubated overnight at 37°C. The following day the medium was replaced with the nanoparticle suspension (10 μg/ml, 0.05 nM) and the plate was incubated for 24 h. At the end of the experiment, the cover slips were washed 4 times with fresh pre-warmed PBS to eliminate the excess of nanoparticles not internalised. Cells were then fixed with a solution of 3% PFA in PBS for 20 min at room temperature. Staining of the cytoplasm was performed with DiO using a working solution of 100 nM in PBS. More specifically, cells were treated with the DiO solution for 30 min at room temperature and then washed with distilled water 4 times. Afterwards, the coverslips having fixed cells on their surface were placed onto microscope slides previously washed with 70% ethanol, after that a drop of 4′,6-diamidino-2-phenylindole (DAPI) solution in mounting media (100 μg/ml) was deposited on each slide. The internalisation of imprinted NPs was evaluated by using two confocal microscopes, a Leica DMI6000B and an Olympus

FV1000 CLSM, both using a 60× UPlanSAPO Olympus objective and a Kalman filter of 4. Rhodamine B-based MIP nanoparticles were excited using Helium Neon laser (543 nm). For imaging of DAPI, 364 nm and 454 nm were used as excitation and emission wavelength respectively. 490 nm (λexc) and 520 (λemiss) were set for DiO imaging. Afterwards, the images were analysed using ImageJ software.

6.2.4 TEM of macrophage cells

TEM of the NR8383 cells treated with MIPs (250 µg/ml of bare MIPs and 100 µg/ml of PEG$_{4000}$-coated MIPs) was carried out after 72 h incubation. NR8383 cells were fixed in 4% formaldehyde/1% glutaraldehyde, post-fixed using 1% osmium tetroxide, dehydrated in ascending concentrations of ethanol and infiltrated with Agar 100 resin. 1 µm toluidine blue stained resin sections were prepared from the resultant resin blocks and examined by light microscopy to locate suitable areas. 90 nm sections were then cut for TEM, placed on copper grids and stained with uranyl acetate (0.5%) and lead citrate (3%) using an automated stainer. TEM sections were examined in an Hitachi H7500 TEM at 60kV or 80kV. Representative images were taken using an AMT XR41 Digital Camera System.

6.3 RESULTS AND DISCUSSION

6.3.1 Size and flow cytometry analyses

The size distribution of bare, PEG$_{1100}$-coated and PEG$_{4000}$-coated MIPs employed in these internalisation studies was assessed by a Nanosight instrument and reported in 3.3.3 (Figure 3-5). The size of nanoMIPs produced by persulfate-initiated polymerisation in water was assessed by DLS and reported in table 7. It should be noted, however, that changing one parameter of the nanoparticle (e.g. surface coating) without affecting the others (charge, hydrodynamic diameter, colloidal stability, etc.) is quite challenging. Hence, variations in biocompatibility or uptake may be due to a combination of such variations.

Table 7. Average size of MIP NPs in water by Nanosight® and DLS at 37°C.

Type of MIPs	Size [nm] by Nanosight[a] in water	Size [nm] by DLS in water[b]
Bare (UV-polym.)	86	126 ± 2
PEG$_{1100}$ shell	94	137 ± 14
PEG$_{4000}$ shell	108	131 ± 9
Bare (Persulfate-polym)	N/A	189 ± 17

(a), mean diameter assessed by Nanosight equipped with NTA software and considering at least 1000 tracks. (b) z-average hydrodynamic diameter extracted by cumulant analysis of the data. The error bars represent the standard deviation of at least four measurements.

As mentioned above, the measurement of MIP NPs produced in water by NanoSight analysis was not reliable because of the low refractive index (probably due to a low cross-linking degree) of such nanoMIPs. This results in the MIPs being "invisible" to the instrument, because of the low amount of scattered light.

Flow cytometry was chosen to preliminarily assess the particle internalisation in cells. MIP NPs imprinted for melamine and trypsin were used as models for UV- and persulfate-initiated polymerisations respectively. Figure 6-1 shows an apparent internalisation for both melamine and trypsin nanoMIPs after 24 h incubation. Flow cytometry is a widely used method capable of analysing thousands of cells/particles per second, by monitoring the fluorescence changes in a sample. The sample is injected in a flow cell, where a liquid stream carries the cells in line through the laser beam for detection. Since multiple laser/filter settings are available, multiplexed analysis is also achievable. It should be noted, however, that the fluorescence detected by flow cytometry is not indicative of internalisation, since nanoparticles bound to the surface of the cells (but not internalised) would be detected. A way to overcome this entails the incubation of the cells to be analysed in a solution of trypan blue[254]. Trypan blue does not enter living cells and, at the same time, quenches the fluorescence from those particles bound on the cell surface.
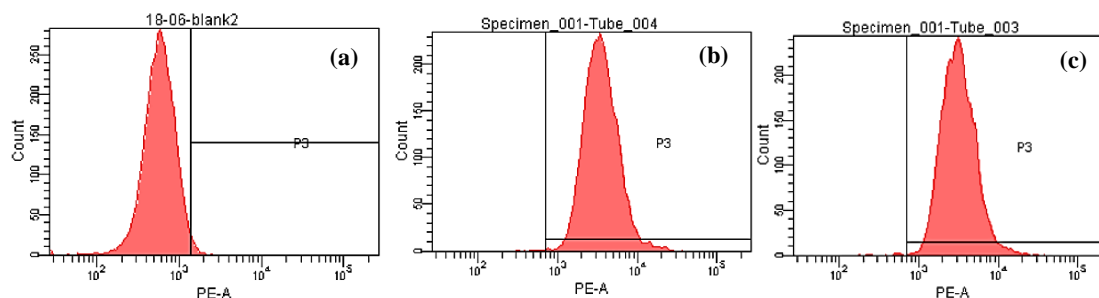
Figure 6-1. Representative plot analysis of fluorescence levels in control cells (a) and cells treated with nanoMIPs imprinted for melamine (b) and trypsin (c). The shift in the PE-A axis is indicative of fluorescence detected in cells exposed to nanoMIPs. Each experiment was performed collecting a minimum of 7500 events.

Another method to assess the particle internalisation without potential artifacts relies in the use of confocal and/or transmission electron microscopy. These two microscopy techniques allow a better localisation of the nanoparticles on the z-axis, thus enabling an improved detection of the particle internalisation. However, these two techniques – especially TEM – are quite expensive and time-consuming. Furthermore, the sample processing for TEM analysis is laborious and includes several steps, which may negatively bias results.

6.3.2 Confocal microscopy analysis

In order to further assess the internalisation of MIP NPs, rhodamine-labelled MIPs imprinted for melamine as a model template were produced by using a polymerisable rhodamine-dye (Figure 6-2), which was included in the polymerisation mixture (0.12% mol compared to the total number of moles of methacrylic acid). UV-polymerised bare and PEGylated MIP NPs (PEG$_{4000}$), together with trypsin nanoMIPs produced by persulfate-initiated polymerisation were analysed. The MIPs obtained were washed 7 times with distilled water to remove any unreacted free monomer, using Amicon Ultra-15 Centrifugal Filter Units (MWCO 30 kDa). The fluorescence spectrum was recorded in distilled water, using a FluoroMax-P (Horiba, USA) and setting 555 nm as excitation

wavelength. The emission peak from the labelled MIPs was detected at 578 nm, confirming the incorporation of the dye within the polymer matrix of the nanoparticles.
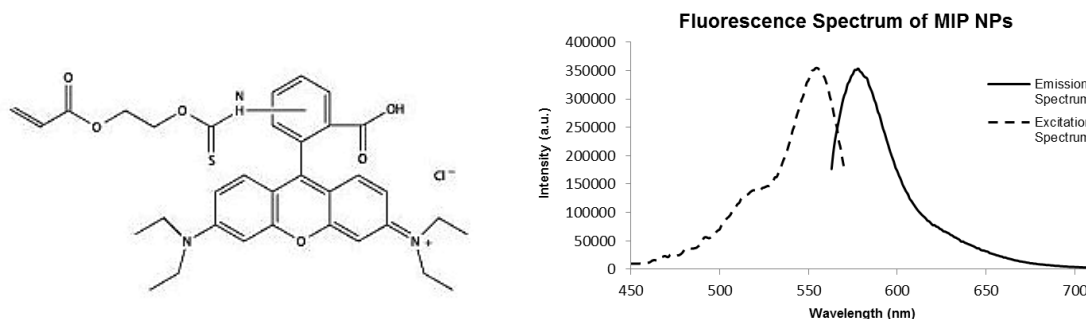
Figure 6-2. On the left, methacryloxyethyl thiocarbamoyl rhodamine B, the fluorescent monomer employed to label the nanoparticles. On the right, fluorescence spectra of rhodamine-labelled MIPs.

Once rhodamine-labelled MIP NPs were obtained, HaCaT cells were incubated at 37°C for 24 h in the presence of these particles (10 µg/ml, 0.05 nM). The number of cells/well was chosen in order to have a roughly 80% confluent monolayer of cells on the coverslip in each well. After incubation in the presence of MIPs, wells were thoroughly washed with PBS to remove the NPs which were not taken up by the cells. The cell nucleus was stained with DAPI (4′,6-diamidino-2-phenylindole) and the cytoplasm with the lipophilic probe DiO (3,3'-dioctadecyloxacarbocyanine perchlorate). Z-stacks images (Figure 6-3) showed that the imprinted NPs (in red) were internalised and localised in the cytoplasm (green). Each optical section represents a specific focal plane, from which the internalisation of bare MIP NPs can be observed.
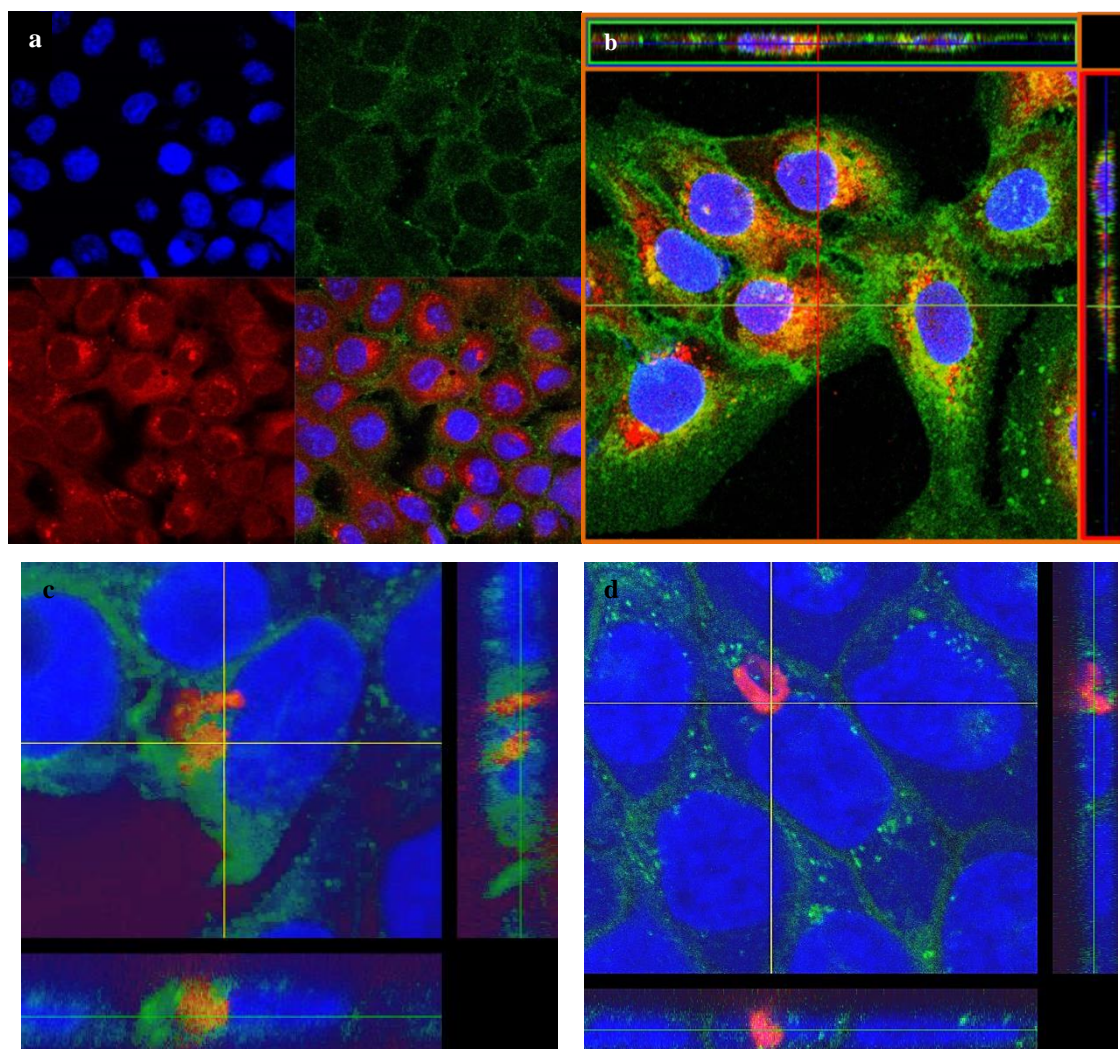
Figure 6-3. Representative confocal images of bare (a-c) and PEG$_{4000}$-coated (d) internalised MIP nanoparticles (red dots) imprinted for melamine after 24 h exposure. The nucleus was stained with DAPI (blue) and the cytoplasm with DiO (green).

Similarly, rhodamine-labelled MIP NPs imprinted for trypsin were tested under the same conditions. HaCaT cells were incubated at 37°C for 24 h in the presence of these particles (10 μg/ml). Figure 6-4 shows a certain level of particle internalisation, although to an apparent lesser extent compared to nanoMIPs produced in acetonitrile.
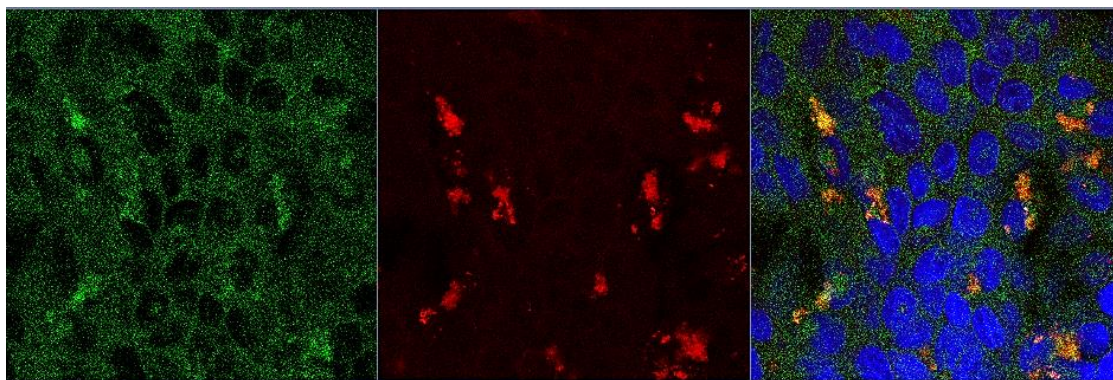
Figure 6-4. Representative confocal images of internalised MIP nanoparticles (red dots) imprinted for trypsin after 24 h exposure. The nucleus was stained with DAPI (blue) and the cytoplasm with DiO (green).

6.3.3 Transmission electron microscopy (TEM)

To better evaluate the particle localisation in cells and the effect of the particle coating on their internalisation, bare and PEG$_{4000}$-coated MIPs were used as models and analysed by TEM. Macrophages treated with bare MIPs (250 µg/ml) or PEG$_{4000}$-coated MIPs (100 µg/ml) contained MIP particles within membrane bound cytoplasmic bodies. The cytoplasmic bodies were considered to be consistent with one or more types of endo-lysosomal compartment (e.g. endosomes or lysosomes). MIPs have a round or ellipsoid shape. Bare MIPs appeared to be of uniform electron density (Figure 6-5) whilst the PEG$_{4000}$-coated MIPs particles had an electron dense outer rim and a less electron dense core (Figure 6-6). PEGylation did not seem to have an obvious effect on particle internalisation. On a few occasions, particles that were not enclosed in the cytoplasmic bodies were seen (Figure 6-5 f). It was not clear whether the particles were always endocytosed individually or sometimes as clusters. The size of some bodies and the fact that the particles were sometimes widely separated in these bodies may indicate uptake by a non-selective mechanism (i.e. macropinocytosis) in which the particles are taken up with the extracellular media. Macropinocytosis is a form of fluid phase endocytosis involved in the uptake of materials of more than 0.2 µm diameter and it is constitutive in macrophages.
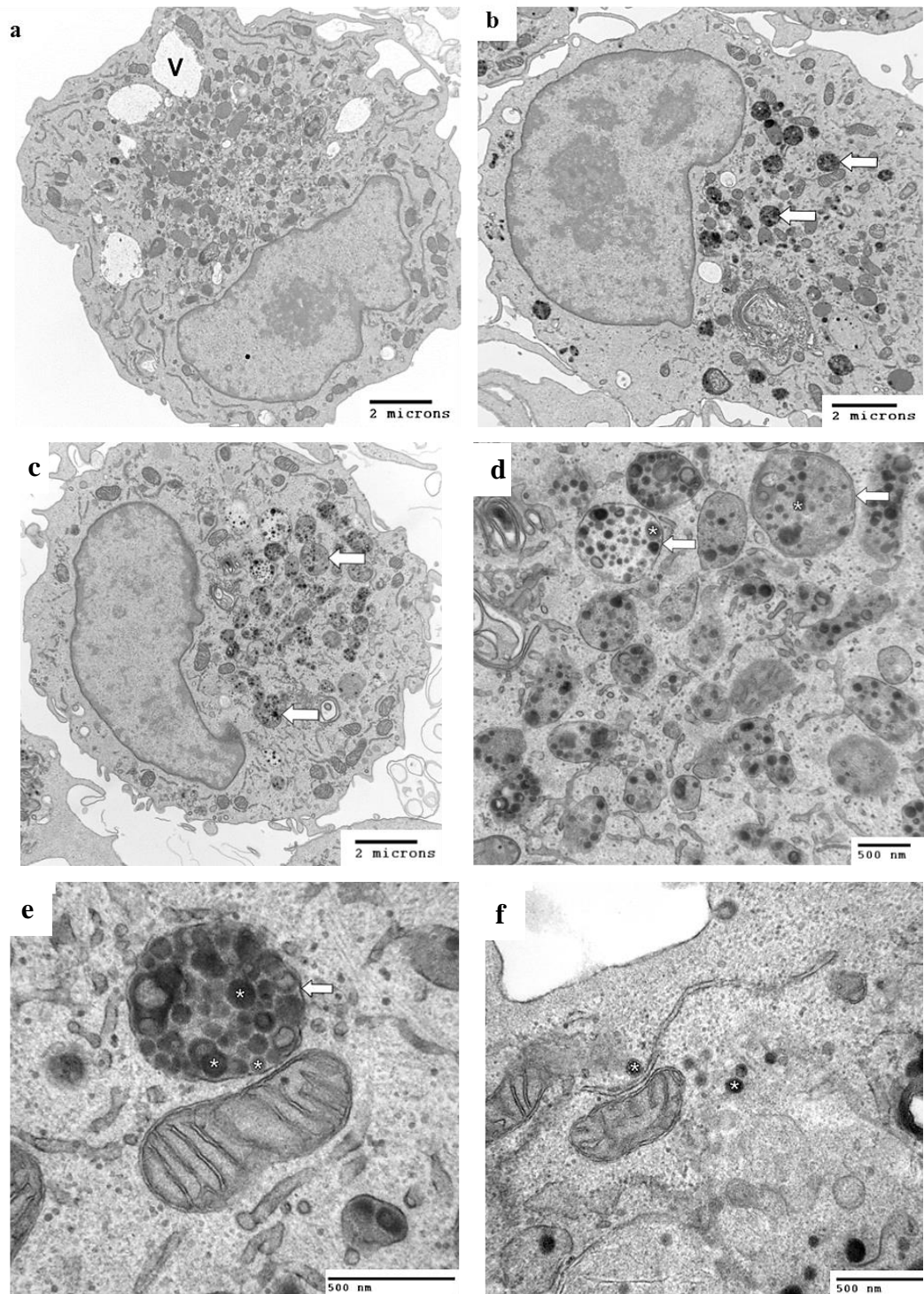
Figure 6-5. Representative TEM images of macrophage-internalised MIPs. Control cell (a); cell treated with bare MIPs (b, c); bare MIPs (*) in a cytoplasmic body (d, e), considered to be an endo-lysosomal compartment (arrow); bare MIPs (*) that are not within endo-lysosomal compartments (f). V= Normally occurring vacuole. Arrows = cytoplasmic bodies (considered to be endo-lysosomal compartments) containing MIP particles.

Some of the internalised MIP particles were larger than their theoretical size. This may be due to TEM sections through conjoined particles or to a certain level of sample polydispersity. There were very few necrotic cells and there was no evidence of cellular toxicity (including mitochondrial damage) in the other cells which were examined. Unfortunately, MIP NPs imprinted by persulfate-initiated polymerisation for trypsin were not visible. This could be caused by their poor electron density due to their low cross-linking degree.
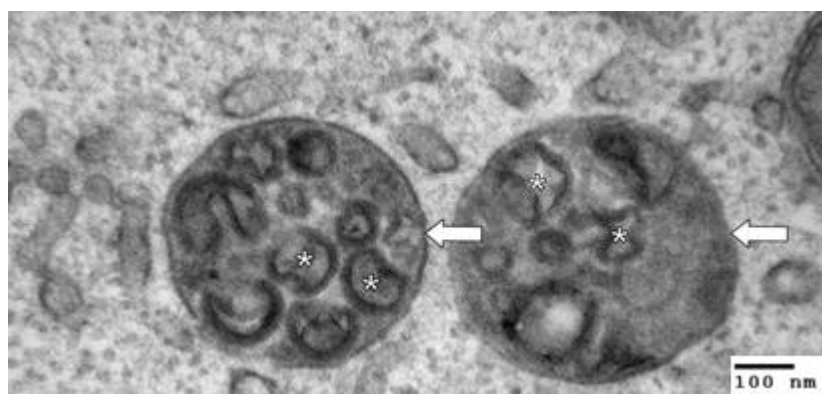
Figure 6-6. TEM image of PEG$_{4000}$-coated MIPs, showing a core-shell structure (*), in endo-lysosomal compartments (arrows).

6.4 CONCLUSIONS

The uptake studies performed here proved that MIP NPs can be internalised, regardless of their imprinting process (in water or in acetonitrile). Either nanoMIPs imprinted in water for an overexpressed protein to be targeted or nanoMIPs imprinted in organics for an hydrophobic drug to be released are two possible nanosystems which can find application for both imaging and therapy. In particular, MIP NPs can be used as intracellular drug delivery systems, for instance by coupling the drug through a cleavable linker such as hydrazone or a peptide, which would get hydrolysed once the nanoparticle is internalised inside the cell. Another option entails the use of a disulfide cross-linker such as *N,N*-bis(acryloyl)cystamine that can undergo reduction by

glutathione (present in cells), thus enhancing the drug release. Both this options are currently under investigation by the Leicester Biotechnology group. Next steps in the assessment of MIP internalisation may include a quantification of the nanoMIPs taken up by cells through cell lysis analysis or using the Cytoviva technology which allows to count even unlabelled MIPs, simultaneously evaluating also the influence of the particle surface coatings.

7 TARGETING OF OVEREXPRESSED PROTEINS IN CELLS

7.1 INTRODUCTION

As mentioned before, nanoMIPs are produced in a size range that is potentially suitable for applications in cells. A fascinating application, very recenlty explored by other research groups, involves the use of nanoMIPs to target overexpressed moieties exposed on the surface of cells. However, only saccharides (sialic and glucuronic acid) have been used as templates for the generation of MIPs, with no examples of peptide/protein imprinting for targeting of surface proteins on cells reported so far. Herein, we assessed whether nanoMIPs could be used to target overexpressed proteins in senescent and cancer cells.
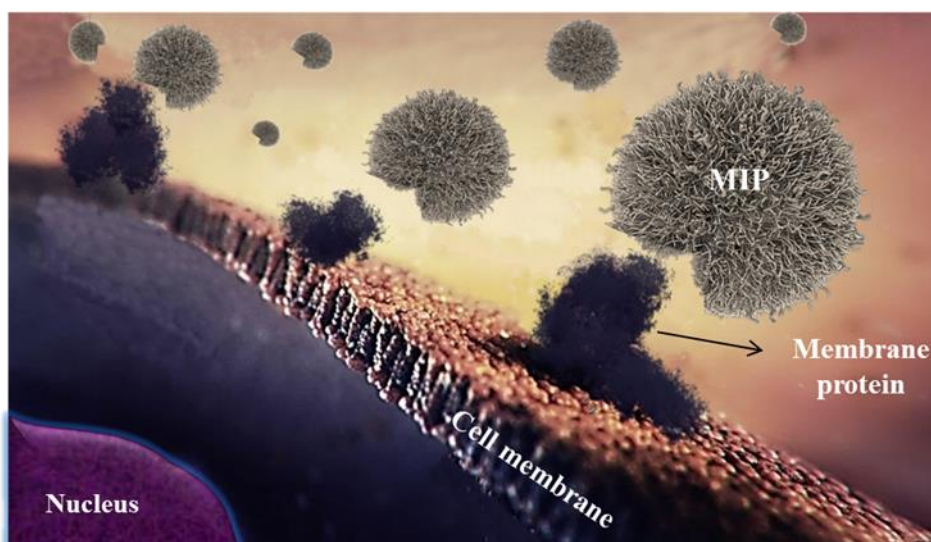
Figure 7-1. Scheme of the principle behind targeting of surface proteins by using nanoMIPs.

Senescence is a state in which cells are still metabolically active but their cell cycle is arrested (i.e. cells cease to divide). Furthermore, other phenotypic modifications appear such as elongation, vacuolisation and multinucleation[255]. Senescence can be caused by exposure to a range of stress stimuli (the so-called "stress induced premature senescence") or by telomere shortening following a high number of cell deivisions (called replicative senescence). Generally speaking, senescence can be seen as a

progressive failure of the physiological cell homeostasis. However, the precise etiology of senescence is still unknown, but there is some evidence suggesting that cellular senescence occurs as a mechanism to prevent the onset of cancer[256]. In fact, senescence referred as a cell-protective mechanism since it stops proliferation of stressed and damaged cells, thus blocking further aberrations. The immune system continuously removes senescent cells from our body, but over the time it becomes less effective, thus leading to accumulation of senescent cells in tissues and contributing to disease development and aging. Pre-malignant stages of cancer are often characterised by accumulation of senescent cells, known to secrete chemokines and growth factors which in turn accelerate angiogenesis, cell migration and proliferation, promoting progession into full malignancy[257]. Therefore early diagnosis of senescent cells is crucial to reduce the chances of cancer development.

Conversely, cancer is characterised by an abnormal cell growth, with the potential to spread and invade other organs, often with fatal effect. With almost 8 million people dead in 2010 (38% more than 20 years ago), cancer is the main cause of death in the developed world[258]. Cancer incindence has been raising in the past two decades because of lifestyle changes (sedentary behaviour) and aging of population. Although a tumour is often thought to be linked only to an uncontrolled proliferation rate of its cells, the following factors - called the hallmarks of cancer[259] - are common to cancer cells:

- Self-sufficiency in growth signals
- Immune system evasion
- Genome instability and mutation
- Apoptosis resistance
- Limitless replicative potential
- Sustained angiogenesis
- Tissue invasion and metastasis
- Altered metabolism
- Tumour-promoting inflammation
- Insensitivity to anti-growth signals

Even in this case, early diagnosis is the key for a positive outcome. Imaging procedures such as MRI, Positron Emission Tomography (PET), ultrasounds and X-rays are currently employed in routine diagnosis. The ultimate goal in the diagnosis of cancer by imaging is the possibility to discriminate cancer cells from the healthy ones with the greatest spatial resolution. Fluorescence-based techniques are a viable alternatives to current clinical methods, however limited to surafce tumours due to limits in light

penetrations. Nevertheless, the development of novel fluorescent nanosystems able to recognise cancer cells with high affinity and specificity is an option that many researchers are now investigating. The aim of this work is to evaluate the performance of nanoMIPs targeted towards overexpressed proteins in senescent and cancer cells, both for potential imaging and therapeutic applications.

7.2 MATERIALS AND METHODS

7.2.1 Chemicals

Puromycin, hygromycin, trypsin, PBS, 6 well plates, 15 ml tubes, BSA, DMEM and PBS were purchased from Fisher Scientific (UK). Anti-B2MG antibodies were obtained from Novus Biologicals (US). EJp16 and lung and breast cancer cell lines (H522, H1299, H1650, SKBR-3, MDA-MB-231 and 468) were purchased from ATCC (UK). Anti-EGFR antibodies were obtained from Abcam (US). DAPI-antifade mountant, γ-tubulin staining secondary Alexa-fluor 546 donkey anti-mouse were obtained from Life Technologies (US), and γ-catenin antibodies from BD Transduction Laboratories (UK).

7.2.2 Preparation of peptide-modified solid-phase and nanoMIPs

Glass beads were first activated by boiling in a 2M NaOH solution for 15 min, then rinsed with deionised water and acetone, desiccated at 80 °C and incubated overnight in 2 % v/v APTMS/toluene solution. This last step leads to beads bearing –NH$_2$ groups. Then 60 g of glass beads were placed in a solution of SIA linker (0.2 mg/ml) in acetonitrile for 2 h in the dark. The succinic moiety allows the linker to react with the solid-phase, and the haloacetyl group enables coupling with the thiol group intentionally added on the N-terminus of the peptide sequence of interest. Afterwards, the beads were washed with 400 ml of acetonitrile and placed in a bottle containing the cysteine-modified peptide of interest in deoxygenated 0.01 M PBS containing 5 mM EDTA (pH 8.2). After overnight incubation, the beads were washed with 500 ml of water in a sintered funnel and used for the synthesis of nanoMIPs.

7.2.3 Synthesis of nanoMIPs

Fluorescent nanoMIPs were produced by persulfate-initiated polymerisation in phosphate buffer 5 mM as reported in 4.2.3.

7.2.4 Cell culture conditions

For the experiments with senescent cells, the culture media (DMEM) for EJp16 cell lines was supplemented with 10% FBS, penicillin–streptomycin (50 unit/ml), puromycin (2 μg/ml) and hygromycin (100 μg/ml) as selective antibiotics for this cell lines. MDA-MB 231, MDA-MB-468 and SKBR-3 cells were cultured in DMEM (GIBCO) supplemented with 10% fetal bovine serum (FBS, GIBCO). In SKBR-3 cells media insulin was added to a final concentration of 1 mg/mL. Cells were incubated in the presence of 100 U/ml penicillin/100 μg/ml streptomycin (P/S) in humidified atmosphere of 5% CO_2 and 95% air at 37°C.

7.2.5 Flow cytometry

Flow cytometry analysis was performed on 90% confluent 6 well plates. Plates were washed with cold PBS and the cells collected by scraping in 0.5 ml cold PBS, and then kept on ice. Trypsin was not used to prevent internalisation of extracellular proteins. Afterwards, cells were centrifuged at 200 g for 5 min (4 °C) and the supernatant discarded. Cells were then resuspended in 200 μl of blocking buffer (0.5% BSA in PBS) and incubated 15 min on ice, then transferred to 96 rounded bottom multi-well plate. These were centrifuged at 500 g for 5 min (4 °C) and the supernatant was removed. Subsequently, cells were resuspended with nanoMIPs (final concentration 30 ug/ml), while control cells were incubated with the required antibodies (FITC-labelled anti-B2MG antibodies, dilution 1:5) at 4 °C in the dark for 45 min. Cells were then washed twice with blocking buffer (150 μl per well) and centrifuged at 500 g for 5 min at 4 °C.

The cell pellet was finally resuspended in 300–500 µl of blocking buffer and the fluorescence was monitored using a flow cytometer.

In the experiments with cancer cells, cells were collected by trypsinisation, resuspended in RPMI and aliquoted by 1.5×10^6 of cells in 2 ml RPMI per experimental condition in 15 ml conical tubes. MIPs were diluted to the concentration of 60 ug/ml in RPMI. 1 ml of diluted MIPs was added to 2 ml of cell suspension to achieve the final concentration of 20 ug/ml. Mixtures were incubated 2 hrs in dark at 37°C with rotation 15 RPM. Following the incubation the samples were centrifuged, washed with PBS and plated in RPMI on 10 cm plates. 48 hrs later all cells both attached and floating were collected, washed with PBS and divided into two parts: one was stored for subsequent Western Blot analysis and another was used for flow cytometry analysis.

7.2.6 Western blotting

EGFR levels were quantified by Western blot analysis from cell lysate using anti-EGFR antibodies. The signal was normalised by blotting the lysate against GAPDH, using anti-GAPDH antibodies. Briefly, cells were trypsinised, washed with PBS and resuspended in lysis buffer in a microcentrifuge tube for 30 min at 4°C. The tube was centrifuged at 4°C and the supernatant saved in a separate tube. An aliquot of the cell lysate was loaded on the SDS-PAGE gel and this was allowed to run. The proteins were then transferred from the gel to the nitrocellulose membrane. The latter was then blocked for 1 h at RT and incubated with anti-EGFR antibodies. After washing, a labelled secondary Ab was introduced and incubated for 1 h. After washing out the excess Ab, the membrane was analysed in a Typhoon instrument.

7.2.7 Confocal microscopy

MIPs binding was assessed on to two different breast cancer cell lines (MDA-468 and SKBR-3, respectively with high and low EGFR expression on the cell surface) at two different time points (2 and 24 h). The day before treatment cell suspension was seeded on gelatin-covered coverslips previously washed with 70% ethanol and twice with PBS

in an amount to estimate the cell confluency 40 – 70% the next day incubated overnight at 37°C. The following day the medium was replaced with the nanoparticle suspension (10 µg/ml) in full media as described earlier and the plate was incubated for 2 h or 24 h. Following the incubation, the cover slips were washed 4 times with fresh pre-warmed PBS to eliminate the excess of nanoparticles that were not internalised. Cells were then fixed with a solution of 4% PFA in PBS for 10 min at room temperature. PFA fixed coverslips were placed in blocking buffer containing 5% BSA and 0,3% Triton-X100 in PBS for 1 hour. The coverslips were then incubated with primary anti γ-catenin antibodies in blocking buffer in a moist chamber for 1 hour (dilution 1:500). After washing with PBS for 5 times coverslips were incubated with secondary Alexa-fluor 546 donkey anti-mouse (1 µg/ml) antibodies in blocking buffer in a moist chamber for 1 hour. After washing with PBS for 5 times coverslips were mounted with DAPI-antifade mountant. Gamma-tubulin staining was employed for membrane staining. Figures were photographed by using TCS SP5 (Leica) confocal microscope and High Content Imaging System Operetta CLS (PerkinElmer).

7.3 RESULTS AND DISCUSSION

7.3.1 Targeting of B2MG proteins in senescent cells

Very recently, novel senescent biomarkers have been identified by Macip's group at the University of Leicester. In a joint collaboration with the latter research group, fluorescent nanoMIPs targeted towards an overexpressed membrane protein (called B2MG) present in senescent cells were tested. B2MG is a membrane protein which is part of the MHCI complex, upregulated in several pathological conditions, and recently proven to be overexpressed in senescent cells[260, 261].

The nanoMIPs were produced by solid-phase imprinting using an epitope (CEYASRVNHVTLSQPKIVKW) of B2MG as a template. The in-house synthesised fluorescent monomer *N*-fluo was employed as a signalling functionality to allow detection by flow cytometry or confocal microscopy. Commercially available anti-

B2MG antibodies were used as a control, to compare the binding of nanoMIPs to senescent and healthy cells. After their synthesis, nanoMIPs were dialysed using Amicon centrifuge units (30 kDa MWCO) to remove traces of unreacted monomers. DLS analysis showed a particle diameter of 235 ± 8 nm in water, while fluorescence analysis confirmed a bright fluorescence emission around 510 nm. Preliminary results obtained by flow cytometry (Figure 7-2) showed fluorescence signal in senescent cells (EJp16) treated both with antibodies and nanoMIPs, at a concentration of 20 μg/ml.
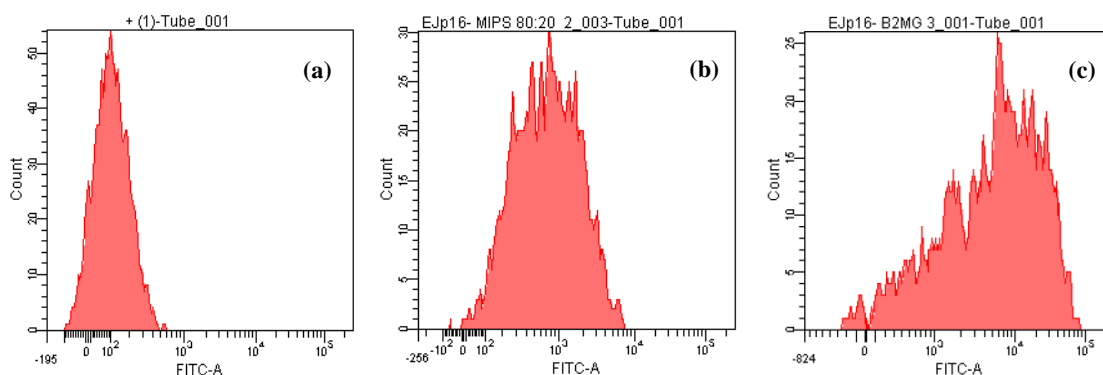
Figure 7-2. Representative fluorescence emission of untreated senescent cells (a), senescent cells treated with MIPs (b) and with antibodies (c) analysed by flow cytometry.

The emission of labelled nanoMIPs and antibodies after 1 h incubation with senescent and healthy cells was then compared and plotted (Figure 7-3). Experiments were performed in triplicate, considering the number of fluorescent events detected (one event corresponds to one cell detected). The difference in fluorescence between antibodies and MIPs (Figure 7-3) is due to the fact that the commercial antibodies employed to target B2MG are labelled with Alexa Fluor 488, which is several times brighter than fluorescein.
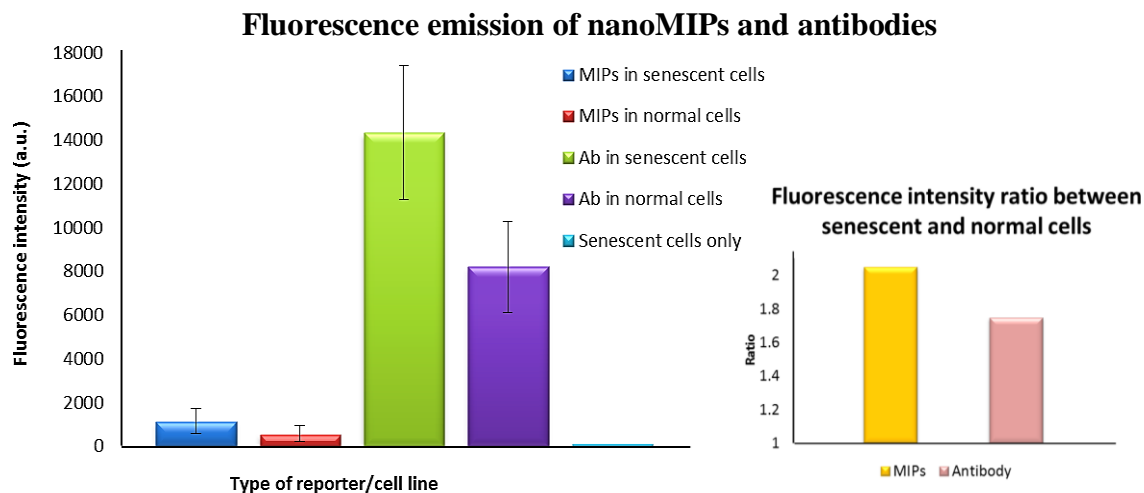
Figure 7-3. Fluorescence emission intensities of labelled nanoMIPs and antibodies in senescent and healthy cells. On the right, fluorescence intensity ratio of the signal detected in senescent and cancer cells, for both nanoMIPs and antibodies.

When evaluating such a difference, one should consider that Alexa Fluor dyes are not sensitive to pH (e.g. no reduction in fluorescence because of changes in pH of the cellular microenvironment), possess a higher quantum yield and lack self-quenching issues. As mentioned above, Alexa Fluor dyes have not been used to label nanoMIPs due to their high cost (around £200/mg). Fluorescein is a much cheaper alternative, however drawbacks such as fast photobleaching, quenching when multiple dyes are in close proximity or under slightly acidic conditions should be carefully considered. However, considering the high fluorescence emission detected even in healthy cells, anti-B2MG antibodies seem to show a considerable amount of non-specific binding. Although the level of fluorescence intensity from fluorescein-labelled nanoMIPs is lower compared to antibodies, nanoMIPs showed good specificity for B2MG, as they were able to bind senescent cells to a higher extent compared to healthy cells. Furthermore, the fluorescence intensity ratio of the signal detected in senescent and healthy cells related to MIPs and antibodies was comparable (Figure 7-3, on the right), suggesting that the level of specificity of the nanoMIPs is similar to the one of antibodies, with less non-specific binding.

7.3.2 EGFR targeting in cancer cells

As widely reported in the literature, EGFR is overexpressed in several malignancies, including lung, breast and colorectal cancers, and is a critical regulator of cancer cell invasiveness. The EGFR structure has been solved and there are several approved antibodies targeted towards EGFR which are currently used in clinic[262]. EGFR is a kinase and is activated by binding of specific ligands, such as epidermal growth factor and transforming growth factor α (TGFα.) Upon binding and activation by its ligands, the receptor undergoes homodimerisation (or heterodimerisation with members of the ErbB receptor family, including ErbB2/Her2/neu). EGFR dimerisation promotes its intrinsic intracellular tyrosine kinase activity. This leads to autophosphorylation of several tyrosine residues in the C-terminal domain of EGFR which, in turn, triggers a cascade of downstream activating signalling proteins. These signalling proteins activate other pathways, such as phosphatidylinositol 3-kinase (PI3K), mitogen-activated protein kinase (MAPK) and the c-Jun N-terminal kinases (JNKs), inducing cell proliferation and cell migration, leading to cancer development/progression (Figure 7-4).[263]

EGFR-specific MIPs (EGFR-nanoMIPs) were produced against a linear sequence (aa 418-435) of the extracellular portion of the receptor. This region overlaps with the EGF binding region and therefore a MIP binding would also prevent the dimerisation/activation of the receptor itself, potentially leading to a reduction in that cascade of downstream proteins, which ultimately induce cell proliferation. In a collaboration with Dr. Larissa Lezina and Dr. Nick Barlev, several breast and lung cancer cell lines, expressing different amounts of EGFR, were tested in the presence of fluorescent nanoMIPs.
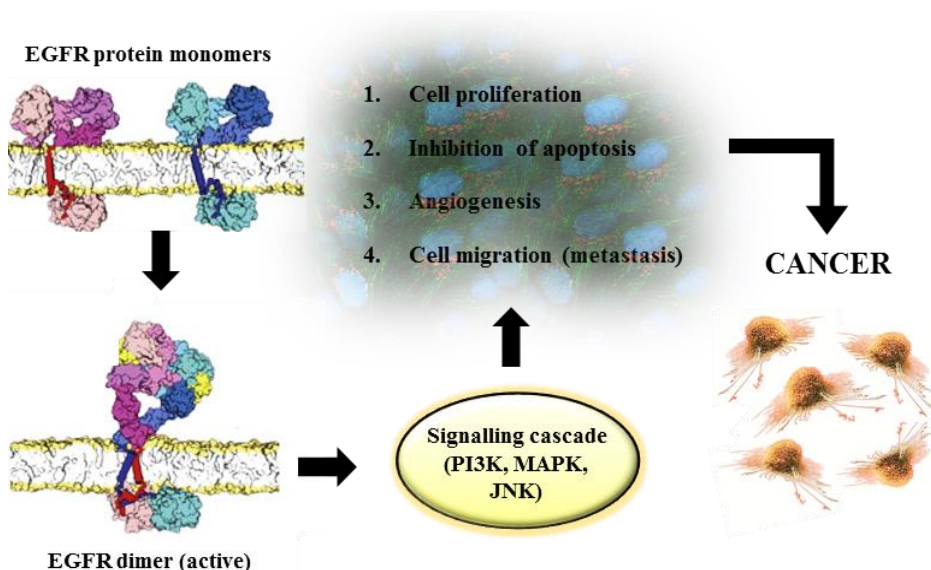
Figure 7-4. Scheme of the main processes involved in EGFR activation.

Specific binding of nanoMIPs to cancer cells – flow cytometry analysis

After their synthesis, an aliquot of fluorescent EGFR-nanoMIPs was dialysed to remove traces of monomers or templates and concentrated down to 0.3 mg/ml. This was necessary to allow the further dilution with the cellular media. The final concentration of nanoMIPs in the presence of cancer cells was between 10 and 40 μg/ml. The fluorescence of these nanoMIPs was previously assessed by means of a fluorimeter, to ensure the incorporation of the fluorescent monomer was successful, and the particles suitable for flow cytometry analysis. The nanoMIPs were incubated for 2 h in the presence of several breast and lung cancer cell lines, expressing different amount of EGFR. The EGFR total expression was assessed by Western Blot (WB) and reported in Figure 7-5. GAPDH is usually employed as a loading control for WB, as it is constitutively expressed in most cells. GAPDH is generally used to normalize the levels of proteins loaded on the gel. From the results reported in Figure 7-5, it is evident that the MDA-MB468 cells (breast cancer) which express the highest amount of EGFR (WB below) also showed the highest binding of EGFR-nanoMIPs. Conversely SKBR3 cells, which express a very low amount of EGFR, did not show any appreciable binding of EGFR-nanoMIPs, suggesting that the binding of nanoparticles to cells is specific.
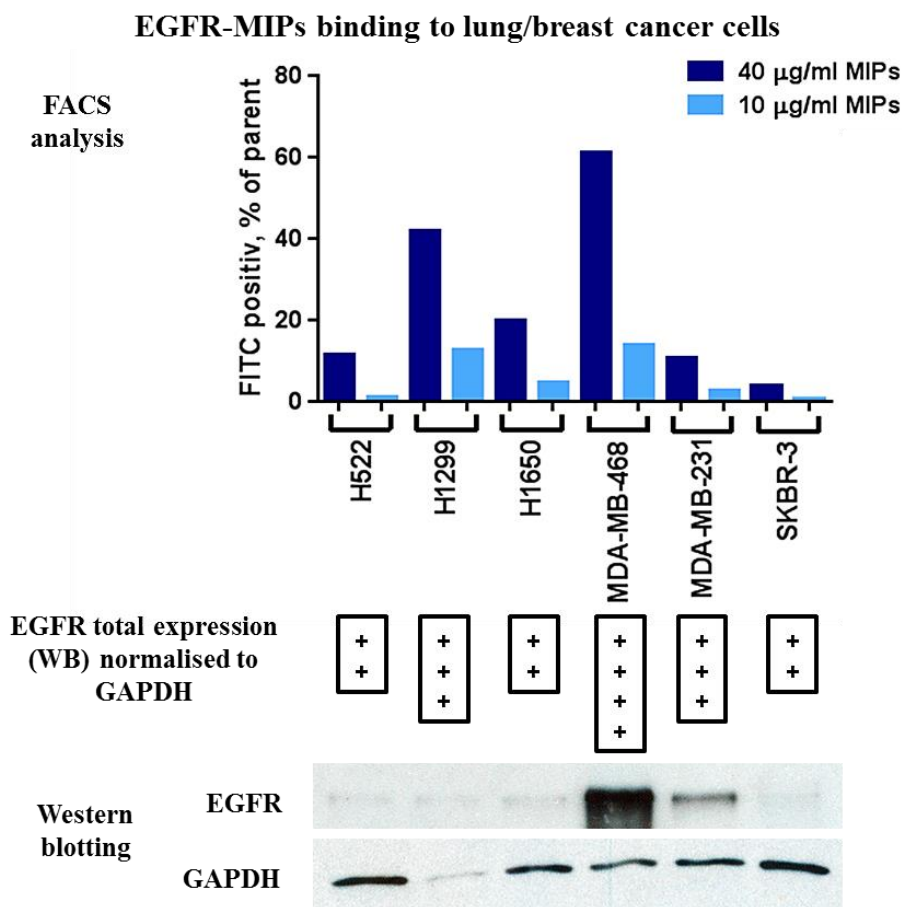
Figure 7-5. Level of nanoMIPs binding to EGFR, normalised by subtracting nonspecific binding (nanoMIPs imprinted for biotin) from total binding for each cell line.

Specific binding of nanoMIPs to cancer cells – confocal microscopy

To further assess the binding of fluorescent nanoMIPs to EGFR, confocal microscopy was performed on MDA-468 and SKBR-3 cells, respectively expressing high and low levels of EGFR on the cell surface (Figure 7-6). The nanoMIPs were first dialysed against distilled water to remove traces of monomers, then diluted in cell culture media at a final concentration of 10 μg/ml, and eventually incubated in the presence of cells for 2 and 24 h. The nucleus was stained with DAPI (blue), while γ-tubulin (red) was employed to stain the cell membrane. NanoMIPs were labelled with the previously synthesised fluorescein-based monomer (*N*-fluo), showing a green emission around 510

nm. Figure 7-7 shows higher binding of the nanoMIPs to cells overexpressing EGFR (MDA-468), whereas an evident lower binding was detected in cells expressing lower levels of EGFR (SKBR-3). These results confirm the previous flow cytometry analysis and demonstrate that the synthesised EGFR-imprinted nanoMIPs are specific for their target even in physiological conditions, and therefore nanoMIPs in general can be potentially used as imaging tools to target overexpressed proteins in specific cell populations.
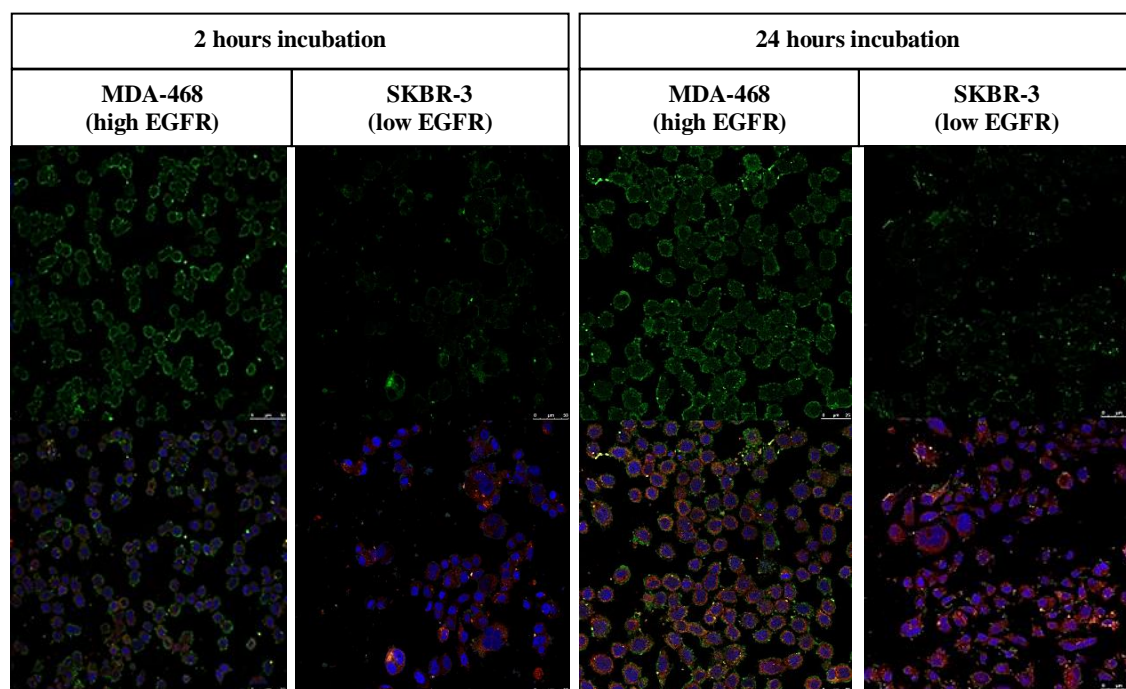
Figure 7-6. Confocal microscopy imges of fluorescent nanoMIPs (green) in MDA-468 and SKBR-3 cells after 2 and 24 h incubation. DAPI was employed to stain the nucleus (blue), and γ-tubulin (red) for the membrane.

7.4 CONCLUSIONS

The work performed on senescent and cancer cells proved that fluorescent nanoMIPs targeted towards overexpressed proteins on the cell surface are specific for their targets under physiological conditions, and could be used as *in vitro* imaging tools. This preliminary work opens the possibility to explore other proteins as potential targets, with the chance to produce MIP NPs imprinted with several targets and labelled with

different dyes, thus achieving multiplexed imaging. The next step involves the assessment of their i*n vivo* performance as imaging tools. In a current collaboration with Dundee University, we are exploring the possibility to use composite QD-MIP NPs to target solid cancer in Zebrafish and mice.

Another potential application of MIP NPs, currently being investigated in our labs, entails their use as drug delivery systems (DDS). In particular, MIP NPs can be polymerised in the presence of two templates, one immobilised on the solid-phase (an epitope of the target protein) and the other free in solution (the drug to be included in the particle). Thus a simultaneous "primary" and "secondary" imprinting would be accomplished, with the MIP NPs being able to specifically bind a given protein while delivering a drug to the target cell. Finally, an intriguing application is the use of MIP NPs to target and block a surface effector protein, thus preventing the relative intracellular effect of that protein, for instance by blocking specific kinases which lead to phosphorylation and activation of intracellular enzymes.

8 GENERAL CONCLUSIONS AND FUTURE WORK

Fluorescent nanoMIPs imprinted for a wide range of targets, ranging from small molecules such as melamine to peptides and proteins, have been produced by means of an innovative solid-phase approach which relies on the immobilisation of the template molecule on a solid support (micro-sized glass beads). This fully automatable method allows simultaneous purification and selection of nanoMIPs with high-affinity for the template in just about 3 hours. Conversely, most of the polymerisation routes to produce nanoMIPs require typically 20-24 hours and a further purification step (e.g. Soxhlet extraction or dialysis) is mandatory to remove template and unreacted monomers.

In this work, several commercially available fluorescent monomers were first tested to assess their suitability to produce nanoMIPs. Some of them showed either poor photochemical stability or inappropriate fluorescence properties for their application as signalling functionalities in cells. For this reason, two fluorescent monomers were synthesised (*N*-fluoresceinylacrylamide and eosin *O*-acrylate). In light of its stability, the fluorescein-based monomer was then used as a fluorescent reporter in all subsequent nanoMIPs. Several fluorescent dyes have been used and successfully polymerised either within the MIP matrix or grafted as polymeric layer around the nanoparticles (core-shell approach). The latter method is very useful for performing surface functionalisation of nanoMIPs, without affecting their recognition properties. For instance, PEGylation proved to be an effective method to improve the colloidal stability of nanoMIPs both in water and in physiological conditions, and enable their use in ELISA-like assays. An interesting modification of the current ELISA protocol with nanoMIPs, currently under investigation, entails the use of two types of nanoMIPs developed against two different epitopes of the same target. One nanoMIP would act as a "capture agent", while the other one would be the analogue of a detection antibiody, much like a sandwich ELISA. The detection MIP could be either fluorescently labelled or modified to bear HRP moieties.

Although nanoMIPs have been successfully applied *in vivo* as demonstrated by Hoshino *et al*., no comprehensive biocompatibility studies have been carried out so far. Even the inflammatory response of nanoMIPs has not been assessed so far, thus preventing them from being considered for any clinical *in vivo* applications. Herein, we demonstrated that nanoMIPs are biocompatible in several cell lines and exhibited a low cytokine

release, making them potentially exploitable as *in vivo* imaging tools. To assess this, *in vivo* experiments in Zebrafish and mice are currently being performed. When considering biological applications, the absence of bacteria/fungi in the MIP solution is unquestionably crucial. In this regard, nanoMIPs demonstrated to be structurally stable after autoclaving and UV treatment, and recent preliminary results showed that their recognition properties remain unaffected after sterilisation. Further tests will be performed to evaluate whether other methods (e.g. azide, gamma irradiation, ethanol treatment) are also viable options. The uptake studies performed in this work proved that MIP NPs can be internalised in cells, regardless of their imprinting method (in water or in acetonitrile), and therefore can be employed as intracellular drug delivery systems (DDS). For this purpose, cleavable linkers such as hydrazone or the use of a disulfide cross-linker such as *N,N*-bis(acryloyl)cystamine that can undergo reduction by intracellular glutathione, represent an interesting option, currently under investigation, to achieve selective drug release. Moreover, magnetic properties could be embedded in the MIP matrix allowing magnetic targeting and, potentially, hyperthermia therapy.

The results obtained on senescent and cancer cells proved that nanoMIPs can be used to target overexpressed proteins on the cell surface. As mentioned above, since a panel of nanoMIPs targeted towards several epitopes can be easily labelled using different reporters, multiplexed imaging is theoretically achievable. The choice of the fluorescent reporter is crucial and depends on the final application. Generally, Alexa Fluor® dyes show excellent photochemical properties but their use may be limited by their high cost. Other fluorescent monomers are currently being synthesised in our labs, such as dansyl-based monomers for detection of hydrophobic compounds and ion-sensitive monomers for detection of heavy metals.

Overall, nanoMIPs demonstrated their great potential in diagnostics, both for quantification of molecules (e.g. ELISA-like assays) and for *in vitro*/*in vivo* imaging. Their ability to specifically bind overexpressed proteins on the cell surface opens the possibility to explore other biomarkers as targets, and paves the way for their use as therapeutic agents, either in the form of DDS or multifunctional nanosystems (e.g. magnetofluorescent NPs). Very recently, it has been verified that even intracellular proteins may be used as targets in cancer therapy. This can be possible because some intracellular proteins produce extracellular epitopes or directly migrate to cell membrane under certain circumstances (stress or cancer)[264]. Therefore, depending on

the physiological trafficking of the protein or its epitopes, targeting of proteins usually located intracellularly is achievable. Finally, another intriguing application for nanoMIPs is their use as "receptor antagonists", able to block a surface effector protein, thus preventing the relative intracellular effect of that protein (e.g. by blocking kinases which lead to phosphorylation and activation of intracellular enzymes).

9 LIST OF PUBLICATIONS

- F. Canfarotta, M. Whitcombe, S. Piletsky. *Polymeric nanoparticles for optical sensing* – Biotechnology Advances, 2013, 31 (8), 1585

- I.P.V. Sansalvador, F. Canfarotta, S. Piletsky. *Synthesis of monodisperse polymeric nano- and microparticles and their application in bioanalysis* – Bioanalytical Reviews, 2013 (book chapter)

- E. Moczko, A. Poma, A. Guerreiro, I.P.V. Sansalvador, S. Caygill, F. Canfarotta, M. Whitcombe, S. Piletsky. *Surface-modified multifunctional MIP nanoparticles* – Nanoscale, 2013, 5 (9), 3733

- F. Canfarotta, S. Piletsky. *Engineered magnetic nanoparticles for biomedical applications* – Advanced Healthcare Materials, 2014, 3 (2), 160

- F. Canfarotta, A. Poma, A. Guerreiro, S. Piletsky. *Solid-phase synthesis of molecularly imprinted nanoparticles* – Nature Protocols, 2016, 11 (3)

- C. Cáceres, F. Canfarotta, I. Chianella, E. Pereira, E. Moczko, C. Esen, A. Guerreiro, E. Piletska, M. Whitcombe and S. Piletsky. *Does size matter? Study of performance of pseudo-ELISAs based on molecularly imprinted polymer nanoparticles prepared for analytes of different sizes* – Analyst, 2016, 141

- F. Canfarotta, A. Waters, R. Sadler, A. Guerreiro, P. McGill, D. Papkovsky, K. Haupt, S. Piletsky. *Biocompatibility and internalisation of molecularly imprinted polymer nanoparticles* – Nano Research, 2016, in press

- J. Czulak, A. Guerreiro, K. Metran, F. Canfarotta, A. Goddard, R. H. Cowan, A. W. Trochimczuk, S. Piletsky. *Formation of target-specific binding sites in enzymes. Solid-phase molecular imprinting of HRP* – Nanoscale, 2016, in press

- F. Canfarotta, K. Smolinska, S. Piletsky. *Development of an ELISA-like assay based on imprinted nanoparticles for detection of vancomycin* – Book chapter in "Methods in Molecular Biology" (Springer), submitted

- F. Canfarotta, L. Lezina, N. Barlev, A. Guerreiro, S. Piletsky. *EGFR targeting in cancer cells with molecularly imprinted nanoparticles* – Submitted to Nature Nanotechnology

- K. Smolinska, A. Guerreiro, F. Canfarotta, C. Fuentes, M. Whitcombe, S. Piletsky – *Performance of antibodies and imprinted polymer nanoparticles in ELISA - a direct comparison* – Submitted to Scientific Reports

- E. Piletska, H. Yawer, F. Canfarotta, K. Smolinska, E. Moczko, S. Piletsky, A. Guerreiro, M. J. Whitcombe, S. Piletsky. *Solid-phase synthesis of molecularly imprinted silica nanoparticles by Ostwald ripening* – Submitted to Nano Today

- Antonio Guerreiro, Mona Qasem, Francesco Canfarotta, Deiene Garcia-Mutio, Alberto Gomez-Caballero, María Aránzazu, Ramón Barrio, Elena Piletska, Sergey Piletsky. *Solid-Phase Molecular Imprinting in the Absence of Cross-linkers: Towards Plastic Aptamers* – Submitted to Nature Communications

- S. Tang, F. Canfarotta, S. Piletsky. *An ELISA-like assay based on molecularly imprinted nanoparticles for detection of gentamicin in real samples* – In preparation

- F. Canfarotta, A. Cecchini, S. Piletsky. *Nano-sized molecularly imprinted polymers as artificial antibodies* – Book chapter in "Molecularly Imprinted Polymers: Analytical Chemistry Applications" (Royal Society of Chemistry), in preparation

- S. Kassem, F. Canfarotta, J. Czulak, S. Piletsky, M. Mohamed, H. Sayour. *Biocompatibility and biodistribution of surface-modified Yttrium nanoparticles in rats for theranostic applications* – in preparation

10 REFERENCES

1. K. K. Jain, *Clinica chimica acta; international journal of clinical chemistry*, 2005, **358**, 37-54.

2. I. L. Medinitz, Tetsuo Uyeda, H., Goldman E.R., Mattussi, H., *Nature Materials*, 2005, **4**, 435 - 446.

3. K. K. Jain, *Clinical chemistry*, 2007, **53**, 2002-2009.

4. Renub-Research, *Global In Vitro Diagnostic (IVD) Market Trends and Future Forecast (2009-2014)*, 2010.

5. RNCOS, *Global in vitro diagnostic market analysis*, 2011.

6. A. P. Demchenko, *Advanced fluorescent reporters in chemistry and biology II*, 2010.

7. J. Hu and S. Liu, *Macromolecules*, 2010, **43**, 8315-8330.

8. Y. Shiraishi, T. Inoue and T. Hirai, *Langmuir*, 2010, **26**, 17505-17512.

9. D. Wang, R. Miyamoto, Y. Shiraishi and T. Hirai, *Langmuir*, 2009, **25**, 13176-13182.

10. K. Cui, X. Lu, J. Guan, Q. Lu, Z. Fei and P. J. Dyson, *Chemistry - A European Journal*, 2013, **19**, 8550-8557.

11. A. P. Demchenko, *Analytical biochemistry*, 2005, **343**, 1-22.

12. J. P. Rao and K. E. Geckeler, *Progress in Polymer Science (Oxford)*, 2011, **36**, 887-913.

13. P. B. Zetterlund, Y. Kagawa and M. Okubo, *Chemical Reviews*, 2008, **108**, 3747-3794.

14. C. Li and S. Liu, *Chemical Communications*, 2012, **48**, 3262-3278.

15. K. J. Y. a. J. T. Y. K. Yang, J. Am. Chem. Soc., 2005, 127, and 16760–16761., *J. Am. Chem. Soc.*, 2005, **127**, 16760–16761.

16. C. H. L. a. S. Y. L. J. M. Hu, Langmuir, 2010, 26, 724–729., *Langmuir*, 2010, **26**, 724–729.

17. Y. Jiang, X. Hu, J. Hu, H. Liu, H. Zhong and S. Liu, *Macromolecules*, 2011, **44**, 8780-8790.

18. Y. Y. Li, H. Cheng, J. L. Zhu, L. Yuan, Y. Dai, S. X. Cheng, X. Z. Zhang and R. X. Zhuo, *Advanced Materials*, 2009, **21**, 2402-2406.

19. M. Q. Zhu, L. Zhu, J. J. Han, W. Wu, J. K. Hurst and A. D. Q. Li, *Journal of the American Chemical Society*, 2006, **128**, 4303-4309.

20. J. Chen, F. Zeng, S. Wu, Q. Chen and Z. Tong, *Chemistry - A European Journal*, 2008, **14**, 4851-4860.

21. M. Q. Zhu, G. F. Zhang, C. Li, M. P. Aldred, E. Chang, R. A. Drezek and A. D. Q. Li, *Journal of the American Chemical Society*, 2011, **133**, 365-372.

22. T. Wu, G. Zou, J. Hu and S. Liu, *Chemistry of Materials*, 2009, **21**, 3788-3798.

23. S. Deshayes, V. Maurizot, M. C. Clochard, C. Baudin, T. Berthelot, S. Esnouf, D. Lairez, M. Moenner and G. Déléris, *Pharmaceutical Research*, 2011, **28**, 1631-1642.

24. K. Miki, K. Oride, S. Inoue, Y. Kuramochi, R. R. Nayak, H. Matsuoka, H. Harada, M. Hiraoka and K. Ohe, *Biomaterials*, 2010, **31**, 934-942.

25. A. Pucci, E. Locatelli, J. Ponti, C. Uboldi, V. Molinari and M. Comes Franchini, *Journal of Nanoparticle Research*, 2013, **15**, 1-6.

26. J. F. Lutz and Z. Zarafshani, *Advanced drug delivery reviews*, 2008, **60**, 958-970.

27. M. Álvarez-Paino, G. Marcelo, A. Muñoz-Bonilla, J. Rodríguez-Hernández and M. Fernández-García, *Polymer Chemistry*, 2013, **4**, 986-995.

28. H. Su, Y. Liu, D. Wang, C. Wu, C. Xia, Q. Gong, B. Song and H. Ai, *Biomaterials*, 2013, **34**, 1193-1203.

29. C. Tissandier, N. Diop, M. Martini, S. Roux, O. Tillement and T. Hamaide, *Langmuir*, 2012, **28**, 209-218.

30.   S. K. Sahoo, S. Parveen and J. J. Panda, *Nanomedicine*, 2007, **3**, 20-31.

31.   A. F. E. Hezinger, J. Teßmar and A. Göpferich, *European Journal of Pharmaceutics and Biopharmaceutics*, 2008, **68**, 138-152.

32.   J. Luo, Z. Xie, J. W. Y. Lam, L. Cheng, H. Chen, C. Qiu, K. Hoi Sing, X. Zhan, Y. Liu, D. Zhu and T. Ben Zhong, *Chemical Communications*, 2001, 1740-1741.

33.   Y. Hong, J. W. Y. Lam and B. Z. Tang, *Chemical Communications*, 2009, 4332-4353.

34.   Y. Hong, J. W. Y. Lam and B. Z. Tang, *Chemical Society Reviews*, 2011, **40**, 5361-5388.

35.   L. Tang, J. K. Jin, A. Qin, W. Zhang Yuan, Y. Mao, J. Mei, J. Zhi Sun and B. Zhong Tang, *Chemical Communications*, 2009, 4974-4976.

36.   E. Y. Bryleva, N. A. Vodolazkaya, N. O. McHedlov-Petrossyan, L. V. Samokhina, N. A. Matveevskaya and A. V. Tolmachev, *Journal of Colloid and Interface Science*, 2007, **316**, 712-722.

37.   J. Tian, H. Chen, L. Zhuo, Y. Xie, N. Li and B. Tang, *Chemistry - A European Journal*, 2011, **17**, 6626-6634.

38.   S. Uchiyama, Y. Matsumura, A. P. De Silva and K. Iwai, *Analytical Chemistry*, 2003, **75**, 5926-5935.

39.   S. Uchiyama, N. Kawai, A. P. De Silva and K. Iwai, *Journal of the American Chemical Society*, 2004, **126**, 3032-3033.

40.   C. Gota, K. Okabe, T. Funatsu, Y. Harada and S. Uchiyama, *Journal of the American Chemical Society*, 2009, **131**, 2766-2767.

41.   K. Zhou, Y. Wang, X. Huang, K. Luby-Phelps, B. D. Sumer and J. Gao, *Angewandte Chemie - International Edition*, 2011, **50**, 6109-6114.

42.   J. R. Casey, S. Grinstein and J. Orlowski, *Nature Reviews Molecular Cell Biology*, 2010, **11**, 50-61.

43.   S. Hornig, C. Biskup, A. Gräfe, J. Wotschadlo, T. Liebert, G. J. Mohr and T. Heinze, *Soft Matter*, 2008, **4**, 1169-1172.

44. C. Fan, S. Wang, J. W. Hong, G. C. Bazan, K. W. Plaxco and A. J. Heeger, *Proceedings of the National Academy of Sciences of the United States of America*, 2003, **100**, 6297-6301.

45. A. Bajaj, O. R. Miranda, I. B. Kim, R. L. Phillips, D. J. Jerry, U. H. F. Bunz and V. M. Rotello, *Proceedings of the National Academy of Sciences of the United States of America*, 2009, **106**, 10912-10916.

46. C. C. You, O. R. Miranda, B. Gider, P. S. Ghosh, I. B. Kim, B. Erdogan, S. A. Krovi, U. H. F. Bunz and V. M. Rotello, *Nature Nanotechnology*, 2007, **2**, 318-323.

47. L. Gai, H. Chen, B. Zou, H. Lu, G. Lai, Z. Li and Z. Shen, *Chemical Communications*, 2012, **48**, 10721-10723.

48. L. Wang and W. Tan, *Nano Letters*, 2006, **6**, 84-88.

49. H. S. Peng, J. A. Stolwijk, L. N. Sun, J. Wegener and O. S. Wolfbeis, *Angewandte Chemie - International Edition*, 2010, **49**, 4246-4249.

50. J. Hu, L. Dai and S. Liu, *Macromolecules*, 2011, **44**, 4699-4710.

51. L. Zhu, W. Wu, M. Q. Zhu, J. J. Han, J. K. Hurst and A. D. Q. Li, *Journal of the American Chemical Society*, 2007, **129**, 3524-3526.

52. B. Ma, S. Wu, F. Zeng, Y. Luo, J. Zhao and Z. Tong, *Nanotechnology*, 2010, **21**.

53. J. Chen, F. Zeng, S. Wu, J. Su, J. Zhao and Z. Tong, *Nanotechnology*, 2009, **20**.

54. M. Frigoli, K. Ouadahi and C. Larpent, *Chemistry - A European Journal*, 2009, **15**, 8319-8330.

55. A. Poma, A. P. Turner and S. A. Piletsky, *Trends in biotechnology*, 2010, **28**, 629-637.

56. N. Lavignac, C. J. Allender and K. R. Brain, *Analytica chimica acta*, 2004, **510**, 139-145.

57. L. Ye and K. Haupt, *Analytical and bioanalytical chemistry*, 2004, **378**, 1887-1897.

58. J. Svenson and I. A. Nicholls, *Analytica chimica acta*, 2001, **435**, 19-24.

59.   E. V. Piletska, A. R. Guerreiro, M. J. Whitcombe and S. A. Piletsky, *Macromolecules*, 2009, **42**, 4921-4928.

60.   S. A. Piletsky, N. W. Turner and P. Laitenberger, *Medical engineering & physics*, 2006, **28**, 971-977.

61.   R. A. Lorenzo, A. M. Carro, C. Alvarez-Lorenzo and A. Concheiro, *International Journal of Molecular Sciences*, 2011, **12**, 4327-4347.

62.   A. G. Mayes and M. J. Whitcombe, *Advanced drug delivery reviews*, 2005, **57**, 1742-1778.

63.   E. L. Holthoff and F. V. Bright, *Analytica chimica acta*, 2007, **594**, 147-161.

64.   D. R. Kryscio and N. A. Peppas, *Acta Biomaterialia*, 2011.

65.   C. Algieri, E. Drioli, L. Guzzo and L. Donato, *Sensors (Switzerland)*, 2014, **14**, 13863-13912.

66.   S. P. Li, H. M. Guan, G. B. Xu and Y. J. Tong, *Fenxi Huaxue/ Chinese Journal of Analytical Chemistry*, 2015, **43**, 294-299.

67.   B. Rezaei, M. K. Boroujeni and A. A. Ensafi, *Biosensors and Bioelectronics*, 2015, **66**, 490-496.

68.   J. Wackerlig and P. A. Lieberzeit, *Sensors and Actuators, B: Chemical*, 2014, **207**, 144-157.

69.   P. S. Sharma, F. D'Souza and W. Kutner, *TrAC - Trends in Analytical Chemistry*, 2012, **34**, 59-76.

70.   Y. T. Wu, Y. J. Liu, X. Gao, K. C. Gao, H. Xia, M. F. Luo, X. J. Wang, L. Ye, Y. Shi and B. Lu, *Chemosphere*, 2015, **119**, 515-523.

71.   S. Tokonami, H. Shiigi and T. Nagaoka, *Analytica chimica acta*, 2009, **641**, 7-13.

72.   D. Gao, Zhang, Z., Wu, M., Xie, C., Guan, G., Wang, D., *Journal of the American Chemical Society*, 2007, **129**, 7859-7866.

73.   E. Asadi, S. Azodi-Deilami, M. Abdouss and S. Khaghani, *Applied Biochemistry and Biotechnology*, 2012, **167**, 2076-2087.

74. K. Rostamizadeh, M. Vahedpour and S. Bozorgi, *International Journal of Pharmaceutics*, 2012, **424**, 67-75.

75. D. Türkmen, N. Bereli, M. E. Çorman, H. Shaikh, S. Akgöl and A. Denizli, *Artificial Cells, Nanomedicine and Biotechnology*, 2014, **42**, 316-322.

76. I. Basozabal, A. Guerreiro, A. Gomez-Caballero, M. Aranzazu Goicolea and R. J. Barrio, *Biosensors and Bioelectronics*, 2014, **58**, 138-144.

77. I. Chianella, A. Guerreiro, E. Moczko, J. S. Caygill, E. V. Piletska, I. M. P. De Vargas Sansalvador, M. J. Whitcombe and S. A. Piletsky, *Analytical Chemistry*, 2013, **85**, 8462-8468.

78. R. V. Shutov, A. Guerreiro, E. Moczko, I. P. De Vargas-Sansalvador, I. Chianella, M. J. Whitcombe and S. A. Piletsky, *Small*, 2014, **10**, 1086-1089.

79. M. J. Abdin, Z. Altintas and I. E. Tothill, *Biosensors and Bioelectronics*, 2015, **67**, 177-183.

80. A. Pardo, L. Mespouille, P. Dubois, B. Blankert and P. Duez, *Chemistry - A European Journal*, 2014, **20**, 3500-3509.

81. Y. Hu, S. Feng, F. Gao, E. C. Y. Li-Chan, E. Grant and X. Lu, *Food Chemistry*, 2015, **176**, 123-129.

82. H. R. Rajabi, M. Shamsipur, M. M. Zahedi and M. Roushani, *Chemical Engineering Journal*, 2015, **259**, 330-337.

83. M. K. Bojdi, M. H. Mashhadizadeh, M. Behbahani, A. Farahani, S. S. H. Davarani and A. Bagheri, *Electrochimica Acta*, 2014, **136**, 59-65.

84. M. Pourfarzib, M. Shekarchi, H. Rastegar, B. Akbari-Adergani, A. Mehramizi and R. Dinarvand, *Journal of Chromatography B: Analytical Technologies in the Biomedical and Life Sciences*, 2015, **974**, 1-8.

85. Z. Zhang, L. Chen, F. Yang and J. Li, *RSC Advances*, 2014, **4**, 31507-31514.

86. X. H. Gu, R. Xu, G. L. Yuan, H. Lu, B. R. Gu and H. P. Xie, *Analytica chimica acta*, 2010, **675**, 64-70.

87. L. Zhao, F. Zhao and B. Zeng, *Biosensors and Bioelectronics*, 2014, **62**, 19-24.

88. C. Guo, B. Wang and J. Shan, *Chinese Journal of Chemistry*, 2014.

89. L. Tan, W. Li, H. Li and Y. Tang, *Journal of Chromatography A*, 2014, **1336**, 59-66.

90. S. E. Shim, Y. Shin, J. W. Jun, K. Lee, H. Jung and S. Choe, *Macromolecules*, 2003, **36**, 7994-8000.

91. V. D. Salian and M. E. Byrne, *Macromolecular Materials and Engineering*, 2013, **298**, 379-390.

92. K. Yang, M. M. Berg, C. Zhao and L. Ye, *Macromolecules*, 2009, **42**, 8739-8746.

93. R. Liu, G. Guan, S. Wang and Z. Zhang, *Analyst*, 2011, **136**, 184-190.

94. H. Niu, Y. Yang and H. Zhang, *Biosensors and Bioelectronics*, 2015, **74**, 440-446.

95. A. B. Descalzo, C. Somoza, M. C. Moreno-Bondi and G. Orellana, *Analytical Chemistry*, 2013, **85**, 5316-5320.

96. S. Ge, J. Lu, L. Ge, M. Yan and J. Yu, *Spectrochimica Acta - Part A: Molecular and Biomolecular Spectroscopy*, 2011, **79**, 1704-1709.

97. Y. Kim, J. B. Jeon and J. Y. Chang, *Journal of Materials Chemistry*, 2012, **22**, 24075-24080.

98. K. Qian, G. Fang and S. Wang, *RSC Advances*, 2013, **3**, 3825-3828.

99. G. Guan, B. Liu, Z. Wang and Z. Zhang, *Sensors*, 2008, **8**, 8291-8320.

100. M. H. Lee, Y. C. Chen, M. H. Ho and H. Y. Lin, *Analytical and bioanalytical chemistry*, 2010, **397**, 1457-1466.

101. C. Lin, A. Joseph, C. Chang and Y. Lee, *Journal of Chromatography A*, 2004, **1027**, 259-262.

102. S. E. Diltemiz, R. Say, S. Buyuktiryaki, D. Hur, A. Denizli and A. Ersoz, *Talanta*, 2008, **75**, 890-896.

103. M. P. Chantada-Vázquez, J. Sánchez-González, E. Peña-Vázquez, M. J. Tabernero, A. M. Bermejo, P. Bermejo-Barrera and A. Moreda-Piñeiro, *Biosensors and Bioelectronics*, 2016, **75**, 213-221.

104. P. Zuo, J. Gao, J. Peng, J. Liu, M. Zhao, J. Zhao and H. He, *Microchimica Acta*, 2016, **183**, 329-336.

105. S. Patra, E. Roy, R. Madhuri and P. K. Sharma, *Biosensors and Bioelectronics*, 2015, **63**, 301-310.

106. L. Feng, L. Tan, H. Li, Z. Xu, G. Shen and Y. Tang, *Biosensors and Bioelectronics*, 2015, **69**, 265-271.

107. M. Bompart, Y. De Wilde and K. Haupt, *Advanced Materials*, 2010, **22**, 2343-2348.

108. W. Wu, J. Shen, Y. Li, H. Zhu, P. Banerjee and S. Zhou, *Biomaterials*, 2012, **33**, 7115-7125.

109. S. Kunath, M. Panagiotopoulou, J. Maximilien, N. Marchyk, J. Sänger and K. Haupt, *Advanced Healthcare Materials*, 2015, **4**, 1322-1326.

110. S. Shinde, Z. El-Schich, A. Malakpour, W. Wan, N. Dizeyi, R. Mohammadi, K. Rurack, A. Gjörloff Wingren and B. Sellergren, *Journal of the American Chemical Society*, 2015, **137**, 13908-13912.

111. D. Yin, S. Wang, Y. He, J. Liu, M. Zhou, J. Ouyang, B. Liu, H. Y. Chen and Z. Liu, *Chemical Communications*, 2015, **51**, 17696-17699.

112. Y. Liu, S. Wang, C. Zhang, X. Su, S. Huang and M. Zhao, *Analytical Chemistry*, 2013, **85**, 4853-4857.

113. K. Fujiwara, Y. Yoshizaki, M. Shin, T. Miyazaki, T. Saita and S. Nagata, *Antimicrobial Agents and Chemotherapy*, 2012, **56**, 5883-5891.

114. L. Gao, J. Zhuang, L. Nie, J. Zhang, Y. Zhang, N. Gu, T. Wang, J. Feng, D. Yang, S. Perrett and X. Yan, *Nature Nanotechnology*, 2007, **2**, 577-583.

115. Y. Hoshino, H. Koide, T. Urakami, H. Kanazawa, T. Kodama, N. Oku and K. J. Shea, *Journal of the American Chemical Society*, 2010, **132**, 6644-6645.

116. Z. Wu, J. Hou, Y. Wang, M. Chai, Y. Xiong, W. Lu and J. Pan, *International Journal of Pharmaceutics*, 2015, **496**, 1006-1014.

117. H. Shi, X. He, Y. Yuan, K. Wang and D. Liu, *Analytical Chemistry*, 2010, **82**, 2213-2220.

118. R. Y. Tsien, *Nature*, 1981, **290**, 527-528.

119. H. A. Clark, R. Kopelman, R. Tjalkens and M. A. Philbert, *Analytical Chemistry*, 1999, **71**, 4837-4843.

120. J. Xu, L. Sun, J. Li, J. Liang, H. Zhang and W. Yang, *Nanoscale Research Letters*, 2011, **6**, 1-7.

121. L. Wang, Wang, K., Santra, S., Zhao, X., Hilliard, L.R., Smith, J.E., Wu, Y., Tan, W., *Analytical Chemistry*, 2006, **78**, 646-654.

122. Y. Wang, Z. Li, W. Zhong, H. Li, D. Xu and H. Chen, *Science China Chemistry*, 2010, **53**, 747-751.

123. D. Knopp, D. Tang and R. Niessner, *Analytica chimica acta*, 2009, **647**, 14-30.

124. F. Gao, F. Luo, J. Yin and L. Wang, *Luminescence*, 2008, **23**, 392-396.

125. T. Kurkina and K. Balasubramanian, *Cellular and molecular life sciences : CMLS*, 2011.

126. A. S. de Dios and M. E. Diaz-Garcia, *Analytica chimica acta*, 2010, **666**, 1-22.

127. J. Kim, H. S. Kim, N. Lee, T. Kim, H. Kim, T. Yu, I. C. Song, W. K. Moon and T. Hyeon, *Angewandte Chemie - International Edition*, 2008, **47**, 8438-8441.

128. V. Salgueiriño-Maceira, M. A. Correa-Duarte, M. Spasova, L. M. Liz-Marzán and M. Farle, *Advanced Functional Materials*, 2006, **16**, 509-514.

129. S. A. Corr, Y. P. Rakovich and Y. K. Gun'Ko, *Nanoscale Research Letters*, 2008, **3**, 87-104.

130. D. W. Hwang, H. Y. Ko, J. H. Lee, H. Kang, S. H. Ryu, I. C. Song, D. S. Lee and S. Kim, *Journal of Nuclear Medicine*, 2010, **51**, 98-105.

131.   H. S. Cho, Z. Dong, G. M. Pauletti, J. Zhang, H. Xu, H. Gu, L. Wang, R. C. Ewing, C. Huth, F. Wang and D. Shi, *ACS Nano*, 2010, **4**, 5398-5404.

132.   S. T. Selvan, P. K. Patra, C. Y. Ang and J. Y. Ying, *Angewandte Chemie - International Edition*, 2007, **46**, 2448-2452.

133.   A. Ranzoni, A. Den Hamer, T. Karoli, J. Buechler and M. A. Cooper, *Analytical Chemistry*, 2015, **87**, 6150-6157.

134.   J. Sudimack and R. J. Lee, *Advanced drug delivery reviews*, 2000, **41**, 147-162.

135.   C. Chen, J. Ke, X. E. Zhou, W. Yi, J. S. Brunzelle, J. Li, E. L. Yong, H. E. Xu and K. Melcher, *Nature*, 2013.

136.   H. Lu, G. Yi, S. Zhao, D. Chen, L. H. Guo and J. Cheng, *Journal of Materials Chemistry*, 2004, **14**, 1336-1341.

137.   S. Wu, G. Han, D. J. Milliron, S. Aloni, V. Altoe, D. V. Talapin, B. E. Cohen and P. J. Schuck, *Proceedings of the National Academy of Sciences of the United States of America*, 2009, **106**, 10917-10921.

138.   T. J. Yoon, J. S. Kim, B. G. Kim, K. N. Yu, M. H. Cho and J. K. Lee, *Angewandte Chemie - International Edition*, 2005, **44**, 1068-1071.

139.   J. Harrison, C. A. Bartlett, G. Cowin, P. K. Nicholls, C. W. Evans, T. D. Clemons, B. Zdyrko, I. A. Luzinov, A. R. Harvey, K. S. Iyer, S. A. Dunlop and M. Fitzgerald, *Small*, 2012, **8**, 1579-1589.

140.   A. Fraix, N. Kandoth, I. Manet, V. Cardile, A. C. E. Graziano, R. Gref and S. Sortino, *Chemical Communications*, 2013, **49**, 4459-4461.

141.   J. An, X. Dai, Z. Wu, Y. Zhao, Z. Lu, Q. Guo, X. Zhang and C. Li, *Biomacromolecules*, 2015, **16**, 2444-2454.

142.   R. Dey, S. Mazumder, M. K. Mitra, S. Mukherjee and G. C. Das, *Journal of Nanomaterials*, 2009, **2009**.

143.   Y. Xing, Z. Xia and J. Rao, *IEEE Transactions on Nanobioscience*, 2009, **8**, 4-12.

144. R. A. Sperling and W. J. Parak, *Philosophical Transactions of the Royal Society A: Mathematical, Physical and Engineering Sciences*, 2010, **368**, 1333-1383.

145. A. A. Burns, J. Vider, H. Ow, E. Here, P. M. Oula, M. Baumgart, S. M. Larson, U. Wiesner and M. Bradbury, *Nano Letters*, 2009, **9**, 442-448.

146. M. Benezra, O. Penate-Medina, P. B. Zanzonico, D. Schaer, H. Ow, A. Burns, E. DeStanchina, V. Longo, E. Herz, S. Iyer, J. Wolchok, S. M. Larson, U. Wiesner and M. S. Bradbury, *The Journal of clinical investigation*, 2011, **121**, 2768-2780.

147. M. Nakamura, M. Shono and K. Ishimura, *Analytical Chemistry*, 2007, **79**, 6507-6514.

148. T. Yu, K. Greish, L. D. McGill, A. Ray and H. Ghandehari, *ACS Nano*, 2012, **6**, 2289-2301.

149. D. Lee, S. Khaja, J. C. Velasquez-Castano, M. Dasari, C. Sun, J. Petros, W. R. Taylor and N. Murthy, *Nature Materials*, 2007, **6**, 765-769.

150. I. Lee, O. Hwang, D. Yoo, G. Khang and D. Lee, *Bulletin of the Korean Chemical Society*, 2011, **32**, 2187-2192.

151. D. Lee, V. R. Erigala, M. Dasari, J. Yu, R. M. Dickson and N. Murthy, *International Journal of Nanomedicine*, 2008, **3**, 471-476.

152. R. Zhang, C. Xiong, M. Huang, M. Zhou, Q. Huang, X. Wen, D. Liang and C. Li, *Biomaterials*, 2011, **32**, 5872-5879.

153. W. J. M. Mulder, K. Castermans, J. R. Van Beijnum, M. G. A. Oude Egbrink, P. T. K. Chin, Z. A. Fayad, C. W. G. M. Löwik, E. L. Kaijzel, I. Que, G. Storm, G. J. Strijkers, A. W. Griffioen and K. Nicolay, *Angiogenesis*, 2009, **12**, 17-24.

154. P. Decuzzi, R. Pasqualini, W. Arap and M. Ferrari, *Pharmaceutical Research*, 2009, **26**, 235-243.

155. M. Liang, X. Liu, D. Cheng, G. Liu, S. Dou, Y. Wang, M. Rusckowski and D. J. Hnatowich, *Bioconjugate Chemistry*, 2010, **21**, 1385-1388.

156. C. Zheng, M. Zheng, P. Gong, D. Jia, P. Zhang, B. Shi, Z. Sheng, Y. Ma and L. Cai, *Biomaterials*, 2012, **33**, 5603-5609.

157. C. M. Lee, H. J. Jeong, S. J. Cheong, E. M. Kim, D. W. Kim, S. T. Lim and M. H. Sohn, *Pharmaceutical Research*, 2010, **27**, 712-721.

158. S. Lee, J. H. Ryu, K. Park, A. Lee, S. Y. Lee, I. C. Youn, C. H. Ahn, S. M. Yoon, S. J. Myung, D. H. Moon, X. Chen, K. Choi, I. C. Kwon and K. Kim, *Nano Letters*, 2009, **9**, 4412-4416.

159. M. K. Yoo, I. K. Park, H. T. Lim, S. J. Lee, H. L. Jiang, Y. K. Kim, Y. J. Choi, M. H. Cho and C. S. Cho, *Acta Biomaterialia*, 2012, **8**, 3005-3013.

160. G. Hong, R. Yuan, B. Liang, J. Shen, X. Yang and X. Shuai, *Biomedical Microdevices*, 2008, **10**, 693-700.

161. W. L. L. Suen and Y. Chau, *Journal of Controlled Release*, 2013, **167**, 21-28.

162. M. K. Yoo, I. Y. Kim, E. M. Kim, H. J. Jeong, C. M. Lee, Y. Y. Jeong, T. Akaike and C. S. Cho, *Journal of Biomedicine and Biotechnology*, 2007, **2007**.

163. M. D. Rowe, D. H. Tham, S. L. Kraft and S. G. Boyes, *Biomacromolecules*, 2009, **10**, 983-993.

164. L. Zhang, H. Xue, C. Gao, L. Carr, J. Wang, B. Chu and S. Jiang, *Biomaterials*, 2010, **31**, 6582-6588.

165. G. Chen, W. Chen, Z. Wu, R. Yuan, H. Li, J. Gao and X. Shuai, *Biomaterials*, 2009, **30**, 1962-1970.

166. T. Dai, N. Li, L. Zhang, Y. Zhang and Q. Liu, *International Journal of Nanomedicine*, 2016, **11**, 203-212.

167. N. Lewinski, V. Colvin and R. Drezek, *Small*, 2008, **4**, 26-49.

168. S. T. Selvan, T. T. Yang Tan, D. Kee Yi and N. R. Jana, *Langmuir*, 2010, **26**, 11631-11641.

169. J. Weng and J. Ren, *Current Medicinal Chemistry*, 2006, **13**, 897-909.

170. X. Gao, Y. Cui, R. M. Levenson, L. W. K. Chung and S. Nie, *Nature biotechnology*, 2004, **22**, 969-976.

171. L. Yildirimer, N. T. K. Thanh, M. Loizidou and A. M. Seifalian, *Nano Today*, 2011, **6**, 585-607.

172. C. He, L. Yin, C. Tang and C. Yin, *Biomaterials*, 2012, **33**, 8569-8578.

173. K. Riehemann, S. W. Schneider, T. A. Luger, B. Godin, M. Ferrari and H. Fuchs, *Angewandte Chemie - International Edition*, 2009, **48**, 872-897.

174. U. Tamer, Y. Gündoğdu, I. H. Boyaci and K. Pekmez, *Journal of Nanoparticle Research*, 2010, **12**, 1187-1196.

175. Z. Yang, J. Leon, M. Martin, J. W. Harder, R. Zhang, D. Liang, W. Lu, M. Tian, J. G. Gelovani, A. Qiao and C. Li, *Nanotechnology*, 2009, **20**.

176. W. J. Stark, *Angewandte Chemie International Edition*, 2011, **50**, 1242-1258.

177. B. Ballou, B. C. Lagerholm, L. A. Ernst, M. P. Bruchez and A. S. Waggoner, *Bioconjugate Chemistry*, 2004, **15**, 79-86.

178. B. Ballou, L. A. Ernst, S. Andreko, T. Harper, J. A. J. Fitzpatrick, A. S. Waggoner and M. P. Bruchez, *Bioconjugate Chemistry*, 2007, **18**, 389-396.

179. I. Brigger, C. Dubernet and P. Couvreur, *Advanced drug delivery reviews*, 2002, **54**, 631-651.

180. X. He, H. Nie, K. Wang, W. Tan, X. Wu and P. Zhang, *Analytical Chemistry*, 2008, **80**, 9597-9603.

181. Z. Yang, S. Zheng, W. J. Harrison, J. Harder, X. Wen, J. G. Gelovani, A. Qiao and C. Li, *Biomacromolecules*, 2007, **8**, 3422-3428.

182. D. E. Owens, 3rd and N. A. Peppas, *Int J Pharm*, 2006, **307**, 93-102.

183. Y. Sheng, C. Liu, Y. Yuan, X. Tao, F. Yang, X. Shan, H. Zhou and F. Xu, *Biomaterials*, 2009, **30**, 2340-2348.

184. J. H. Park, L. Gu, G. Von Maltzahn, E. Ruoslahti, S. N. Bhatia and M. J. Sailor, *Nature Materials*, 2009, **8**, 331-336.

185. M. Ferrari, *Nature Nanotechnology*, 2008, **3**, 131-132.

186. H. Duan and S. Nie, *Journal of the American Chemical Society*, 2007, **129**, 3333-3336.

187. P. Decuzzi and M. Ferrari, *Biophysical Journal*, 2008, **94**, 3790-3797.

188. J. Shim, V. Solovyeva, D. Estrada, S. Banerjee, J. Rivera, E. Pop and R. Bashir, Proceedings of the IEEE Conference on Nanotechnology, 2012.

189. D. B. Wells, M. Belkin, J. Comer and A. Aksimentiev, *Nano Letters*, 2012, **12**, 4117-4123.

190. C. D. Chin, V. Linder and S. K. Sia, *Lab on a Chip - Miniaturisation for Chemistry and Biology*, 2012, **12**, 2118-2134.

191. W. R. Algar, D. Wegner, A. L. Huston, J. B. Blanco-Canosa, M. H. Stewart, A. Armstrong, P. E. Dawson, N. Hildebrandt and I. L. Medintz, *Journal of the American Chemical Society*, 2012, **134**, 1876-1891.

192. J. Safari and Z. Zarnegar, *Journal of Saudi Chemical Society*, 2014, **18**, 85-99.

193. M. A. Vetten, C. S. Yah, T. Singh and M. Gulumian, *Nanomedicine: Nanotechnology, Biology, and Medicine*, 2014, **10**, 1391-1399.

194. D. P. Duxbury, *Chemical Reviews*, 1993, **93**, 381-433.

195. L. Ferrari, L. Rovati, P. Fabbri and F. Pilati, *Sensors (Switzerland)*, 2013, **13**, 484-499.

196. T. Robertson, F. Bunel and M. Roberts, *Cells*, 2013, **2**, 591.

197. G. Cirillo, F. Iemma, F. Puoci, O. I. Parisi, M. Curcio, U. G. Spizzirri and N. Picci, *Journal of Drug Targeting*, 2009, **17**, 72-77.

198. Y. Hoshino, T. Kodama, Y. Okahata and K. J. Shea, *Journal of the American Chemical Society*, 2008, **130**, 15242-15243.

199. A. R. Guerreiro, I. Chianella, E. Piletska, M. J. Whitcombe and S. A. Piletsky, *Biosensors and Bioelectronics*, 2009, **24**, 2740-2743.

200. S. Korposh, I. Chianella, A. Guerreiro, S. Caygill, S. Piletsky, S. W. James and R. P. Tatam, *Analyst*, 2014, **139**, 2229-2236.

201.   A. Poma, A. Guerreiro, S. Caygill, E. Moczko and S. Piletsky, *RSC Advances*, 2014, **4**, 4203-4206.

202.   A. Poma, A. Guerreiro, M. J. Whitcombe, E. V. Piletska, A. P. F. Turner and S. A. Piletsky, *Advanced Functional Materials*, 2013, n/a-n/a.

203.   E. Moczko, A. Poma, A. Guerreiro, I. Perez De Vargas Sansalvador, S. Caygill, F. Canfarotta, M. J. Whitcombe and S. Piletsky, *Nanoscale*, 2013, **5**, 3733-3741.

204.   H. Sheng and B. C. Ye, *Applied Biochemistry and Biotechnology*, 2009, **152**, 54-65.

205.   E. Moczko, A. Guerreiro, E. Piletska and S. Piletsky, *Langmuir*, 2013, **29**, 9891-9896.

206.   A. Poma, A. Guerreiro, M. J. Whitcombe, E. V. Piletska, A. P. F. Turner and S. A. Piletsky, *Advanced Functional Materials*, 2013, **23**, 2821-2827.

207.   X. D. Liu, S. Tokura, M. Haruki, N. Nishi and N. Sakairi, *Carbohydrate Polymers*, 2002, **49**, 103-108.

208.   M. M. Titirici, A. J. Hall and B. Sellergren, *Chemistry of Materials*, 2002, **14**, 21-23.

209.   S. A. Piletsky, E. V. Piletska, K. Karim, K. W. Freebairn, C. H. Legge and A. P. F. Turner, *Macromolecules*, 2002, **35**, 7499-7504.

210.   S. A. Piletsky, I. Mijangos, A. Guerreiro, E. V. Piletska, I. Chianella, K. Karim and A. P. F. Turner, *Macromolecules*, 2005, **38**, 1410-1414.

211.   T. Otsu, *Journal of Polymer Science, Part A: Polymer Chemistry*, 2000, **38**, 2121-2136.

212.   N. Marchyk, J. Maximilien, S. Beyazit, K. Haupt and B. T. Sum Bui, *Nanoscale*, 2014, **6**, 2872-2878.

213.   A. R. Kannurpatti, S. Lu, G. M. Bunker and C. N. Bowman, *Macromolecules*, 1996, **29**, 7310-7315.

214.   J. M. Rabanel, P. Hildgen and X. Banquy, *Journal of Controlled Release*, 2014, **185**, 71-87.

215. A. S. Karakoti, S. Das, S. Thevuthasan and S. Seal, *Angew Chem Int Ed Engl*, 2011, **50**, 1980-1994.

216. P. Carnell and S. Newell, *American Laboratory*, 2013, **45**.

217. W. Anderson, D. Kozak, V. A. Coleman, T. K. Jämting and M. Trau, *Journal of Colloid and Interface Science*, 2013, **405**, 322-330.

218. E. A. Mun, C. Hannell, S. E. Rogers, P. Hole, A. C. Williams and V. V. Khutoryanskiy, *Langmuir*, 2014, **30**, 308-317.

219. P. Zarogoulidis, W. Hohenforst-Schmidt, K. Darwiche, L. Krauss, D. Sparopoulou, L. Sakkas, A. Gschwendtner, H. Huang, F. J. Turner, L. Freitag and K. Zarogoulidis, *Gene Therapy*, 2013, **20**, 1022-1028.

220. D. Grasseschi, F. S. Lima, M. Nakamura and H. E. Toma, *Micron*, 2015, **69**, 15-20.

221. A. Mukhopadhyay, C. Grabinski, A. R. M. N. Afrooz, N. B. Saleh and S. Hussain, *Applied Biochemistry and Biotechnology*, 2012, **167**, 327-337.

222. I. Surugiu, B. Danielsson, L. Ye, K. Mosbach and K. Haupt, *Analytical Chemistry*, 2001, **73**, 487-491.

223. I. Surugiu, L. Ye, E. Yilmaz, A. Dzgoev, B. Danielsson, K. Mosbach and K. Haupt, *Analyst*, 2000, **125**, 13-16.

224. Y. Yonamine, Y. Hoshino and K. J. Shea, *Biomacromolecules*, 2012, **13**, 2952-2957.

225. S. A. Piletsky, E. V. Piletska, A. Bossi, K. Karim, P. Lowe and A. P. F. Turner, *Biosensors and Bioelectronics*, 2001, **16**, 701-707.

226. D. Zhao, X. Qiao, Z. Xu, R. Xu and Z. Yan, *Journal of Immunoassay and Immunochemistry*, 2013, **34**, 16-29.

227. J. A. Cadée, M. J. Van Steenbergen, C. Versluis, A. J. R. Heck, W. J. M. Underberg, W. Den Otter, W. Jiskoot and W. E. Hennink, *Pharmaceutical Research*, 2001, **18**, 1461-1467.

228. X. D. Feng, X. Q. Guo and K. Y. Qiu, *Polymer Bulletin*, 1987, **18**, 19-26.

229. M. Shirangi, J. Sastre Toraño, B. Sellergren, W. E. Hennink, G. W. Somsen and C. F. Van Nostrum, *Bioconjugate Chemistry*, 2015, **26**, 90-100.

230. C. J. Wienken, P. Baaske, U. Rothbauer, D. Braun and S. Duhr, *Nature Communications*, 2010, **1**.

231. M. Jerabek-Willemsen, T. André, R. Wanner, H. M. Roth, S. Duhr, P. Baaske and D. Breitsprecher, *Journal of Molecular Structure*, 2014, **1077**, 101-113.

232. A. Guerreiro, A. Poma, K. Karim, E. Moczko, J. Takarada, I. P. de Vargas-Sansalvador, N. Turner, E. Piletska, C. S. de Magalhães, N. Glazova, A. Serkova, A. Omelianova and S. Piletsky, *Advanced Healthcare Materials*, 2014.

233. N. Desai, *AAPS Journal*, 2012, **14**, 282-295.

234. X. A. Ton, V. Acha, K. Haupt and B. Tse Sum Bui, *Biosensors and Bioelectronics*, 2012, **36**, 22-28.

235. J. C. K. Lai, G. Ananthakrishnan, S. Jandhyam, V. V. Dukhande, A. Bhushan, M. Gokhale, C. K. Daniels and S. W. Leung, *International Journal of Nanomedicine*, 2010, **5**, 715-723.

236. J. Aragonés, P. Fraisl, M. Baes and P. Carmeliet, *Cell Metabolism*, 2009, **9**, 11-22.

237. A. V. Zhdanov, C. Favre, L. O'Flaherty, J. Adam, R. O'Connor, P. J. Pollard and D. B. Papkovsky, *Integrative biology : quantitative biosciences from nano to macro*, 2011, **3**, 1135-1142.

238. A. V. Zhdanov, V. I. Ogurtsov, C. T. Taylor and D. B. Papkovsky, *Integrative biology : quantitative biosciences from nano to macro*, 2010, **2**, 443-451.

239. P. Aggarwal, J. B. Hall, C. B. McLeland, M. A. Dobrovolskaia and S. E. McNeil, *Advanced drug delivery reviews*, 2009, **61**, 428-437.

240. M. Cui, R. Liu, Z. Deng, G. Ge, Y. Liu and L. Xie, *Nano Research*, 2014, **7**, 345-352.

241. C. D. Walkey and W. C. W. Chan, *Chemical Society Reviews*, 2012, **41**, 2780-2799.

242.   T. Pellegrino, S. Kudera, T. Liedl, A. M. Javier, L. Manna and W. J. Parak, *Small*, 2005, **1**, 48-63.

243.   K. Natte, J. F. Friedrich, S. Wohlrab, J. Lutzki, R. von Klitzing, W. Österle and G. Orts-Gil, *Colloids and Surfaces B: Biointerfaces*, 2013, **104**, 213-220.

244.   A. Verma and F. Stellacci, *Small*, 2010, **6**, 12-21.

245.   T. M. Göppert and R. H. Müller, *International Journal of Pharmaceutics*, 2005, **302**, 172-186.

246.   L. Vroman, A. L. Adams, G. C. Fischer and P. C. Munoz, *Blood*, 1980, **55**, 156-159.

247.   J. C. von Kleist-Retzow, H. T. Hornig-Do, M. Schauen, S. Eckertz, T. A. D. Dinh, F. Stassen, N. Lottmann, M. Bust, B. Galunska, K. Wielckens, W. Hein, J. Beuth, J. M. Braun, J. H. Fischer, V. Y. Ganitkevich, K. Maniura-Weber and R. J. Wiesner, *Experimental Cell Research*, 2007, **313**, 3076-3089.

248.   P. J. Murray and T. A. Wynn, *Nature Reviews Immunology*, 2011, **11**, 723-737.

249.   A. Sindrilaru, T. Peters, S. Wieschalka, C. Baican, A. Baican, H. Peter, A. Hainzl, S. Schatz, Y. Qi, A. Schlecht, J. M. Weiss, M. Wlaschek, C. Sunderkötter and K. Scharffetter-Kochanek, *Journal of Clinical Investigation*, 2011, **121**, 985-997.

250.   D. Finco, C. Grimaldi, M. Fort, M. Walker, A. Kiessling, B. Wolf, T. Salcedo, R. Faggioni, A. Schneider, A. Ibraghimov, S. Scesney, D. Serna, R. Prell, R. Stebbings and P. K. Narayanan, *Cytokine*, 2014, **66**, 143-155.

251.   D. Drescher, G. Orts-Gil, G. Laube, K. Natte, R. W. Veh, W. Österle and J. Kneipp, *Analytical and bioanalytical chemistry*, 2011, **400**, 1367-1373.

252.   E. C. Cho, Q. Zhang and Y. Xia, *Nature Nanotechnology*, 2011, **6**, 385-391.

253.   F. Joris, B. B. Manshian, K. Peynshaert, S. C. De Smedt, K. Braeckmans and S. J. Soenen, *Chemical Society Reviews*, 2013, **42**, 8339-8359.

254.   E. O. L. Santos, A. E. C. S. Azzolini and Y. M. Lucisano-Valim, *Journal of Pharmacological and Toxicological Methods*, 2015, **72**, 67-71.

255. M. Collado and M. Serrano, *Nature Reviews Cancer*, 2010, **10**, 51-57.

256. E. Simboeck, J. D. Ribeiro, S. Teichmann and L. Di Croce, *Biochemical Pharmacology*, 2011, **82**, 1361-1370.

257. M. Collado, J. Gil, A. Efeyan, C. Guerra, A. J. Schuhmacher, M. Barradas, A. Benguría, A. Zaballos, J. M. Flores, M. Barbacid, D. Beach and M. Serrano, *Nature*, 2005, **436**, 642.

258. R. Lozano, M. Naghavi, K. Foreman, S. Lim, K. Shibuya, V. Aboyans, J. Abraham, T. Adair, R. Aggarwal, S. Y. Ahn, M. Alvarado, H. R. Anderson, L. M. Anderson, K. G. Andrews, C. Atkinson, L. M. Baddour, S. Barker-Collo, D. H. Bartels, M. L. Bell, E. J. Benjamin, D. Bennett, K. Bhalla, B. Bikbov, A. B. Abdulhak, G. Birbeck, F. Blyth, I. Bolliger, S. Boufous, C. Bucello, M. Burch, P. Burney, J. Carapetis, H. Chen, D. Chou, S. S. Chugh, L. E. Coffeng, S. D. Colan, S. Colquhoun, K. E. Colson, J. Condon, M. D. Connor, L. T. Cooper, M. Corriere, M. Cortinovis, K. C. De Vaccaro, W. Couser, B. C. Cowie, M. H. Criqui, M. Cross, K. C. Dabhadkar, N. Dahodwala, D. De Leo, L. Degenhardt, A. Delossantos, J. Denenberg, D. C. Des Jarlais, S. D. Dharmaratne, E. R. Dorsey, T. Driscoll, H. Duber, B. Ebel, P. J. Erwin, P. Espindola, M. Ezzati, V. Feigin, A. D. Flaxman, M. H. Forouzanfar, F. G. R. Fowkes, R. Franklin, M. Fransen, M. K. Freeman, S. E. Gabriel, E. Gakidou, F. Gaspari, R. F. Gillum, D. Gonzalez-Medina, Y. A. Halasa, D. Haring, J. E. Harrison, R. Havmoeller, R. J. Hay, B. Hoen, P. J. Hotez, D. Hoy, K. H. Jacobsen, S. L. James, R. Jasrasaria, S. Jayaraman, N. Johns, G. Karthikeyan, N. Kassebaum, A. Keren, J. P. Khoo, L. M. Knowlton, O. Kobusingye, A. Koranteng, R. Krishnamurthi, M. Lipnick, S. E. Lipshultz, S. L. Ohno, J. Mabweijano, M. F. MacIntyre, L. Mallinger, L. March, G. B. Marks, R. Marks, A. Matsumori, R. Matzopoulos, B. M. Mayosi, J. H. McAnulty, M. M. McDermott, J. McGrath, G. A. Mensah, T. R. Merriman, C. Michaud, M. Miller, T. R. Miller, C. Mock, A. O. Mocumbi, A. A. Mokdad, A. Moran, K. Mulholland, M. N. Nair, L. Naldi, K. M. V. Narayan, K. Nasseri, P. Norman, M. O'Donnell, S. B. Omer, K. Ortblad, R. Osborne, D. Ozgediz, B. Pahari, J. D. Pandian, A. P. Rivero, R. P. Padilla, F. Perez-Ruiz, N. Perico, D. Phillips, K. Pierce, C. A. Pope Iii, E. Porrini, F. Pourmalek, M. Raju, D. Ranganathan, J. T. Rehm, D. B. Rein, G. Remuzzi, F. P. Rivara, T. Roberts, F.

R. De León, L. C. Rosenfeld, L. Rushton, R. L. Sacco, J. A. Salomon, U. Sampson, E. Sanman, D. C. Schwebel, M. Segui-Gomez, D. S. Shepard, D. Singh, J. Singleton, K. Sliwa, E. Smith, A. Steer, J. A. Taylor, B. Thomas, I. M. Tleyjeh, J. A. Towbin, T. Truelsen, E. A. Undurraga, N. Venketasubramanian, L. Vijayakumar, T. Vos, G. R. Wagner, M. Wang, W. Wang, K. Watt, M. A. Weinstock, R. Weintraub, J. D. Wilkinson, A. D. Woolf, S. Wulf, P. H. Yeh, P. Yip, A. Zabetian, Z. J. Zheng, A. D. Lopez and C. J. L. Murray, *The Lancet*, 2012, **380**, 2095-2128.

259. D. Hanahan and R. A. Weinberg, *Cell*, 2011, **144**, 646-674.

260. T. B. Drüeke and Z. A. Massy, *Seminars in Dialysis*, 2009, **22**, 378-380.

261. M. Althubiti, L. Lezina, S. Carrera, R. Jukes-Jones, S. M. Giblett, A. Antonov, N. Barlev, G. S. Saldanha, C. A. Pritchard, K. Cain and S. MacIp, *Cell Death and Disease*, 2014, **5**.

262. J. Martinez-Useros and J. Garcia-Foncillas, *Oral Oncology*, 2016, **51**, 423-430.

263. J. Zhou, T. Du, B. Li, Y. Rong, A. Verkhratsky and L. Peng, *ASN Neuro*, 2015, **7**.

264. Y. Wang, X. Wang, C. R. Ferrone, J. H. Schwab and S. Ferrone, *Molecular Oncology*, 2015, **9**, 1982-1993.